# INCREMENTAL REDUNDANCY LOW-DENSITY PARITY-CHECK CODES FOR HYBRID FEC/ARQ SCHEMES

A Dissertation
Presented to
The Academic Faculty

by

Woonhaing Hur

In Partial Fulfillment
of the Requirements for the Degree
Doctor of Philosophy in the
School of Electrical and Computer Engineering

Georgia Institute of Technology
May 2007

# INCREMENTAL REDUNDANCY LOW-DENSITY PARITY-CHECK CODES FOR HYBRID FEC/ARQ SCHEMES

Approved by:


Dr. Steven W. McLaughlin, Advisor
School of Electrical and Computer Engineering
*Georgia Institute of Technology*

Dr. Douglas B. Williams
School of Electrical and Computer Engineering
*Georgia Institute of Technology*

Dr. John A. Copeland
School of Electrical and Computer Engineering
*Georgia Institute of Technology*

Dr. Biing Hwang (Fred) Juang
School of Electrical and Computer Engineering
*Georgia Institute of Technology*

Dr. Thomas D. Morley
School of Mathematics
*Georgia Institute of Technology*



Date Approved: January 18, 2007

*To my wife Kyunga, my son Kyungmoo (Andy), my daughter Jimin (Jenny), and my family*

# ACKNOWLEDGEMENTS

This dissertation could not be completed without the aid and support of countless people over the past several years. I would like to thank everyone who influenced this work.

First of all, I would like to express my deep appreciation to Dr. Steven W. McLaughlin, my dissertation advisor, for his support, encouragement, attention to detail, and guidance. It has been an honor and a pleasure to work with him during my stay at Georgia Institute of Technology. I cannot imagine a better advisor.

I am truly grateful to Dr. Douglas W. Williams, Dr. John A. Copeland, Dr. Biing Hwang Juang, and Dr. Thomas D. Morley for serving on my thesis committee. Their valuable advice has improved the quality of this thesis.

I also would like to extend many thanks to all friends of my LAB and Georgia Tech., both past and present, for their helps and friendship. Their friendship has made my graduate studies more enjoyable, and it has been a great pleasure to have worked with them.

I am forever indebted to my wife Kyunga for her all love and support. Also, my son, Andy (Kyungmoo) and my daughter Jenny (Jimin) gave me great happiness whenever I see their face.

I dedicate this thesis to my family; my parents, Mr. Byungson Hur and Mrs. Yangsoon Whang, my parents-in law, Mr. Shinheung Kim and Mrs. Dongrye Kwon, and all the others in my family. This thesis would not have been possible without their unending love and support.

# TABLE OF CONTENTS

# LIST OF TABLES

# LIST OF FIGURES

# LIST OF ACRONYMS

| | |
|---|---|
| **ACK** | Acknowledgement |
| **ARQ** | Automatic repeat request |
| **AWGN** | Additive white Gaussian noise |
| **BER** | Bit error rate |
| **FEC** | Forward error correction |
| **FER** | Frame error rate |
| **IRA** | Irregular repeat accumulate |
| **LDPC** | Low-density parity-check |
| **LLR** | Log-likelihood ratio |
| **NAK** | Negative acknowledgement |
| **MAP** | Maximum a posterior probability |
| **MIMO** | Multiple-input multiple-output |
| **MMSE** | Minimum mean square error |
| **QPSK** | Quadrature phase shift keying |
| **SNR** | Signal to noise ratio |
| **V-BLAST** | Vertical Bell Labs layered space-time |
| **ZF** | Zero Forcing |

# LIST OF ABBREVIATIONS

| | |
|---|---|
| **DCAC** | Dedicated coded adaptive coding |
| **FPAC** | Finite-length punctured adaptive coding |
| **IR-HybridARQ** | Incremental redundancy hybrid FEC/ARQ |
| **IR-LDPC** | Incremental redundancy low-density parity-check |
| **RPAC** | Random punctured adaptive coding |

# SUMMARY

The objective of this dissertation is to investigate incremental redundancy low-density parity-check (IR-LDPC) codes for hybrid forward error correction / automatic repeat request (HybridARQ) schemes. Powerful capacity-approaching IR-LDPC codes are one of the key functional elements in high-throughput HybridARQ schemes and provide a flexible rate-compatible structure, which is necessary for low-complexity HybridARQ schemes.

This dissertation first studies the design and performance evaluation of IR-LDPC codes, which have good error rate performance at short block lengths. The subset codes of the IR-LDPC codes will be compared to conventional random punctured codes and multiple dedicated codes. This step is necessary for designing IR-LDPC codes because throughput performance of HybridARQ schemes strongly depends on the error rate performance of a subset of IR-LDPC codes. As a system model for this work, an adaptive LDPC coded system is presented. This adaptive system can confront the nature of time-varying channels and approach the capacity of the system with the aid of LDPC codes. This system shows remarkable throughput improvement over a conventional punctured system and, for systems that use multiple dedicated codes, provides comparable performance with low-complexity at every target error rate.

This dissertation also focuses on IR-LDPC codes with a wider operating code range because the previous IR-LDPC codes exhibited performance limitation related to the maximum achievable code rate. For this reason, this research proposes a new way to increase the maximum code rate of the IR-LDPC codes, which provides throughput

improvement at high throughput regions over conventional random punctured codes. Also presented is an adaptive code selection algorithm using threshold parameters. This algorithm reduces the number of the unnecessary traffic channels in HybridARQ schemes.

This dissertation also examines how to improve throughput performance in HybridARQ schemes with low-complexity by exploiting irregular repeat accumulate (IRA) codes. The proposed adaptive transmission method with adaptive puncturing patterns of IRA codes shows higher throughput performance in all of operating code ranges than does any other single mode in IR-HybridARQ schemes.

# CHAPTER 1

# INTRODUCTION

## 1.1 Overview and Motivation

Recently, the demand for efficient and reliable digital transmissions for high-speed and high-quality wireless systems has received considerable attention. This demand requests flexible and powerful error control coding schemes such as automatic repeat request (ARQ) and forward error correction (FEC) codes. These schemes are also required to support different variable-data-rates and quality-of-service requirements over time-varying wireless channels [1][2], which have tremendous impairments due to multipath fading effects.

Multipath fading is a harsh and complex phenomenon in mobile communication that induces performance degradation in wireless systems. Conventional wireless systems employing single antenna transmission have many challenges from interference of the transmitted signal in multipath environments. This phenomenon results when an antenna receives radio signals by two or more paths simultaneously. This multipath is caused by reflection, refraction, shadowing and a moving user. Reducing the fading effects in single antenna systems has become a challenging and burdensome task.

To attack such multipath fading effects and enhance the throughput performance of the wireless systems, ongoing current wireless standards [3] use a Multiple-Input Multiple-Output (MIMO) transmission technique [4][5][6], which uses multiple antennas in both the transmitter and receiver. Unlike single antenna systems, MIMO systems exploit the multipath channels by sending different information by multiple transmit

antennas and receiving the information at multiple receive antennas. This concurrent transmission can solve the multipath fading effects and provide high-data-rate transmission with large capacities [7] and high-throughput.

Currently, the International Telecommunication Union (ITU), which leads the specification of fourth-generation wireless systems [8], is considering the proper combination of ARQ and FEC coding techniques in MIMO antenna environments [9][10][11] to enhance their throughput and spectrum efficiency.

Transmission errors in multipath fading wireless communication systems can be controlled by two error control techniques [12][13][14], FEC codes and ARQ schemes. FEC codes use a powerful error correcting code that increases the noise immunity of transmitted information by adding redundancy to the information sequence to minimize the transmission errors. The primary purpose of FEC codes is to provide high coding gain so that the throughput of such systems keeps constant at equal code rates. However, these systems cannot achieve high system reliability when there are burst errors in time-varying channels. ARQ schemes [15][16], on the other hand, have better throughput performance than FEC schemes in burst channel environments. ARQ systems use a retransmission protocol and available feedback channels in a two-way communication link to combat unavoidable channel errors. However, when channel error rate increases, the throughput of this scheme also has a severe problem. The receiver of these systems requests retransmission continuously to the transmitter until an uncorrectable error is correctly decoded. For a system with large round-trip delay and high-data-rate transmission, ARQ schemes become inefficient, and their throughput rapidly diminishes in deep fading time-varying channels.

These facts above provide the motivation for this dissertation to investigate the proper combination of hybrid FEC/ARQ schemes in time-varying channels in multiple antenna environments. To establish a reliable communication link with less redundancy in codes and higher throughput, both schemes can be combined. This combined scheme is referred to as a hybrid FEC/ARQ (HybridARQ) scheme [17][18][19]. This HybridARQ scheme can maintain higher throughput over a wide range of channel error rates if FEC codes for error correction and ARQ schemes with a retransmission protocol are properly chosen.

In this dissertation, we consider the incremental redundancy HybridARQ (IR-HybridARQ) scheme [20][21] to provide near-capacity performance using powerful rate-compatible error correction codes. The IR-HybridARQ scheme [22][23] requires incremental redundancy characteristics of a family of error correction codes to improve data throughput by transmitting a small fraction of its parity bits gradually according to the channel state in time-varying channels. In this scheme, the throughput of the HybridARQ scheme is strongly affected by the power of the mother code and its family codes, which support a wide range of code rates. Previous research on IR-HybridARQ schemes [24][25][26][27][28] considered using low-density parity-check (LDPC) codes, which are recently known to be powerful error correction codes with feasible decoding complexity. We also exploit the LDPC codes as a family of powerful error correction codes for the IR-HybridARQ schemes. From this objective comes the name of incremental redundancy LDPC (IR-LDPC) codes.

The goal of this dissertation is to investigate IR-LDPC codes, which are used as FEC codes in IR-HybridARQ schemes in time-varying MIMO channels. This research on

IR-LDPC codes is aimed at improving the throughput performance of the IR-HybridARQ scheme for the next generation of wireless communications, which will be pursuing reliable high-data-rate transmission with low-complexity in multiple antenna environments.

## 1.2 Research Approach and Contribution

The approaches to using LDPC codes for HybridARQ schemes are investigated in [24][25][26][27][28]. In these schemes, the information bits are encoded by a mother code. Then, a selected number of parity bits are transmitted. If a retransmission is requested, only additional selected bits are transmitted. This procedure is repeated until the entire codeword of the mother code is transmitted after each subsequent retransmission request. To prepare the subset codes of a mother code, this approach uses a puncturing scheme. Given the number of parity bits for each retransmission by the puncturing scheme, the punctured parity bits are omitted in the transmission data. In this case, the throughput of HybridARQ schemes is strongly affected by the power of the mother code used in the system and the family of codes obtained by puncturing. It should be noted that previous approaches used a simple random puncturing method and a rate-compatible puncturing algorithm suitable for LDPC codes with long-block lengths. Therefore, the performance limitation is shown at higher punctured code rates. To solve the previous problems and to research IR-LDPC codes for high-data-rate transmission with low-complexity, this dissertation focuses on following three contributions.

**Contribution 1: Throughput improvements of adaptive LDPC coded systems**

In this contribution, we study the design on IR-LDPC codes in a rate-compatible fashion for IR-HybridARQ schemes. The error rate performance of the IR-LDPC codes

is also evaluated over time-varying channels. The throughput performance of IR-HybridARQ schemes strongly depends on the frame error rate performance of the subset codes of IR-LDPC codes [25]. Therefore, the family of IR-LDPC codes, which includes the mother code, needs to be designed carefully. In this contribution, we also present a new adaptive coding system with the well-designed IR-LDPC codes to solve the problems posed by time-varying channels and to maximize the capacity of Vertical Bell Lab Layered Space-Time (V-BLAST) MIMO systems. This adaptive coding reduces the complexity of the receiver by using only one channel code to support variable data rate service while showing the comparable performance of a dedicated (i.e. non-punctured, multiple code) coded system which reaches the upper limit of the capacity-approaching schemes with high-complexity. Our proposed adaptive LDPC coded V-BLAST system shows a remarkable transmission rate improvement over a conventional punctured system and provides comparable performance of a system that uses multiple dedicated codes at every target BER in time-varying MIMO channels.

**Contribution 2: Incremental redundancy LDPC codes for hybrid FEC/ARQ scheme**

The throughput of IR-HybridARQ schemes strongly depends on the design of an ensemble of error correction codes. In this contribution, we prepare ensembles of rate-compatible LDPC codes with a modified intentional puncturing algorithm to achieve good frame error rate performance at each operating rate, which can improve the throughput performance of V-BLAST systems in IR-HybridARQ schemes. Our IR-HybridARQ scheme over LDPC coded V-BLAST systems using these ensembles shows high throughput improvement over a conventional randomly punctured LDPC coded system in time-varying channels. We also propose an adaptive IR-HybridARQ scheme

with a code selection algorithm to reduce the traffic of a feedback channel. With the proposed adaptive code selection algorithm, we greatly reduce the traffic of the feedback channel for NAK signaling without any significant throughput loss.

**Contribution 3: Incremental redundancy irregular repeat-accumulate codes for hybrid FEC/ARQ schemes**

In this contribution, incremental redundancy irregular repeat accumulate (IRA) codes [29] are exploited for throughput improvement of IR-HybridARQ schemes with low complexity. IRA codes can be good FEC codes for HybridARQ scheme with the aid of their simple structure and low-complexities with good error rate performance. However, the structure of these codes, which have many degree 2 nodes in parity parts, leads to high error rate performance in burst channels. To deal with this, we propose a new adaptive transmission method with rate-compatible puncturing patterns for these IRA codes to maximize the throughput performance. For the MIMO system for high-data-rate transmission, we consider QR decomposition based V-BLAST system models for a low-complexity approach because minimum mean square error (MMSE) based V-BLAST systems require prohibitive computational complexities. We verify that our IR-HybridARQ scheme, which uses adaptive puncturing patterns of IRA codes and a QR decomposition based detector, has good throughput performance in all of SNR regions and that its performance adapts well to the time-varying channels.

## 1.3 Organization of the Dissertation

This dissertation is organized as follows. Chapter 2 begins with brief backgrounds on LDPC codes and hybrid FEC/ARQ schemes. Chapter 3 investigates the design on IR-LDPC codes and presents the adaptive coded system with those codes. Chapter 4

approaches the throughput improvement of IR-HybridARQ scheme using the proposed IR-LDPC codes and the adaptive code selection algorithm. In chapter 5, we design the low-complexity IR-HybridARQ scheme using adaptive puncturing patterns of IRA codes and a low-complexity QR based detector. Finally, chapter 6 presents a summary of results and suggestions for future research.

# CHAPTER 2

# BACKGROUND RESEARCH

## 2.1 Low-Density Parity-Check Codes

LDPC codes are a class of linear error-correcting block codes. In 1963, Gallager [30] introduced the LDPC codes and showed that random regular LDPC codes are asymptotically good and perform close to the Shannon capacity limit when the block length increases. Unfortunately, LDPC codes were almost forgotten for more than thirty years because there was no available practical decoding technique that was able to achieve the expected near-Shannon performance.

Only recently, LDPC codes have been rediscovered following the invention of turbo codes by Berrou *et al*. in 1993 [31]. MacKay and Neal [32] showed empirically that long LDPC codes offer near optimum performance with iterative decoding algorithms [33], just as turbo code does. In particular, irregular LDPC codes have been shown to perform better than turbo codes. When decoding the irregular LDPC codes with relatively simple and practical iterative decoding algorithm, it is shown that their empirical performance can approach the Shannon limit in [34]. In addition, Richardson *et al.* [35] [36] showed that for very long codes realized from a given ensemble, arbitrarily small bit error probability can be achieved below a certain noise threshold which is computed by the decoding analysis. More recently, Chung *et al*. [37] presented that simulation with large block lengths has shown a bit error rate only 0.0045 dB away from the Shannon capacity limit of the binary input AWGN channel.

### 2.1.1 Structure of LDPC Codes

LDPC codes can be described by a sparse parity-check matrix $\boldsymbol{H}$ containing a sparse number of non-zero entries. The term low-density means that the number of ones in each column and row of the parity-check matrix is small compared to the block size. Linear codes are defined in terms of generator and parity-check matrices. Generator matrix $\boldsymbol{G}$ maps information $\boldsymbol{u}$ to transmitted blocks $\boldsymbol{x}$ called codewords. For a generator matrix $\boldsymbol{G}$, there is a parity-check matrix $\boldsymbol{H}$ which is related as $\boldsymbol{G}\cdot\boldsymbol{H}^{\mathrm{T}}=0$. All codewords must satisfy $\boldsymbol{x}\cdot\boldsymbol{H}^{\mathrm{T}}= 0$ in terms of the parity-check matrix $\boldsymbol{H}$.

If the parity-check matrix $\boldsymbol{H}$ has the same weight per row and the same weight per column, the resulting LDPC codes is called regular. We use a two tuple ($d_v$, $d_c$) to represent a regular LDPC code whose column weight is $d_v$ and row weight is $d_c$. When the weight in every column is not the same in the parity-check matrix, the code is known as an irregular LDPC code. Irregular LDPC codes have a better asymptotic performance and can practically reach channel capacity as shown in [34].

LDPC codes can be represented in a simple bipartite graph representation [38], which consists of two types of nodes: *variable* nodes and *check* nodes. Each variable (check) node corresponds to the column (row) of the parity-check matrix $\boldsymbol{H}$. The edges in the graph indicate the variable nodes participating in the corresponding check node. Thus, a one located at position ($i$, $j$) of $\boldsymbol{H}$ corresponds to an edge between variable node $i$ and the check node $j$.

As an example of a Tanner graph [38], a regular LDPC code of length $n$ = 10 and $k$ = 5 is shown in Figure 1. The equivalent bipartite graph representing this code is also

shown in Figure 2. In this code, every variable node has degree three and each check node has degree six. Thus, this code is called a (3,6) regular LDPC code.

$$\boldsymbol{H} = \begin{bmatrix} 1 & 0 & 0 & 0 & 1 & 1 & 0 & 1 & 1 & 1 \\ 0 & 1 & 0 & 1 & 1 & 0 & 1 & 1 & 1 & 0 \\ 0 & 1 & 1 & 1 & 0 & 1 & 0 & 1 & 0 & 1 \\ 1 & 0 & 1 & 1 & 0 & 0 & 1 & 0 & 1 & 1 \\ 1 & 1 & 1 & 0 & 1 & 1 & 1 & 0 & 0 & 0 \end{bmatrix}$$

**Figure 1. Parity-check matrix *H* of a (3,6) regular LDPC code.**

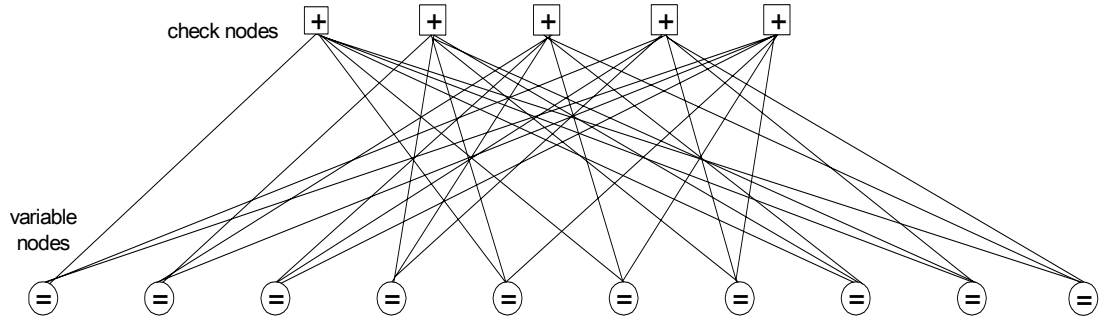


**Figure 2. Equivalent graphical representation of (3,6) regular LDPC code.**

On the other hand, an irregular LDPC code is specified by a degree distribution pair ($\lambda(x)$, $\rho(x)$). The $\lambda(x)$ ($\rho(x)$) represent the fraction of edges emanating from variable (check) nodes of various degrees as indicated by the powers of the place holding variables $x^{i-1}$ , as shown in equation (1) and (2). Let $d_v$ and $d_c$ be the maximum degrees of the variable and check nodes respectively.

$$\lambda(x) = \sum_{i=1}^{d_v} \lambda_i x^{i-1} \quad . \tag{1}$$

$$\rho(x) = \sum_{i=1}^{d_c} \rho_i x^{i-1} \,. \tag{2}$$

The coding rate $R$ of LDPC codes specified by a degree distribution pair, ($\lambda(x)$, $\rho(x)$) is given by

$$R(\lambda, \rho) = 1 - \frac{\frac{\rho_i}{i}}{\frac{\lambda_i}{i}} = 1 - \frac{\int_0^1 \rho(x)dx}{\int_0^1 \lambda(x)dx} \,. \tag{3}$$

To understand the characteristics of LDPC codes, we need to introduce the concepts of cycle, stopping set, and girth in the Tanner graphical representation shown in Figure 3. This representation of LDPC codes is useful since their decoding algorithm can be explained by the exchange of information along the edges of these graphs.

A *cycle* in a Tanner graph [39] is defined as a sequence of connected vertices which start and end at the same vertex in the graph, and which contain other vertices no more than once. The length of a cycle is the number of edges it contains.

A *stopping set* in this graph is a set of variable nodes, so that all neighbors of stopping set are connected to the stopping set at least twice. In particular, the empty set is also a stopping set. The number of variable nodes in a stopping set is called its size.

A *global girth* $g$ of a graph is defined as the size of its smallest cycle. The *local girth* $g_i$ of a variable node is defined as the shortest cycle from the variable node back to itself, if any edge is used not more than once. The global girth $g$ has the relationship with the local girth $g_i$ as shown in equation (4) .

$$g = \min_j (g_j) \,. \tag{4}$$

Figure 3 shows an example of stopping sets and local girths in a Tanner graph. The circles and the squares of this graph represent variable nodes and check nodes, respectively.

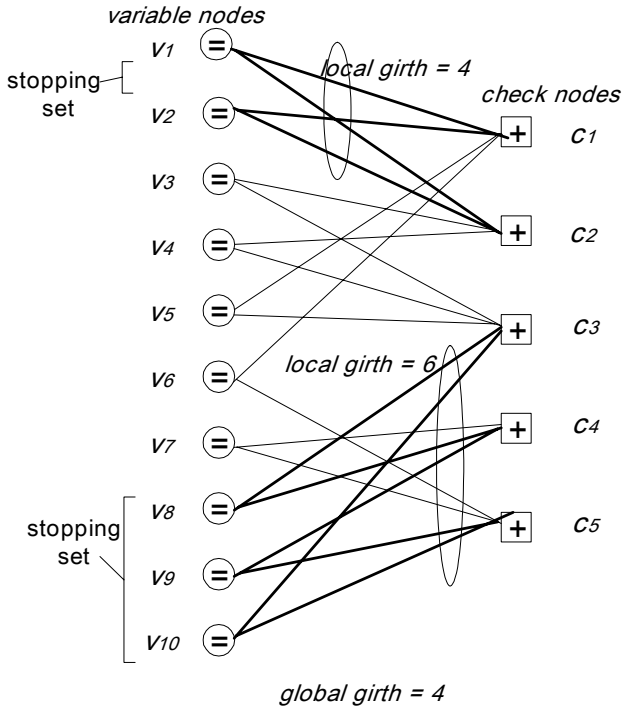


**Figure 3. Stopping sets and local girths.**

The upper set $\{v_1, v_2\}$ and the lower set $\{v_8, v_9, v_{10}\}$ are shown as examples of a stopping set. The global girth of this Tanner graph is 4, while the upper local girths $g_0 = g_1 = 4$, and the lower local girths $g_8 = g_9 = g_{10} = 6$.

### 2.1.2 Encoding Algorithm

The encoding algorithm is usually less complex than the decoding algorithm because the encoding algorithm computes the number of arithmetic operations for a binary linear code. However, LDPC codes have a weak point at their encoding process because the sparse parity-check matrix does not have necessarily a sparse generator

matrix. Encoding process using a dense generator matrix $\boldsymbol{G}$ yields to an $\boldsymbol{N}^2$ computational complexity that is linear with respect to the block length. In this section, two encoding schemes are presented. The first encoding scheme is to deal with the generator matrix, and the second encoding scheme is to deal with lower triangular shape parity-check matrix.

2.1.2.1 Encoding Algorithm with Generator Matrix

Consider a linear block code with a generator matrix $\boldsymbol{G}$. This encoding algorithm can be expressed by

$$x = u \cdot \boldsymbol{G}, \tag{5}$$

where the matrix $\boldsymbol{G}$ is of dimension $k \times n$, $u$ is the information bits of dimension $1 \times k$, and $x$ is the resulting codeword of dimension $1 \times n$. Using Gaussian-Jordan elimination and column ordering, it is always possible to obtain a generator matrix with following form.

$$\boldsymbol{H}_{(n-k)\times n} = \left[ \boldsymbol{P}_{(n-k)\times k} \boldsymbol{I}_{(n-k)\times(n-k)} \right] \Leftrightarrow \boldsymbol{G}_{k\times n} = \left[ \boldsymbol{I}_k \boldsymbol{P}^T_{k\times(n-k)} \right], \tag{6}$$

where the matrix $\boldsymbol{I}$ is an identity matrix and the matrix $\boldsymbol{P}$ is a binary matrix.

The generator matrix of LDPC codes is usually not sparse because of inversion. Cleary, when a data block $u$ is encoded using a systematic generator matrix $\boldsymbol{G}$ in equation (6) and (7) , it is embedded without any modification in the last $k$ coordinates of the resulting codeword. This encoding process requires $k\cdot$ ($n$ – $k$) operations and has a computational complexity that is quadratic in the block length. Thus, this method is not suited for encoding LDPC codes with long block lengths.

2.1.2.2 Encoding Algorithm with Lower-Triangular Shape Parity-Check Matrix

To lower the complexity of the encoding process in the previous section, a parity-check matrix with an almost lower-triangular shape is created in [35][40], as depicted in Figure 4. The idea in this method is to minimize the constant factor $g$ in front of the quadratic dependency. Instead of computing the product $\boldsymbol{x}=\boldsymbol{u}\cdot\boldsymbol{G}$, the equation $\boldsymbol{H}\cdot\boldsymbol{x}^{\mathrm{T}} = 0$ is solved.

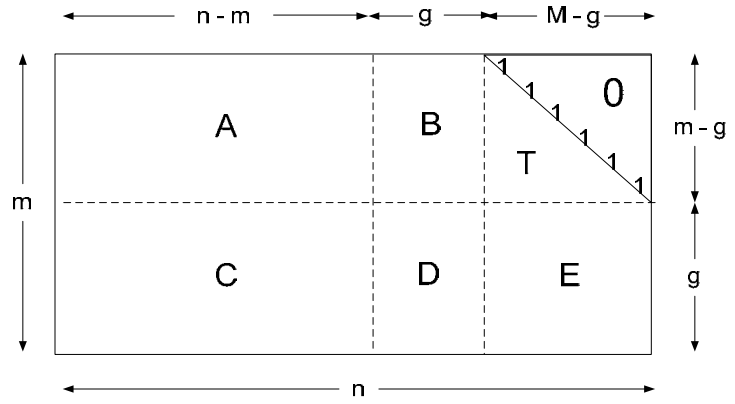


**Figure 4. Parity-check matrix in approximate lower triangular form.**

Let the parity-check matrix be changed into the form indicated in Figure 4 by performing row and column permutations only. Assume that the matrix is transformed into the form

$$H_{(n-k)\times n} = \begin{pmatrix} A_{(m-g)\times(n-m)} & B_{(m-g)\times g} & T_{(m-g)\times(m-g)} \\ C_{g\times(n-m)} & D_{g\times g} & E_{g\times(m-g)} \end{pmatrix}, \tag{7}$$

where $\boldsymbol{T}$ is a lower-triangular matrix with ones along the diagonal. Multiplying this matrix in the equation (8) from the left by

$$\begin{pmatrix} I & 0 \\ -ET^{-1} & I \end{pmatrix}, \tag{8}$$

the matrix will be

$$\begin{pmatrix} A & B & T \\ -ET^{-1}A + C & -ET^{-1}B + D & 0 \end{pmatrix}. \tag{9}$$

Let $\boldsymbol{x} = (m, p_1, p_2)$, where $m$ denotes the systematic part, and $p_1$ and $p_2$ combined denote the parity parts of a codeword $\boldsymbol{x}$. Then, from the equation $\boldsymbol{H} \cdot \mathbf{x}^{\mathrm{T}} = 0$, the following equations are generated [40]:

$$Am^T + Bp_1^T + Tp_2^T = 0, \tag{10}$$

$$\left(-ET^{-1}A + C\right)m^T + \left(-ET^{-1}B + D\right)p_1^T = 0. \tag{11}$$

By defining $\phi = -ET^{-1}B + D$ that is assumed as a non-singular value, equations (12) and (13) are derived as follows:

$$p_1^T = -\phi^{-1}\left(-ET^{-1}A + C\right)m^T. \tag{12}$$

$$p_2^T = -T^{-1}\left(Am^T + Bp_1^T\right). \tag{13}$$

Therefore, the computational complexities of $\boldsymbol{H} \cdot \boldsymbol{x}^{\mathrm{T}} = 0$ can be reduced by computing $p_1$ and $p_2$ effectively with several smaller steps [40]. In this encoding scheme, the overall encoding complexity scales down, minimizing $g$ and maintaining the characteristics of sparseness of the $\boldsymbol{H}$ matrix.

### 2.1.3 Sum-Product Decoding Algorithm

The standard message-passing algorithm is known as a sum-product algorithm [36][41] or a belief propagation algorithm [33]. This simple algorithm converges iteratively to a sub-optimal solution that may not be the maximum likelihood solution. The sum-product decoder is a graph-based decoder operating on the constraint graph of a

parity-check matrix $\boldsymbol{H}$. This sum-product decoding process comprises three steps: initialization, message passing shown in Figure 5(a) from check nodes to variable nodes, and message passing from variable nodes to check nodes shown in Figure 5(b). This process exchanges messages along the edges of the code's constraint graph until a valid codeword satisfying $\boldsymbol{H} \cdot \boldsymbol{x}^{\mathrm{T}} = 0$ is found.

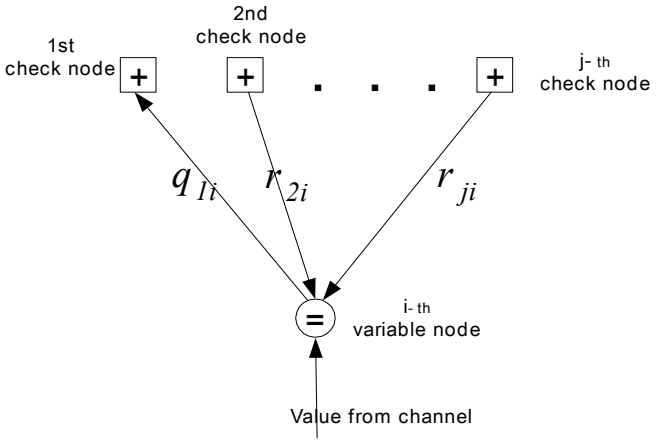


(a)

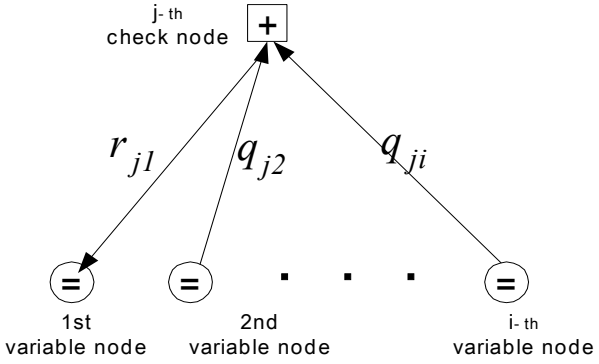


(b)

**Figure 5. Sum-product message passing flow: (a) variable node update and (b) check node update.**

In the initialization step, the messages $r_{ji}$ from the check nodes to the variable nodes are zero. In the first part of iteration, the message $q_{ji}$ from variable nodes to check

nodes are computed based on the observed value of the variable node and some of the message passed from the neighboring check nodes to that variable node. Note that the message that is sent from a variable node *i* to a check node *j* must exclude the message sent in the previous round from a check node *j* to a variable node *i.* This routine is for updating check nodes. In the second part of iteration, every check node sends out a message over an edge by using all messages received from the other edges in previous round. These two alternating parts of the decoding algorithm are updated iteratively until the tentative decoding satisfies the equation $\boldsymbol{H}\cdot\boldsymbol{x}^{\mathrm{T}} = 0$ at variable nodes.

The sum-product algorithm can be changed into the Log-MAP algorithm, representing the messages in a log-likelihood ratio (LLR) symbol set. The log-domain version of sum-product algorithm is to be preferred because involved multiplications can be replaced with additions. Here, we first define the following LLR values [42].

$$L(x_i) = \log\left(\frac{\Pr(x_i = 0 \mid y_i)}{\Pr(x_i = 1 \mid y_i)}\right), \tag{14}$$

where $y_{\mathrm{i}}$ is the input value from the channel at the $i_{\mathrm{th}}$ variable node.

$$L(r_{ji}) = \log\left(\frac{r_{ji}(0)}{r_{ji}(1)}\right). \tag{15}$$

$$L(q_{ji}) = \log\left(\frac{q_{ij}(0)}{q_{ij}(1)}\right). \tag{16}$$

$$L(Q_i) = \log\left(\frac{Q_i(0)}{Q_i(1)}\right). \tag{17}$$

Now using the fact that $\tanh[1/2\log(p_0 / p_1) = p_0 - p_1 = 1 - 2p_1$, we need to show the following results.

$$1-2r_{ji}(1)=\prod_{i^{'}\in V_j\backslash i}(1-2q_{i^{'}j}(1))\Leftrightarrow \tanh(\tfrac{1}{2}L(r_{ji}))=\prod_{i^{'}\in V_j\backslash i}\tanh(\tfrac{1}{2}L(q_{i^{'}j}))\,. \tag{18}$$

The log-domain decoding algorithm involves the following steps using the LLR equations above [42].

Step 1. Initialization:

For $i = 0, 1, \ldots, n\text{-}1$, initialize $L(q_{ij})$ for all $i, j$ for which $\boldsymbol{H}_{ij} = 1$.

$$L(q_{ji})=L(x_i)=\log\frac{(1+e^{-2y_i/\sigma^2})^{-1}}{(1+e^{2y_i/\sigma^2})^{-1}}=2y_i/\sigma^2\,. \tag{19}$$

Step 2. Check-to-variable node message passing:

Update $L(r_{ji})$ at variable nodes.

$$L(r_{ji})=(\prod_{i^{'}\in V_j\backslash i}\alpha_{i^{'}j})\cdot\Phi(\sum_{i^{'}\in V_j\backslash i}\Phi(\beta_{i^{'}j}))\,, \tag{20}$$

where $\alpha_{ij}\triangleq sign(L(q_{ij}))$, $\beta_{ij}\triangleq\left|L(q_{ij})\right|$, and $\Phi(x)\triangleq-\log\tanh(x/2)$.

Step 3. Variable-to-check node message passing:

Update $L(q_{ij})$ at check nodes.

$$L(q_{ji})=L(x_i)+\sum_{j^{'}\in C_i\backslash j}L(r_{j^{'}i})\,. \tag{21}$$

Step 4. Decision:

Update $L(Q_i)$ and check the codeword satisfying $\boldsymbol{H}\cdot\boldsymbol{x}^{\mathrm{T}}=0$.

$$L(Q_i)=L(x_i)+\sum_{j\in C_i}L(r_{ji})\,. \tag{22}$$

The decision is given by $\boldsymbol{x} = [x_i]$ such that $x_i = 1$ if $L(Q_i) < 0$; otherwise, $x_i = 0$. If $\boldsymbol{x}$ is a valid codeword satisfying $\boldsymbol{H} \cdot \boldsymbol{x}^T = 0$, the algorithm halts; otherwise, the routines from step 2 to step 4 are repeated until some maximal number of iterations is reached without a valid decoding.

## 2.2 ARQ Schemes for Link-Level Adaptation Technique

### 2.2.1 Data Link Layer

The data link layer is layer two of the seven-layer open systems interconnection (OSI). The task of the data link layer is to interpret the bit stream of physical layer as a sequence of data blocks and forward them to the network layer. This data link layer provides reliable data transfer across two physical links using higher layer protocols, which include flow control, error checking, acknowledgements, and retransmission. Higher layer protocols can use error detection or correction codes protect data from transmission errors. Also, this protocol utilizes a feedback channel to request message retransmission, which is called ARQ retransmission. The ARQ schemes can be classified into two categories based on their complexities: simple ARQ schemes and hybrid ARQ schemes. The following sections describe the operation of two ARQ schemes.

### 2.2.2 Simple ARQ Schemes

ARQ schemes are usually divided into three types: send-and-wait ARQ, go-back-*N* ARQ, and selective-repeat ARQ. The send-and-wait ARQ scheme is the simplest of these three schemes. The transmitter sends a codeword and then is required to wait for acknowledgement (ACK) that this codeword has been received before the next codeword can be sent. When the transmitter gets a negative acknowledgement (NAK), it will resend

the previous codeword to the receiver. A NAK means the receiver detects some errors in the previous codeword. An obvious problem with this scheme is that while the transmitter is waiting for acknowledgements, transmission time is wasted and throughput can be deteriorated. When round-trip delays are long, throughput suffers appreciably. This problem can be alleviated with the use of go-back-*N* ARQ scheme.

For go-back-*N* ARQ scheme shown in Figure 6(a), the transmitter does not wait for acknowledgements but rather continually sends successive codewords until a request for a retransmission is received. After a round-trip delay, the transmitter will receive an ACK or a NAK. If the NAK is received, the transmitter stops, backs up to the codeword that was not successfully decoded, and restarts the transmission with that codeword. In this scheme, the transmitter requires sufficient buffer to store all the unacknowledged codewords. This ARQ scheme is called continuous ARQ scheme, which is more effective than the send-and-wait ARQ scheme. However, this ARQ scheme can be inefficient for a large round-trip delay and high data transmission rates because many of the codewords that are retransmitted may have already been successfully received as error-free codewords. Thus, if only those codewords that contain detected errors are selectively retransmitted, the throughput of this scheme can be enhanced. This enhanced scheme is called the selective-repeat ARQ scheme, as shown in Figure 6(b).

In this scheme, when the receipt of a defective codeword is detected, only the codeword that is defective is selectively requested. The codewords that arrive in the meantime are not rejected but are filed in a storage buffer at the receiver side. For this operation, the transmitter must keep the transmitted codewords in a storage buffer until an ACK has received for them. If the buffer size is not sufficiently large at transmitter

and receiver side, the buffer will be overflowed. If ARQ scheme has enough storage to buffer NAK transmissions, this selective-repeat ARQ can be the most efficient ARQ scheme among the three basic ARQ schemes in terms of throughput efficiency.

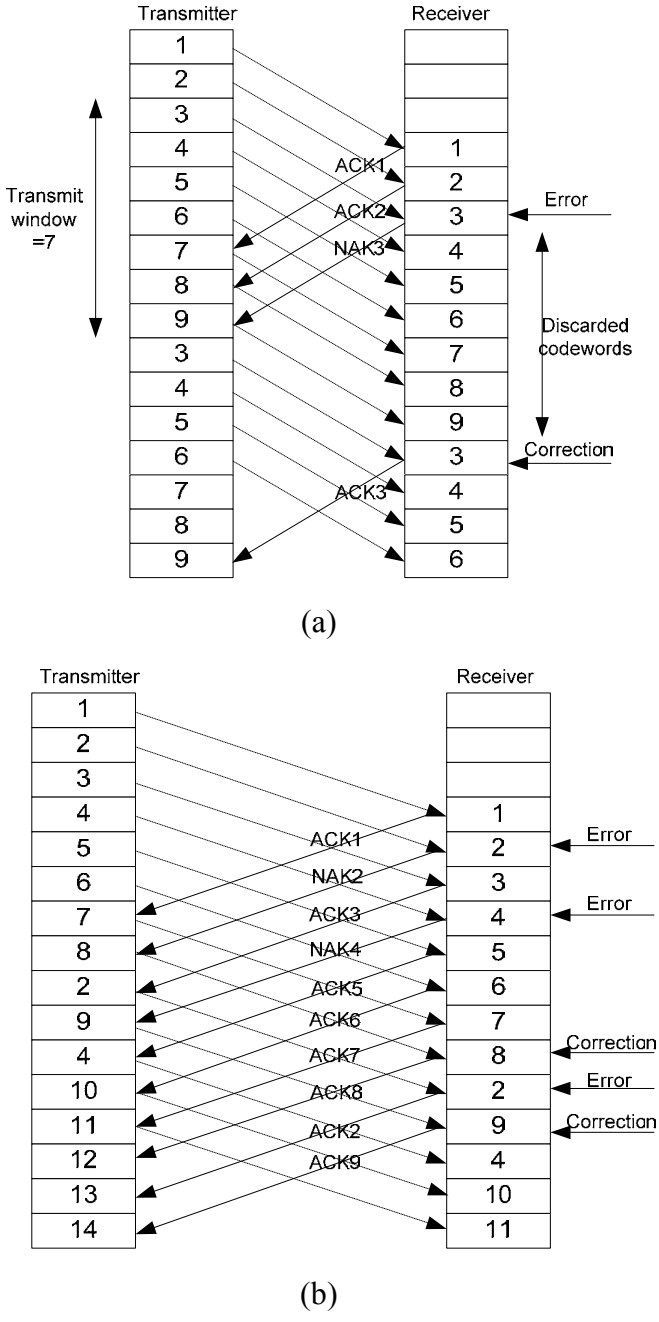


**Figure 6. ARQ schemes: (a) go-back-*N* ARQ scheme and (b) selective-repeat ARQ scheme.**

### 2.2.3 Hybrid ARQ Schemes

Simple ARQ schemes provide a high level of transmission reliability, which can be maintained when channels are severely disrupted. However, their throughput efficiency falls rapidly when channel error rate increases. FEC systems provide constant channel throughput regardless of the channel error rate, but the level of transmission reliability decreases when the channel becomes more error-prone. To obtain high system reliability in FEC systems, powerful long codes must be used, which make decoding hard to implement and expensive. To establish a reliable communication link and to overcome the drawbacks in both ARQ and FEC schemes, two error control schemes are properly combined. This kind of combination is referred to as a hybrid ARQ scheme. This hybrid scheme consists of an FEC subsystem contained in an ARQ strategy. In this section, two types of hybrid ARQ schemes are presented: type I hybrid ARQ scheme and type II hybrid ARQ scheme.

The type I hybrid ARQ scheme is the simplest of the hybrid protocols using a linear code for both error detection and error correction. This scheme can be implemented using either one-code or two-code systems. When a received codeword is detected in error, the receiver first attempts to find and correct the errors. If the linear code can correct the number of errors within its error-correcting capability, the errors are corrected and the decoded message is passed to the data sink. If the receiver detects an uncorrectable error pattern, it rejects the received codeword and requests a retransmission to the transmitter. If the retransmitted codeword is received after a round-trip delay, the receiver again finds and corrects the errors in that codeword. These steps above will be repeated until the receiver decodes the codeword successfully. This type I hybrid ARQ

scheme provides higher throughput than the corresponding ARQ scheme when channel error rate is high because the error correcting capability of the combined linear code reduces the frequency of retransmission.

The disadvantage of the type I hybrid ARQ scheme is that when channel error rate is low, it has lower throughput than its corresponding ARQ scheme. The extra parity-check bits for error correction must be sent in each transmission regardless of the channel error rate. It makes lower throughput.

The second type of hybrid ARQ scheme, type II hybrid ARQ scheme is devised to avoid this situation. In this scheme, the amount of redundant parity-check bits for error correction is varied according to the channel error rate during transmission and retransmission and a received codeword is combined with the previously received codeword. This scheme exploits the channel capacity more efficiently and is suitable for applications in time-varying channels where different levels of error protection are required. The type II hybrid ARQ scheme uses of a set of FEC codes from high rates to low rates. The lower rate codes are derived from higher rate codes in a rate-compatible fashion. When a transmission is initiated in this scheme, the transmitter sends information message encoded by an error detection code. If the receiver finds errors after error detection, it saves the erroneous message in a buffer and requests retransmission to the transmitter. The transmitter then sends a block of parity-check bits formed based on the original message. The receiver attempts again to detect and correct errors of the erroneous message stored in the buffer with the aid of addition parity-check information. If the error correction is unsuccessful, the receiver requests more parity-check bits to the transmitter until the original codeword is recovered. If the code used for error correction

and the retransmission strategy of ARQ scheme is properly chosen in this hybrid ARQ scheme, this type II hybrid ARQ scheme provides better throughput efficiency than the type I hybrid ARQ scheme. In addition, this scheme is more attractive for high-speed data communication systems where error rate is non-stationary in time-varying channels than the type I hybrid ARQ scheme.

## 2.3 Multiple Antenna Systems for High-Data-Rate Wireless Communications

In wireless communications, the fading effect of communication systems is important. Unlike SISO, MIMO requires the multipath fading environment. MIMO system deems the multipath channel not as impairment but as resource which enhances the transmission performance by applying multi antennas [43] for a transmission. If multiple transmitters broadcast different information to a multipath channel [44] and multiple receivers can obtain different information from the multipath channel, multipath channel will become resource for the enhancement of the transmission performance as well as the multipath fading environment itself will be solved. This multiplexing is called space division multiplexing. MIMO system consists of multiple antennas for a single user, and is a concurrent transmission process in space by using multipath channels. This MIMO system mainly uses for high-data-rate data transmission in wireless communication.

### 2.3.1 Multiple-Input Multiple-Output Channel

In a typical multipath propagation environment in wireless communications, the received signal envelope is normally Rayleigh distributed, which results in the Rayleigh fading channel. The probability distribution function of the received signal to noise ratio is exponentially distributed in equation (23).

$$\Pr(\gamma) = \frac{1}{\gamma_0} e^{(-\frac{\gamma}{\gamma_0})}, \quad \gamma > 0, \tag{23}$$

where $\gamma_0$ is the average signal to noise ratio.

Wireless fading channels [45] are also characterized by the time variation of the received signal, which is caused by the motion of the mobile unit. It can be expressed by the Doppler frequency effect. The maximum Doppler frequency, $f_m$, is defined by

$$f_m = \frac{v}{\lambda}, \tag{24}$$

where $\lambda$ is the wavelength, and $v$ is the speed of the mobile unit.

In MIMO system as shown in Figure 7, multipath channels are represented by $M \times N$ antennas. $M$ is the number of transmit antennas and $N$ is that of receive antennas. Multipath channels can be expressed as $M \times N$ channel gain matrix $\boldsymbol{H}$, which characterize the impulse response of every channel within multipaths. This complex matrix is given by

$$\boldsymbol{H} = [h_{ij}] = \begin{pmatrix} h_{11} & \cdots & h_{1N} \\ \vdots & \ddots & \vdots \\ h_{M1} & \cdots & h_{MN} \end{pmatrix}, \tag{25}$$

where $h_{i,j}$ is the channel gain matrix from transmit antenna $j$ to receive antenna $i$. The elements of $\boldsymbol{H}$ are zero-mean complex Gaussian random variables with unit variance. The received signal $y_i$ at the $i_{th}$ receive antenna is

$$y_i = \sqrt{\frac{\rho}{N}} \sum_{j=1}^{n} h_{i,j} x_j + w_i, \tag{26}$$

where $\rho$ ($E_s/N_o$) is the total transmit power per symbol versus total spectral density of the noise. The subscript for time-domain is omitted for simplifying equations.

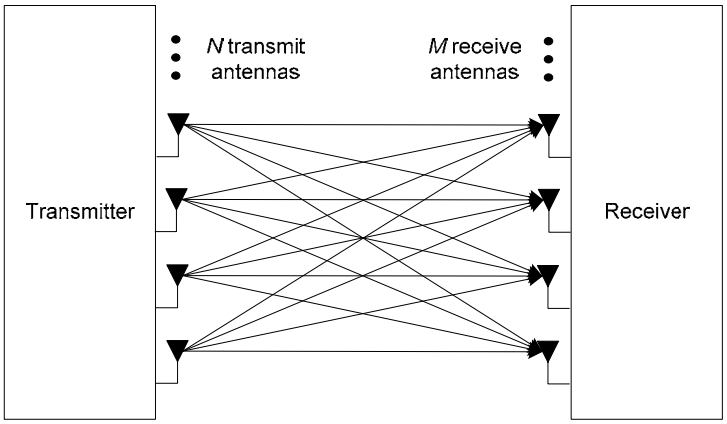


**Figure 7. MIMO channel representation with *M* receive antennas and *N* transmit antennas.**

### 2.3.2 Layered Space-Time Architecture

MIMO system uses multiple transmit and receive antennas to implement concurrent transmission [46]. This transmission can be performed with diversity in space and time domain. Foschini and Gans [10] showed that a high bandwidth efficient communication can be achieved with multiple-element antennas over the rich-scattering wireless channel. This technology is called Layered Space-Time (LST) architecture. In [9], the spread data substream from LST architecture [47] can exist without conflicting each other in multiple transmit and receive antenna environments, and this substream can be exploited to increase the capacity. To achieve this capacity, there are three types of proposed LST architectures, horizontal LST (H-LST), diagonal LST (D-LST) and vertical LST (V-BLAST). In H-LST, the data stream is transmitted in horizontal. Each data stream is always transmitted at the same antenna. D-LST scheme [48], which is considered the applied architecture of H-LST, rotates the encoded data symbols and transmit them from the different antenna at the different timing. This architecture is proposed by Foschini [9], which can reach capacities near the Shannon limit. However,

the complexities of D-LST implementation led to V-BLAST scheme, which is a simplified version of D-LST. In the next chapters, this V-BLAST architecture and detection algorithm are described and used.

# CHAPTER 3

# THROUGHPUT IMPROVEMENTS OF ADAPTIVE LDPC CODED SYSTEMS

## 3.1 Introduction

Time-varying channels in wireless MIMO communications come from much fundamental impairment such as multipath fading, scattering, shadowing, and Doppler spread of mobile speed. To confront the nature of time-varying channels and enhance spectral efficiency over wireless MIMO fading channels, many researchers have been focusing on adaptive transmission techniques [49] such as adaptive coding [50], adaptive modulation [51], adaptive power control, and adaptive transmit antenna diversity [1].

The demand for adaptive coding originates from the fact that some standards request the wireless transceiver to confront fast channel variations by changing the code rate. However an adaptive coding system requires multiple codes for each supporting data rate, which can make system more complex than is necessary. To solve this problem, we need powerful and reconfigurable forward error correction codes with low complexity. Irregular LDPC codes [34] are attractive forward error correction codes [52][53] in the sense that these codes can perform extremely close to the Shannon capacity for long block-lengths. Ha *et al.* introduced good rate-compatible irregular LDPC codes that are well designed at short block lengths with a finite-length puncturing algorithm [54].

One of the most important MIMO systems is the V-BLAST architecture [9] that is proposed for high-data rate systems without transmit diversity [55]. The conventional layered V-BLAST system architecture uses a single code at each layer as a component

code. We will modify this system to use a fraction of this single code in all of the vertical antennas. In this chapter, the combination [56] of rate-compatible LDPC coded adaptive coding system and modified V-BLAST systems is examined as a good candidate for low-complexity, high-capacity approaching schemes over time-varying MIMO channels.

This chapter is organized as follows. In Section 3.2 and 3.3, we discuss our adaptive LDPC coded V-BLAST system models using a single LDPC code in a rate-compatible fashion. Also, we describe the procedure of threshold determination for adaptive transmission and explain the operation of our adaptive LDPC coded V-BLAST systems for supporting variable data rate. In Section 3.4, we show simulation parameter and results. In final section 3.5, we conclude with a brief summary about how our proposed adaptive coded system is well designed with low-complexity and moderate performance loss over time-varying MIMO channels.

## 3.2 Adaptive LDPC Coded Systems

In this section, we design IR-LDPC codes in a rate-compatible fashion to support the incremental redundancy transmission of IR-HybridARQ schemes in next chapter. For a system model, we construct an adaptive coded system using IR-LDPC codes prepared by intentional puncturing and random punctured methods at short block lengths. To change code rates adaptively over time-varying channels for good throughput performance, we also propose an adaptive code selection algorithm. These works improve the throughput performance of our adaptive LDPC coded system.

To evaluate throughput performance of IR-LDPC codes over time-varying channels, we construct adaptive LDPC coded systems, which change the code rate adaptively according to the channel state information. It guarantees throughput

improvement if each subset code of IR-LDPC codes and an adaptive operation method are properly chosen. To compare the performance of IR-LDPC codes to the capacity bound of each rate, we also construct a dedicated coded system, which requires several encoder/decoder pairs for supporting every rate. This system shows near-capacity performance, but its complexity is increased by the number of encoder/decoder pairs. In this section, we consider preparing only one encoder/decoder pair using a family of IR-LDPC codes, which have low-complexity and support all of the required variable code rates. All of the subset codes of IR-LDPC are punctured from a well-designed mother code by an intentional puncturing [30] and random puncturing method [26], which are presented in the next section.

### 3.2.1 Construction of Low-Density Parity-Check Codes

For our adaptive coded system, we prepare rate-compatible IR-LDPC codes by puncturing the mother code that is optimized [57] with a specific puncturing algorithm at short block lengths [58]. These IR-LDPC codes are designed in a rate-compatible fashion, which perform well at all given code rates. The essential work for IR-LDPC codes is to design a mother code carefully because all of the subset codes of IR-LDPC codes are embedded in the lower rate mother code and can be decoded on the same Tanner graph. In wireless environments, the transmitted symbols can be lost in a deep fading channel. The receiver will have practically no information about these symbols, which look likely to be erased in the channel. In addition, the punctured bits can be considered as erasures that occur on determined locations while the channel erasures occur in the random locations in actual case. Considering all of these situations, the design of IR-LDPC codes is considered over the binary erasure channel.

Our main rule of designing IR-LDPC codes is to find the LDPC codes, which can overcome the higher erasure probability at the given binary erasure channel with certain erasure probabilities. Well-designed LDPC codes over the erasure channel can recover all of erasures through few iterative decoding steps in the given channel.

Let us define the probability $e^{(k)}$, which an LLR message of a variable node at the $k_{th}$ iteration during message-passing decoding is equal to zero. This probability [60] can be computed in the Tanner graph as

$$P(v^{(k)} = 0) = e^{(0)}(\varepsilon^{(k-1)})^{d_v - 1}, \tag{27}$$

where $v^{(k)}$ is the message of neighbors of a variable node and $d_v$ is the number of neighbors of a variable node. This probability must be zero when the iteration of decoding approaches infinity. To design good LDPC codes which have the resilience against erasure and puncturing, this channel erasure probability above needs to be maximized. Thus, the following function $f(e)$ [60] of given LDPC codes is maximized.

$$f(e_m) = R_m \,/\, (1 - e_m), \tag{28}$$

where $R_m$ is the mother code rate and $e_m$ is the maximum amount of erasures . In this equation, the largest value of $f(e_m)$ means the highest achievable code rate when we puncture the mother code of which code rate is $R_m$.

The probability density of a variable node message can be calculated with the following recursive formula.

$$\begin{aligned} e^{(k)} &= P(v^{(k)} = 0) \\ &= e^{(0)}\lambda(\varepsilon^{(k-1)}) \\ &= e^{(0)}\lambda(1 - \rho(1 - e^{(k-1)})) \end{aligned}, \tag{29}$$

where $\lambda(x)$ and $\rho(x)$ are degree distribution of LDPC codes defined by equations (1) and (2) and $\varepsilon^{(k)}$ is the probability that a check node messages is equal to zero.

To solve the recursive equation (29), let us define [59]

$$\beta(x) = e^{(0)}(1-\rho(1-x)) . \tag{30}$$

Thus, the following relationship can be derived

$$\begin{array}{lll} \sum_{i=2}^{d_v} \beta^{(i-1)}(e^{(0)})\lambda_i & < & e^{(0)} \\ \sum_{i=2}^{d_v} \beta^{(i-1)}(e^{(1)})\lambda_i & < & e^{(1)} \\ \vdots \qquad\qquad \vdots & & \vdots \qquad , \\ \sum_{i=2}^{d_v} \beta^{(i-1)}(e^{(\Omega-1)})\lambda_i & < & e^{(\Omega-1)} \end{array} \tag{31}$$

where $\Omega$ is the number of inequalities in equation (31), $\rho(x)$ is chosen to be $0.4x^5 + 0.6x^6$. It is known [37] that good LDPC codes have the degree distribution of check nodes with the form $\rho(x) = \rho_d x^{(d-1)} + (1-\rho_d)x^{d-2}$.

In this linear equation routine, we will find a degree distribution of variable nodes that satisfies equation (31). If we find such a sequence, new recursive equations can be solved with larger value *e* until the maximum *e* is found. The degree distribution of variable nodes has following restrictions in this routine.

$$\sum_{j=2}^{d_v} \lambda_j = 1 \quad \text{and} \quad \int_0^1 \lambda(x)dx = \frac{1}{R_m}\int_0^1 \rho(x)dx . \tag{32}$$

In this method, we tried to find the optimal degree distribution by varying $\lambda_2$ from 0.30 to 0.50. Finally, we obtained the mother code with the following degree distribution pair with 45% erasure probability:

$$\lambda(x) = 0.283x + 0.399x^2 + 0.318x^7 , \tag{33}$$

$$\rho(x) = 0.6x^5 + 0.4x^6 . \tag{34}$$

The performance of this mother code is also improved using a progressive edge-growth (PEG) construction algorithm [61] to have good error rate performance at short block lengths.

To prepare the subset codes of IR-LDPC codes from this mother code, a finite-length puncturing method [54] is exploited for a systematic design of rate-compatible LDPC codes at short block lengths [62]. In Figure 8, a typical recovery tree for describing this algorithm is shown.

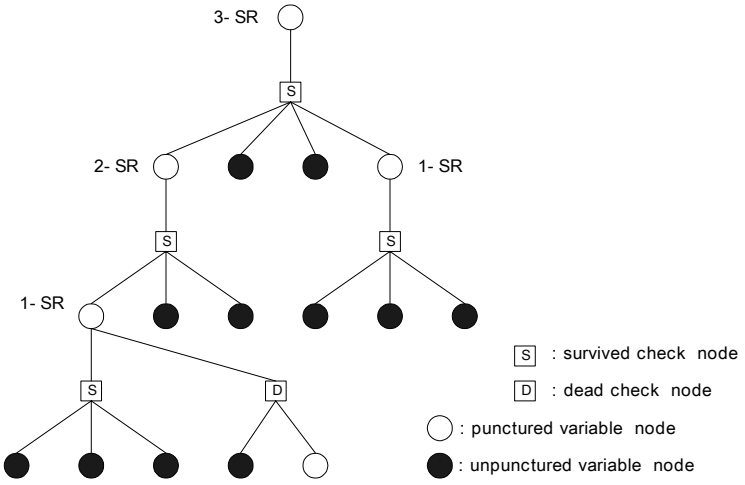


**Figure 8. Typical recovery tree with variable and check nodes.**

A *survived check node* is a check node connected with all unpunctured variable nodes, except one punctured variable node, a so-called *N*-step recovery (*N*-SR) node. A *dead check node* is a check node that has two more punctured variable nodes among all of the neighboring variable nodes. The *N*-SR node is a variable node that is recovered after exactly *N* iterations of a decoding algorithm with at least one neighboring survived check node. If the punctured *N*-SR node is recovered with a non-zero message from one of the neighboring survived check nodes, the node is considered to be recovered, even

though the node may have an incorrect value. All intentional punctured *N*-SR nodes have to be recovered with the message from the unpunctured nodes after a finite number of iterations. In this algorithm, the maximum achievable code rate $R_{\max}$ is defined as equation (35) in the typical recovery tree.

$$R_{\max} = \frac{R_0}{1 - \sum_{n=1}^{k} |G_n| / L}, \tag{35}$$

where $G_n$ is the group of the *N*-SR nodes, $R_0$ is the rate of a mother code, $k$ is the number of groups, and $L$ is the block length. The required number $P_{req}$ of punctured nodes for a designed rate $R_d$ is given by

$$P_{req} = \left\lfloor \frac{L(R_d - R_0)}{R_d} \right\rfloor. \tag{36}$$

To find puncturing locations in the recovery tree, a two-step search algorithm is used. The first step is a grouping algorithm that separates all variable nodes in the typical recovery tree into several groups that have different recovery-error probability [54]. The first group is defined as the set of variable nodes that can be recovered statistically earlier, which consists of *1*-SR variable nodes. After maximizing the number of variable nodes in the first group, the next groups are selected sequentially by the grouping algorithm. The variable nodes of the $N_{\text{th}}$ group include the puncturing locations of $(N\text{-}1)_{\text{th}}$ group in a rate-compatible fashion. If all of the groups are assigned exactly, the order of puncturing locations in the same variable node group is determined using a sorting algorithm, which is the second step of this approach. This step selects the variable nodes first with the smallest number of the dead check node and the largest number of the survived check node in the typical recovery tree.

Unlike the finite-length puncturing method, the random puncturing method selects the locations of punctured symbols arbitrarily. This results in performance loss at high puncturing rates where most of parity bits are punctured. This is referred to as the conventional puncturing method.

### 3.2.2 Operation of Adaptive LDPC Coded Systems

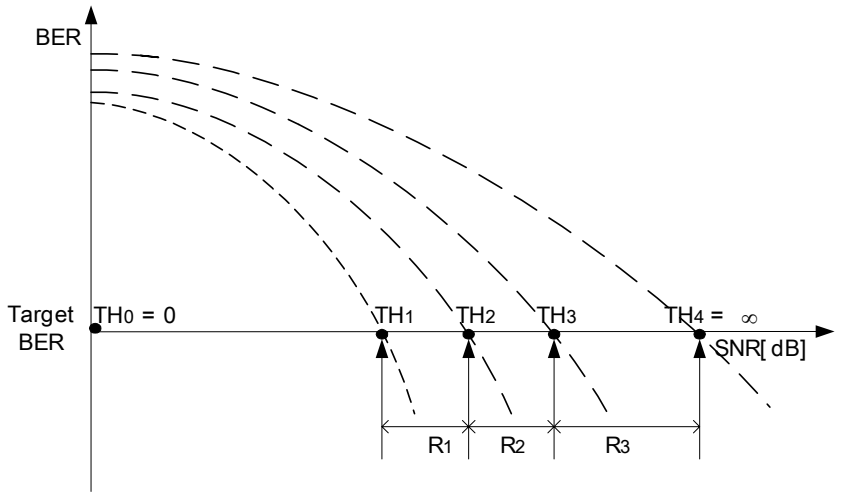


**Figure 9. Adaptation threshold parameters for adaptive coded transmission.**

To construct an adaptive LDPC coded system, the adaptation threshold parameters need to be determined, which the transmitter uses for the code rate selection in the next frame. It is assumed that the receiver knows the received signal-to-noise ratio (SNR) exactly and sends this information to the transmitter without delay. To calculate these threshold parameters, the predicted channel states are partitioned into five segments, shown in Figure 9. In each segment, the transmitter uses a specific code rate for satisfying a target bit error rate (BER). The example of threshold parameters is shown in tables in section 3.4, which are set experimentally by observing the error rate performance of each LDPC coded system in a normal fading condition. In this example,

the transmitter selects the code rate $R_1$ between $TH_1$ and $TH_2$, $R_2$ between $TH_2$ and $TH_3$, and $R_3$ above $TH_3$.

### 3.3 Simulation System Models

The original V-BLAST system uses different channel codes in different layers. It will be modified to use a fraction of the same channel code at each layer. The output of a single channel code is separated, as shown in Figure 10. This V-BLAST system is a simplified version of diagonal-BLAST [9] for reducing its computational complexity and does not have transmit diversity.

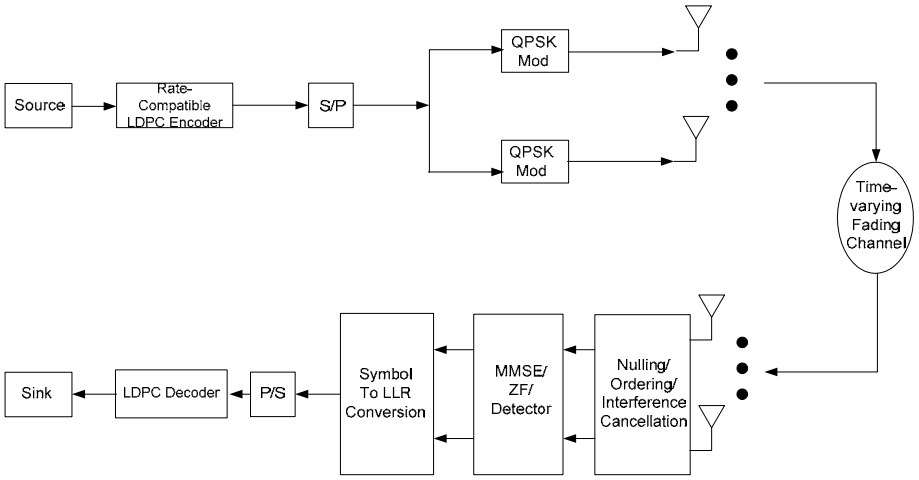


**Figure 10. Modified V-BLAST system.**

The system has $N$ transmit antennas and $M$ receive antennas, where $N \leq M$, in a frequency-flat Rayleigh fading channel. At the transmitter, source data bits are encoded with an LDPC encoder to generate encoded information data bits, which are separated into $N$ substreams and mapped onto quadrature phase shift keying (QPSK) constellation points. All symbols in a certain layer are transmitted into the same antenna over frequency-flat fading channels. Each layer of the V-BLAST system has its own

horizontal antenna. The total transmit power of all antennas is normalized to 1. At the receiver side, the transmission can be expressed mathematically as

$$\boldsymbol{Y} = \boldsymbol{H} \cdot \boldsymbol{X} + \boldsymbol{N} \,, \tag{37}$$

where $\boldsymbol{X}$ and $\boldsymbol{Y}$ are complex $N \times 1$ input and $1 \times M$ output vectors, respectively, and $\boldsymbol{N}$ is a complex Gaussian noise $1 \times M$ vector with variance $\sigma^2$. The average noise power is $N_0$ at each receive antenna. The complex $M \times N$ channel matrix is $\boldsymbol{H}$, which consists of channel coefficients of MIMO frequency-flat fading channels. At the receiver, received symbols are processed by nulling and ordering operation. Those received vectors $\boldsymbol{Y}$ are used as the inputs of successive interference cancellation [63]. After interference cancellation, these data are passed through the minimum mean square error (MMSE) or zero forcing (ZF) detector, which makes a soft decision on the channel inputs. Each received soft bit stream from the detector is multiplexed into one stream and converted into log-likelihood ratio values which a log-domain LDPC decoder uses for soft-decision. The details for MMSE and ZF detection are explained in next section.

### 3.3.1 Nulling and Interference Cancellation

In equations (25) and (37), the received symbols $y$ can be rewritten as

$$\begin{aligned}
&\mathrm{y}_1 = x_1\mathrm{h}_{11} + x_2\mathrm{h}_{12} + \cdots + x_k\mathrm{h}_{1k} + \cdots + x_m\mathrm{h}_{1m} + \mathrm{n}_1 \\
&\mathrm{y}_2 = x_1\mathrm{h}_{21} + x_2\mathrm{h}_{22} + \cdots + x_k\mathrm{h}_{2k} + \cdots + x_m\mathrm{h}_{2m} + \mathrm{n}_2 \\
&\vdots \qquad\qquad\qquad \vdots \qquad\qquad\qquad \vdots \\
&\mathrm{y}_n = x_1\mathrm{h}_{n1} + x_2\mathrm{h}_{n2} + \cdots + x_k\mathrm{h}_{nk} + \cdots + x_m\mathrm{h}_{nm} + \mathrm{n}_n \,, \\
&\qquad\qquad\qquad\qquad \Downarrow \\
&\mathbf{y} = x_1\mathbf{h}_1 + x_2\mathbf{h}_2 + \cdots + x_k\mathbf{h}_k + \cdots + x_m\mathbf{h}_m + \mathbf{n}
\end{aligned} \tag{38}$$

where the $h_{nk}$ is denoted as a $k_{\text{th}}$ column coefficient of $\boldsymbol{H}$ in $n_{th}$ transmit antenna and $x_k$ is the transmitted symbol from the $k_{th}$ transmit antenna. These equations can be also transformed into a simple vector equation, where $\boldsymbol{h}_{\text{k}}$ is the $k_{\text{th}}$ column of $\boldsymbol{H}$. To detect the

desired symbols in equations above, linear combinational nulling can be performed by choosing a weighting vector $\mathbf{w}_i$ to null out all the other symbols based on the ZF or MMSE criterion. When we detect the symbol in a specific layer, the other remaining symbols in the other layers can be considered as interferers. The ZF nulling vector is chosen such that

$$\mathbf{w}_k^T \mathbf{h}_j = \delta_{kj} = \begin{cases} 0 & for\ k \neq j \\ 1 & for\ k = j \end{cases}, \tag{39}$$

where $\mathbf{w}^{\mathrm{T}}$ indicates transpose of $\mathbf{w}$ and $\boldsymbol{h_j}$ is the $j_{\mathrm{th}}$ column of $\boldsymbol{H}$. $\delta$ is the Kronecker delta function. Thus, the decision statistics for the symbol in a $k_{\mathrm{th}}$ substream is given by

$$\begin{aligned} x_k^{\,d} &= \mathbf{w}_k^{\,T} \mathbf{y} \\ &= x_1 \mathbf{w}_k^T \mathbf{h}_1 + x_2 \mathbf{w}_k^T \mathbf{h}_2 + \cdots + x_k \mathbf{w}_k^T \mathbf{h}_k + \cdots + x_m \mathbf{w}_k^T \mathbf{h}_m + \mathbf{w}_k^T \mathbf{n} \\ &= 0 + 0 + \cdots + x_k + \cdots + 0 + \mathbf{w}_k^T \mathbf{n} \ . \end{aligned} \tag{40}$$

The slice operation is used to decode the transmitted symbol $\hat{x}_k$.

$$\hat{x}_k = Q(x_k^d), \tag{41}$$

where Q(.) denotes quantization operation relating to the constellation in use.

On the other hand, this linear nulling operation can have a superior performance if nonlinear techniques such as interference cancellation are combined. In this symbol cancellation operation, the first row of symbols is detected, and interference from already-detected symbols can be subtracted from the remaining received symbols, rather than detecting all of the symbols together. The received symbol vector after $k_{\mathrm{th}}$ layer interference cancellation is formulated by

$$\mathbf{y}_{k+1} = \mathbf{y}_k - \hat{x}_k \mathbf{h}_k, \tag{42}$$

where $\hat{x}_k$ is the decoded symbol in the $k_{\mathrm{th}}$ layer.

The performance of this successive interference cancellation depends on the

decision taken on each layer. However, in actual case, the signals with the weakest SNR will dominate the error performance of the system because such signals are sensitive to the inferences. To avoid this issue, the symbols containing strongest SNR need to be detected first. Next, we will show how to determine a specific ordering to improve the decoding performance of the system.

### 3.3.2 Optimal Detection Order

As mentioned earlier, the system performance depends on the order of detection. For the ordering scheme, we need to determine the signal with the biggest post-detection SNR. This algorithm is called ordered successive cancellation. Using the effective ordering, the ordered interference cancellation obviously reduces error rate performance.

The post-detection SNR [10] for the $k_{\text{th}}$ detected symbol of vector ***y*** is obtained by substituting (37) and (39) into (40), and taking expected values, i.e.

$$\rho_k = \frac{< |x_k|^2 >}{\sigma^2(\|w_k\|^2)}, \tag{43}$$

where $\sigma^2$ is the noise power and $< \cdot >$ denotes the expectation taken over the constellation set.

### 3.3.3 Detection Algorithm using the ZF and MMSE Nulling Vector

In a zero-forcing linear detector, the received signal vector ***y*** is multiplied by nulling matrix ***G*** with the form of Moore-Penrose pseudo-inverse of the channel matrix ***H***.

$$\mathbf{G}_{ZF} = \mathbf{H}^{+} = (\mathbf{H}^H\mathbf{H})^{-1}\mathbf{H}^H, \tag{44}$$

where $^{+}$ denotes the pseudo-inverse.

Then, the decision on the signal vector ***y*** is given by

$$\mathbf{x}_{ZF} = \mathbf{G}_{ZF}\mathbf{y} = \mathbf{H}^{+}\mathbf{y} = (\mathbf{H}^H\mathbf{H})^{-1}\mathbf{H}^H\mathbf{y} = \mathbf{x} + (\mathbf{H}^H\mathbf{H})^{-1}\mathbf{H}^H\mathbf{n}. \tag{45}$$

The MMSE detector minimizes the mean squared error between the transmitted signals and the output of the linear detector. The nulling matrix G is given by

$$\mathbf{G}_{MMSE} = (\mathbf{H}^H \mathbf{H} + \sigma_n^2 \mathbf{I})^{-1} \mathbf{H}^H , \tag{46}$$

where $\sigma_n^2$ is the noise power. Thus the decision on the received signal vector is given by

$$\mathbf{x}_{MMSE} = \mathbf{G}_{MMSE} \mathbf{y} = (\mathbf{H}^H \mathbf{H} + \sigma_n^2 \mathbf{I})^{-1} \mathbf{H}^H \mathbf{y} . \tag{47}$$

Compared to ZF criterion, this MMSE criterion has the advantage to cancel both the noise and interference signal while ZF criterion doesn't have the noise term in the nulling matrix. The full ZF V-BLAST detection algorithm [10] can be described recursively as follows.

- **Initialization**

  Step 1. $\mathbf{G}_1 = \mathbf{H}^+ \; at \; i = 1$

  Step 2. $k_1 = \arg\min_j \left\| \langle \mathbf{G}_1 \rangle_j \right\|^2$

- **Recursion**

  Step 3. $\mathbf{w}_{k_i} = \langle G_i \rangle_{k_i}$

  Step 4. $x_{k_i} = \mathbf{w}_{k_i}^T \mathbf{y}_i$ and $\hat{x}_{k_i} = Q(x_{k_i})$

  Step 5. $\mathbf{y}_{i+1} = \mathbf{y}_i - \hat{x}_{k_i} \mathbf{H}_{k_i}$

  Step 6. $\mathbf{G}_{i+1} = \mathbf{H}_{\bar{k}_i}^+$

  Step 7. $k_{i+1} = \arg\min_{j \notin \{k_1, k_2, \ldots, k_i\}} \left\| \langle \mathbf{G}_{i+1} \rangle_j \right\|^2$, $i = i+1$ , go to step 3.

**Figure 11. Detection algorithm.**

In this algorithm, $\mathbf{H}_{\bar{k}_{i-1}}$ is obtained from $\boldsymbol{H}$ by zeroing the columns $k_1, k_2, \ldots, k_{i-1}$ of $\boldsymbol{H}$. All of steps are iterated as a recursive procedure including determination of the optimal ordering.

## 3.4 Performance Results

Adaptive LDPC coded V-BLAST systems are considered as a system model that employs multiple transmit and receive antennas. A mother code is prepared as a half-rate irregular LDPC code with a block length of 4096. Its degree distribution pairs are given in equations (33) and (34) in previous section. The other code rates are punctured by a finite-length puncturing method and a conventional random puncturing method. For the dedicated LDPC coded system, non-punctured LDPC codes are prepared for every rate. The LDPC coded V-BLAST systems are simulated by Monte Carlo methods over frequency-flat fading channels generated by a modified Jake's fading model. A normalized Doppler spread is $f_D T_S = 0.01$ in a normal fading condition. A fast fading condition is set at $f_D T_S = 0.02$, and a slow fading condition is set at $f_D T_S = 0.001$.

### 3.4.1 Bit Error Rate Performance of LDPC Coded V-BLAST Systems

The adaptive LDPC coded system, which has punctured LDPC codes prepared by a finite-length puncturing method, is called a finite-length punctured adaptive coding (FPAC) system. In Figure 12 and Figure 13, the bit error rate performance of the FPAC system is compared at code rates 0.5, 0.625, and 0.75 in different fading conditions. It is assumed that the transmitter and the receiver know the channel state information perfectly. The normalized Doppler spread is changed from 0.02 to 0.001.

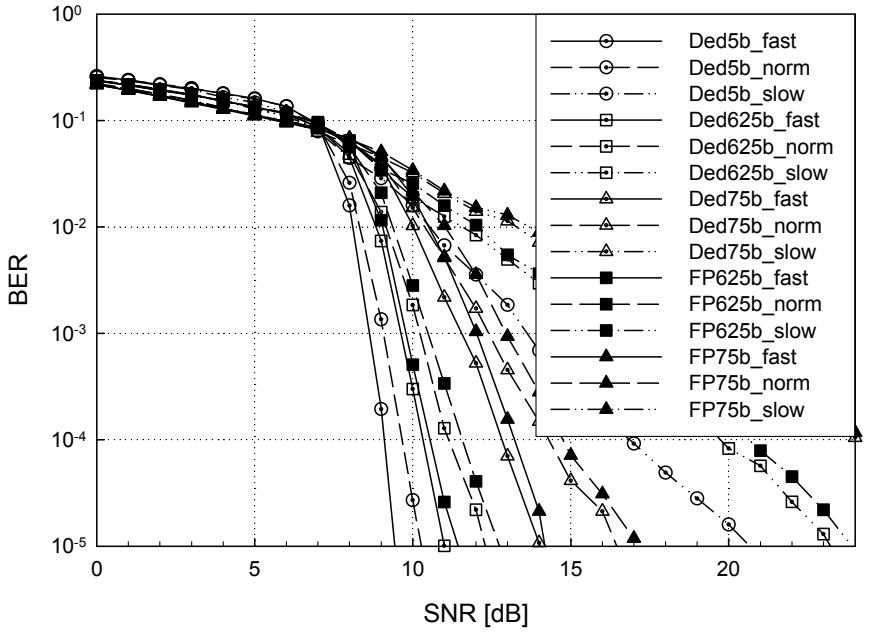


**Figure 12. Comparisons of bit error rate performance of adaptive LDPC coded 2x2 ZF V-BLAST systems in different fading channel conditions.**

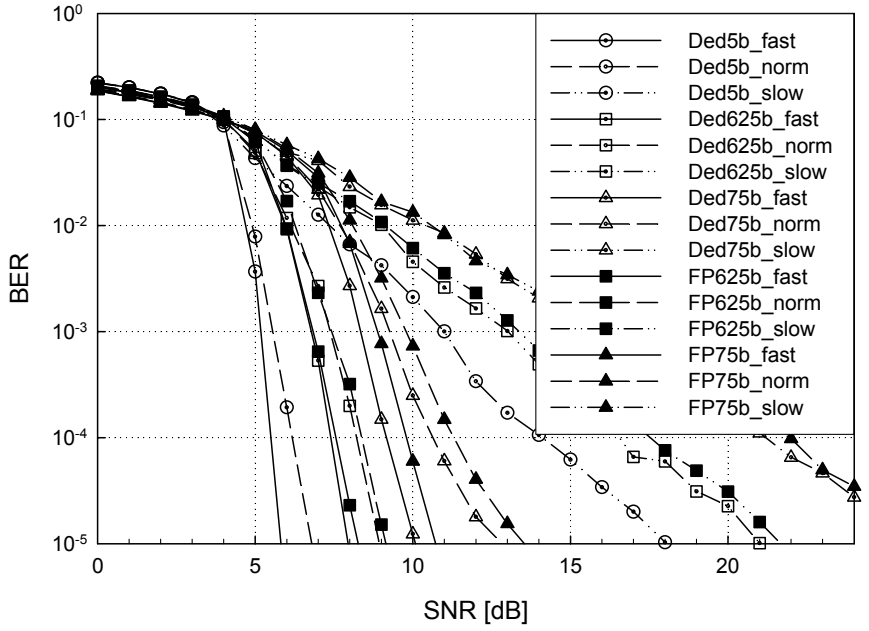


**Figure 13. Comparisons of bit error rate performance of adaptive LDPC coded 2x2 MMSE V-BLAST systems in different fading channel conditions.**

The FPAC system has better BER performance in a faster fading condition at every rate. The BER of the FPAC system at rate 0.5 is 0.9 dB better at target BER $10^{-5}$ in a fast fading condition than in a normal fading condition. In addition, the BER of the FPAC system at rate 0.5 is 10.2 dB in ZF VBLAST and 11.2 dB in MMSE VBLAST worse at target BER $10^{-5}$ in a slow fading condition than in a normal fading condition. It is shown that LDPC coded systems can exploit more the time-diversity characteristics of the channel in a faster fading condition than in a slower fading condition. All of the other punctured codes at rates 0.625 and 0.75 have the same error rate characteristics as the mother code at rate 0.5 in three different fading conditions.

The adaptive system, which uses the random punctured LDPC codes, is called a random punctured adaptive coding (RPAC) system. This conventional punctured system is compared to the FPAC system to verify the performance of punctured LDPC codes prepared by the finite-length puncturing method. In addition, the dedicated coded adaptive coding (DCAC) system, which consists of only dedicated LDPC codes at every rate, is compared to the FPAC system. The performance of the DCAC system is considered as an upper limit of the capacity-approaching schemes with high-complexity.

In Figure 14, Figure 15, Figure 16, and Figure 17, bit error rate performance of the three different LDPC coded systems is compared at code rates 0.5, 0.625, and 0.75. Each coded system is simulated in ZF and MMSE V-BLAST system. The code rates of 0.625 and 0.75 are prepared by puncturing the half-rate mother code with a finite-length puncturing method and a random puncturing method. The FPAC system shows better BER performance at higher code rates of 0.625 and 0.75 than the conventional RPAC system. It is shown that a large percentage of punctured bits in the RPAC system

deteriorate the performance of the iterative soft decision decoder. On the other hand, the FPAC system shows good performance at higher rates, of which performance is not degraded severely compared to the DCAC system. This is because the intentional punctured bits at higher rate LDPC codes are recovered fast, resulting in the fast convergence of the iterative decoder.

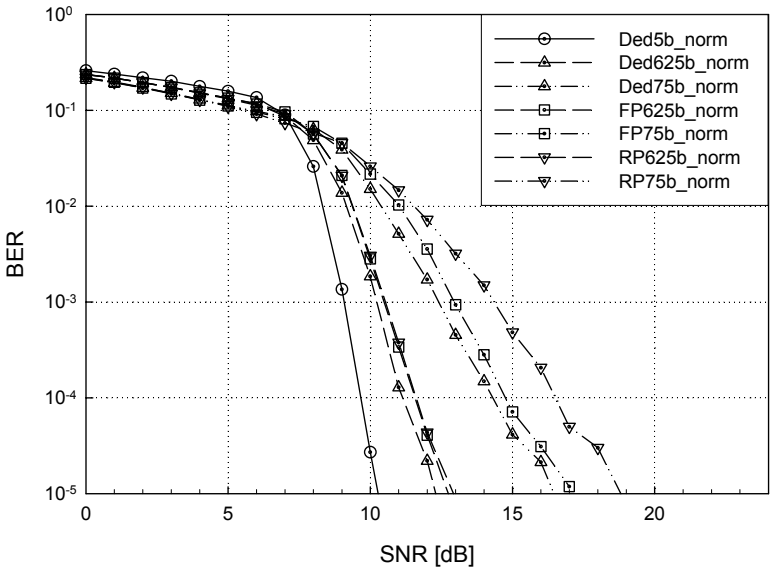


**Figure 14. Comparisons of bit error rate performance of adaptive LDPC coded 2x2 ZF V-BLAST systems in a normal fading condition.**

In ZF V-BLAST systems, the BER gain of the FPAC system over the RPAC system is 0.2 dB at rate 0.625 and 1.8 dB at rate 0.75 for a target BER of $10^{-5}$. The BER performance loss of the FPAC system over the DCAC system is 0.4 dB in 2x2 system and 0.2dB in 4x4 system at rate 0.625 and 0.4 dB in 2x2 system and 0.1dB in 4x4 system at rate 0.75 for a target BER of $10^{-5}$. In MMSE V-BLAST systems, the BER gain of the FPAC system over the RPAC system is 0.2 dB at rate 0.625 in 2x2 and 4x4 systems, and 1.7 dB in 2x2 system and 1.0dB in 4x4 system at rate 0.75 for a target BER of $10^{-5}$. The BER performance loss of the FPAC system over the DCAC system is 0.1 dB at rate 0.625

and 0.4 dB in 2x2 system and 0.4dB in 2x2 system and 0.1dB in 4x4 system at rate 0.75 for a target BER of $10^{-5}$.

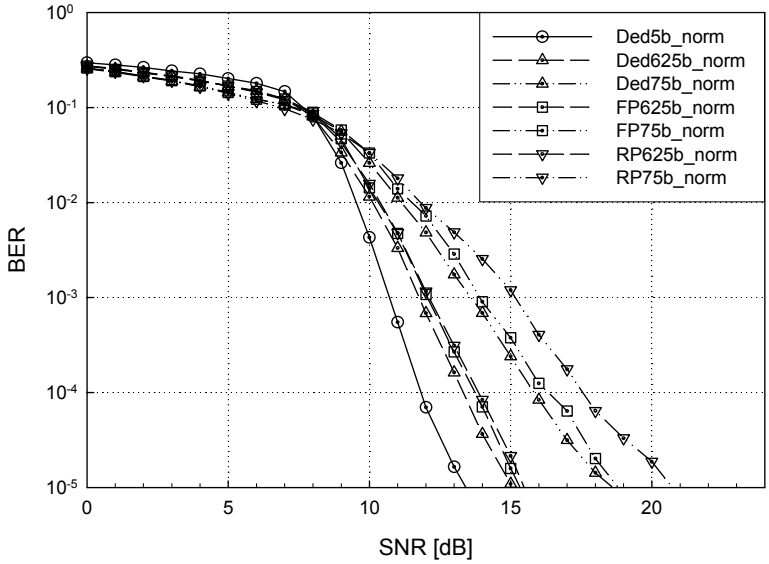


**Figure 15. Comparisons of bit error rate performance of adaptive LDPC coded 4x4 ZF V-BLAST systems in a normal fading condition.**

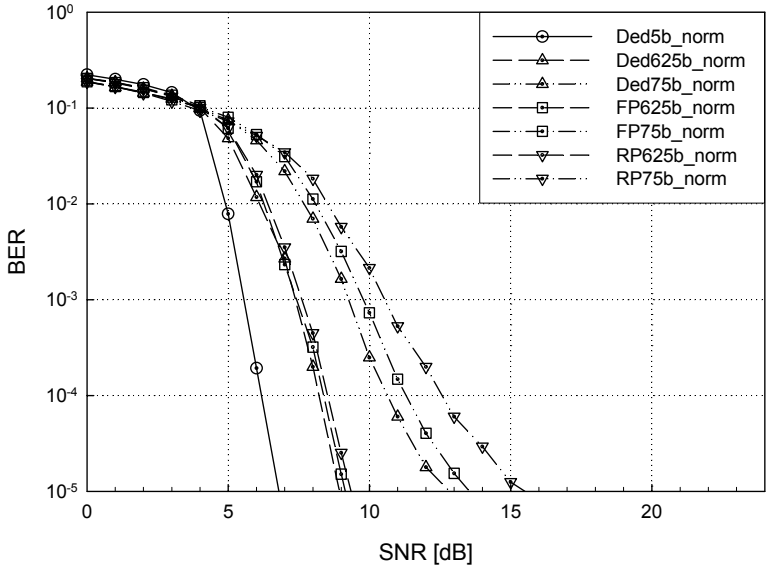


**Figure 16. Comparisons of bit error rate performance of adaptive LDPC coded 2x2 MMSE V-BLAST systems.**

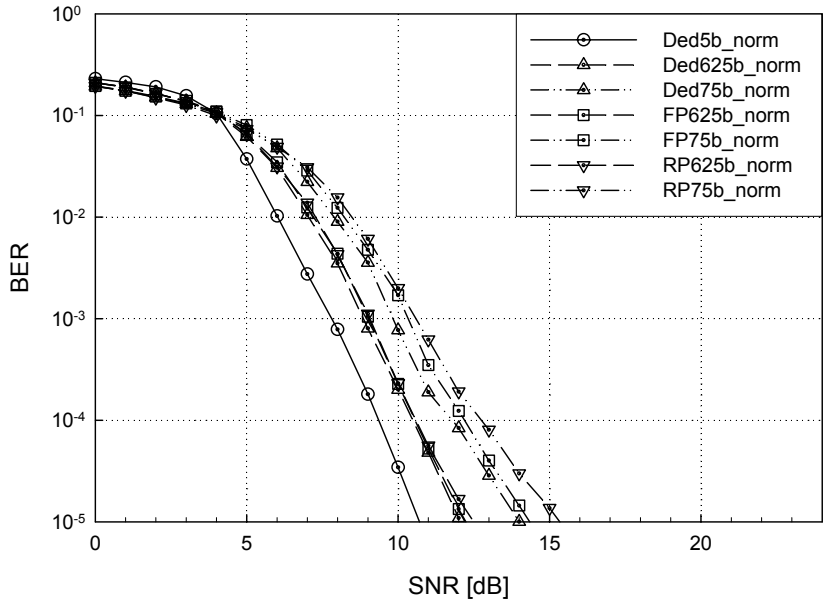


**Figure 17. Comparisons of bit error rate performance of adaptive LDPC coded 4x4 MMSE V-BLAST systems.**

In the previous result, we used optimal detection ordering at the receiver with perfectly known SNR information. In the following simulations, we compared the BER performance of the systems with optimal detection ordering and without optimal detection ordering. The BER performance of the three different LDPC coded systems with/without optimal detection ordering is shown in Figure 18, Figure 19, Figure 20, and Figure 21. The normalized Doppler spread is at $f_D T_S = 0.01$. Compared to the adaptive LDPC coded systems with optimal ordering detection shown in each simulation, the performance of the 2x2 ZF (MMSE) V-BLAST systems without optimal detection ordering shows about 1.0 (1.2) dB $E_b/N_o$ loss at code rate 0.625, and 1.4 (4.2) dB $E_b/N_o$ loss at code rate 0.75 for a BER of $10^{-5}$. In 4x4 ZF (MMSE) V-BLAST systems, the systems without optimal detection ordering have much more loss to the systems with optimal detection ordering because the inference from the multiple antennas is increased

according to the number of antennas. The performance loss of the systems without optimal ordering is about 3.8 (6.5) dB $E_b/N_o$ loss at code rate 0.625, and 4.2 (9.2) dB $E_b/N_o$ loss at code rate 0.75 for a BER of $10^{-5}$.

From these all of the results, the FPAC system outperforms the RPAC system at code rates 0.625 and 0.75 in ZF and MMSE V-BLAST system with multiple antennas, showing the comparable performance to the DCAC system. Also, the performance gap from the systems with and without optimal detection ordering is increased as the number of antenna is increased. Also, the MMSE V-BLAST system is much more sensitive to the interference from the multiple antennas.

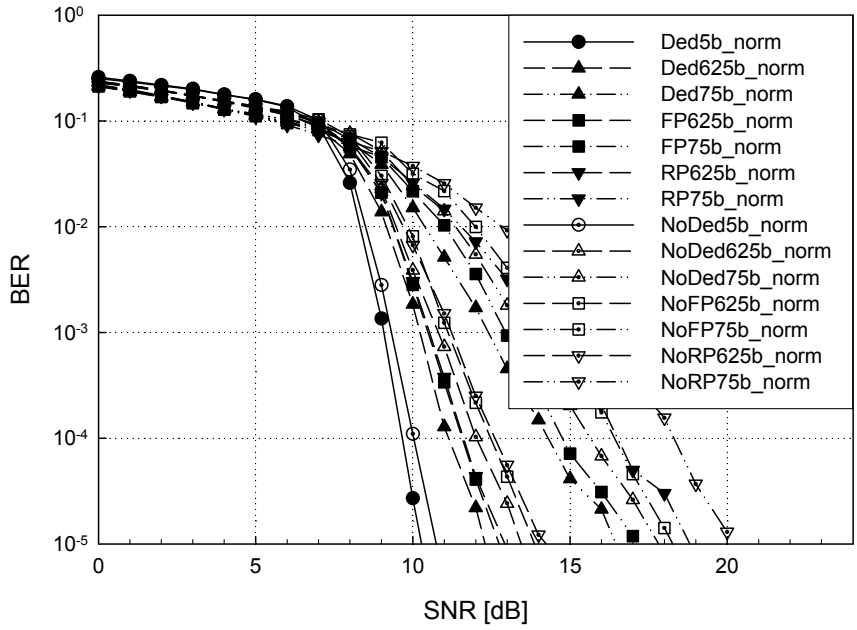


**Figure 18. Comparisons of bit error rate performance of adaptive LDPC coded 2x2 ZF V-BLAST systems with/without optimal ordering.**

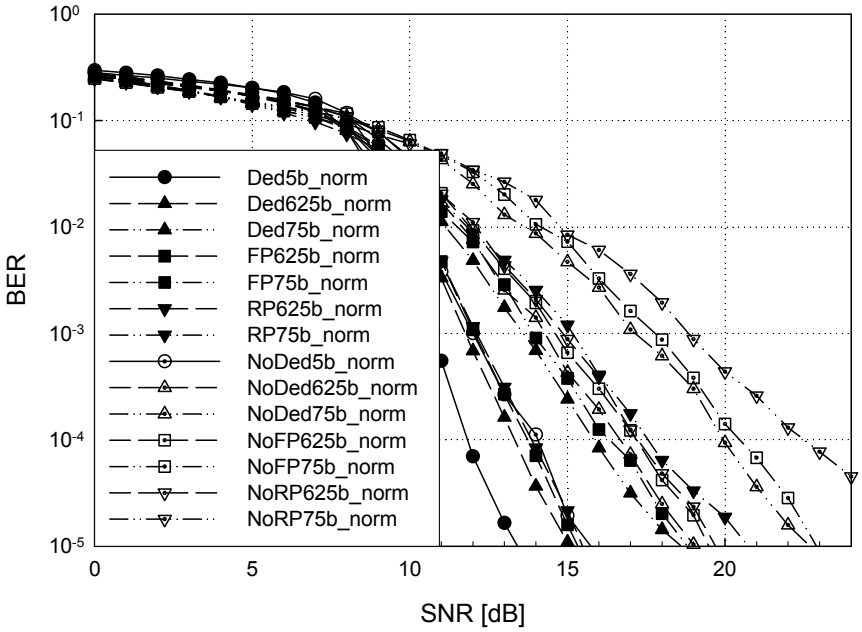


**Figure 19. Comparisons of bit error rate performance of adaptive LDPC coded 4x4 ZF V-BLAST systems with/without optimal ordering.**

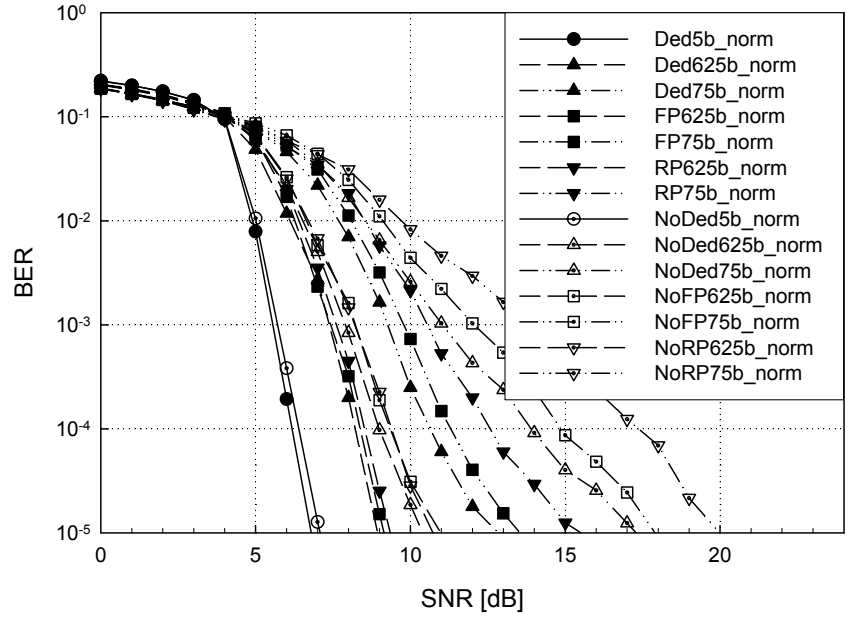


**Figure 20. Comparisons of bit error rate performance of adaptive LDPC coded 2x2 MMSE V-BLAST systems with/without optimal ordering.**

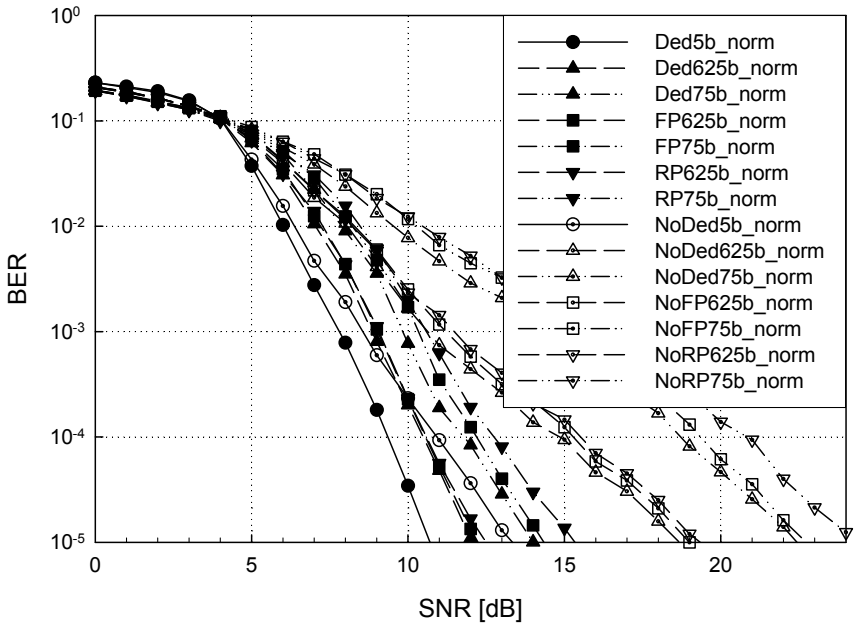


**Figure 21. Comparisons of bit error rate performance of adaptive LDPC coded 4x4 MMSE V-BLAST systems with/without optimal ordering.**

### 3.4.2 Throughput of Adaptive LDPC Coded V-BLAST Systems at Constant BER Operation

For a constant BER operation, the adaptation threshold parameters are set to the values in a specific SNR range between $TH_1$ and $TH_4$, as shown in Table 1, 2, 3, and 4. At high SNR, a higher throughput is preferred by choosing a higher code rate. On the other hand, at low SNR, throughput performance is given up to maintain the minimum error level by choosing a lower code rate. To qualify error rate performance less than the target BER $10^{-3}$, $10^{-4}$, and $10^{-5}$, the transmitter of adaptive LDPC coded systems uses the specific code rates when the estimated SNR at the receiver is above the specific threshold parameters in the tables. In Figure 22, Figure 23, Figure 24, and Figure 25, the throughput performance of the FPAC, the RPAC, and the DCAC systems is compared at

every target BER. This result shows the FPAC system has better throughput performance than the conventional RPAC system. At each target BER, the FPAC system outperforms the RPAC system by 2% more average transmission rate. Compared to the DCAC system, the FPAC system still has good throughput performance, which is within 1% of the performance of the DCAC system.

**Table 1. Adaptation threshold parameters of ZF V-BLAST systems with(without) optimal ordering in 2x2 antennas**

| | Target BER | $Th_0$ | $Th_1$ | $Th_2$ | $Th_3$ | $Th_4$ |
|---|---|---|---|---|---|---|
| [a]FPAC | $10^{-3}$ | 0 (0) | 9.0 (9.3) | 9.3 (11.1) | 11.0 (14.4) | ∞ |
| [b]RPAC | $10^{-3}$ | 0 (0) | 9.0 (9.3) | 9.3 (11.2) | 11.4 (15.9) | ∞ |
| [c]DCAC | $10^{-3}$ | 0 (0) | 9.0 (9.3) | 9.2 (10.8) | 10.4 (13.4) | ∞ |
| FPAC | $10^{-4}$ | 0 (0) | 9.7 (10.0) | 10.5 (12.5) | 12.9 (16.4) | ∞ |
| RPAC | $10^{-4}$ | 0 (0) | 9.7 (10.0) | 10.6 (12.7) | 14.4 (18.3) | ∞ |
| DCAC | $10^{-4}$ | 0 (0) | 9.7 (10.0) | 10.2 (12.0) | 12.4 (15.7) | ∞ |
| FPAC | $10^{-5}$ | 0 (0) | 10.3 (10.7) | 12.7 (13.8) | 17.0 (18.2) | ∞ |
| RPAC | $10^{-5}$ | 0 (0) | 10.3 (10.7) | 13.0 (14.1) | 18.8 (20.2) | ∞ |
| DCAC | $10^{-5}$ | 0 (0) | 10.3 (10.7) | 12.3 (13.4) | 16.4 (17.8) | ∞ |

[a]FPAC : finite-length punctured adaptive coding (FPAC) system

[b]RPAC : conventional random punctured adaptive coding (RPAC) system

[c]DCAC : dedicated coded adaptive coding (DCAC) system

**Table 2. Adaptation threshold parameters of ZF V-BLAST systems with(without) optimal ordering in 4x4 antennas**

| | Target BER | $Th_0$ | $Th_1$ | $Th_2$ | $Th_3$ | $Th_4$ |
|---|---|---|---|---|---|---|
| [a]FPAC | $10^{-3}$ | 0 (0) | 10.7 (12.0) | 12.0 (14.6) | 14.0 (17.8) | ∞ |
| [b]RPAC | $10^{-3}$ | 0 (0) | 10.7 (12.0) | 12.1 (14.8) | 15.2 (19.0) | ∞ |
| [c]DCAC | $10^{-3}$ | 0 (0) | 10.7 (12.0) | 11.8 (14.3) | 13.8 (17.0) | ∞ |
| FPAC | $10^{-4}$ | 0 (0) | 11.8 (14.1) | 13.7 (17.0) | 16.4 (20.3) | ∞ |
| RPAC | $10^{-4}$ | 0 (0) | 11.8 (14.1) | 13.9 (17.1) | 17.6 (22.6) | ∞ |
| DCAC | $10^{-4}$ | 0 (0) | 11.8 (14.1) | 13.3 (16.8) | 15.8 (19.9) | ∞ |
| FPAC | $10^{-5}$ | 0 (0) | 13.4 (15.7) | 15.3 (19.4) | 18.8 (22.8) | ∞ |
| RPAC | $10^{-5}$ | 0 (0) | 13.4 (15.7) | 15.5 (19.8) | 20.8 (27.8) | ∞ |
| DCAC | $10^{-5}$ | 0 (0) | 13.4 (15.7) | 15.0 (19.0) | 18.6 (22.6) | ∞ |

**Table 3. Adaptation threshold parameters of MMSE V-BLAST systems with(without) optimal ordering in 2x2 antennas**

| | Target BER | $Th_0$ | $Th_1$ | $Th_2$ | $Th_3$ | $Th_4$ |
|---|---|---|---|---|---|---|
| [a]FPAC | $10^{-3}$ | 0 (0) | 5.6 (5.7) | 7.5 (8.2) | 9.8 (12.0) | ∞ |
| [b]RPAC | $10^{-3}$ | 0 (0) | 5.6 (5.7) | 7.6 (8.2) | 10.6 (14.0) | ∞ |
| [c]DCAC | $10^{-3}$ | 0 (0) | 5.6 (5.7) | 7.4 (8.0) | 9.2 (11.0) | ∞ |
| FPAC | $10^{-4}$ | 0 (0) | 6.2 (6.4) | 8.4 (9.3) | 11.3 (14.8) | ∞ |
| RPAC | $10^{-4}$ | 0 (0) | 6.2 (6.4) | 8.6 (9.5) | 12.6 (17.4) | ∞ |
| DCAC | $10^{-4}$ | 0 (0) | 6.2 (6.4) | 8.2 (9.0) | 10.6 (14.0) | ∞ |
| FPAC | $10^{-5}$ | 0 (0) | 6.8 (7.1) | 9.1 (10.7) | 13.4 (17.8) | ∞ |
| RPAC | $10^{-5}$ | 0 (0) | 6.8 (7.1) | 9.4 (11.0) | 15.4 (20.0) | ∞ |
| DCAC | $10^{-5}$ | 0 (0) | 6.8 (7.1) | 9.0 (10.4) | 12.8 (17.3) | ∞ |

**Table 4. Adaptation threshold parameters of MMSE V-BLAST systems with(without) optimal ordering in 4x4 antennas**

| | Target BER | $Th_0$ | $Th_1$ | $Th_2$ | $Th_3$ | $Th_4$ |
|---|---|---|---|---|---|---|
| [a]FPAC | $10^{-3}$ | 0 (0) | 7.8 (8.5) | 9.0 (11.0) | 10.4 (15.2) | ∞ |
| [b]RPAC | $10^{-3}$ | 0 (0) | 7.8 (8.5) | 9.1 (11.2) | 10.6 (16.0) | ∞ |
| [c]DCAC | $10^{-3}$ | 0 (0) | 7.8 (8.5) | 8.9 (10.7) | 9.8 (14.5) | ∞ |
| FPAC | $10^{-4}$ | 0 (0) | 9.4 (11.0) | 10.6 (15.1) | 12.2 (19.3) | ∞ |
| RPAC | $10^{-4}$ | 0 (0) | 9.4 (11.0) | 10.6 (15.5) | 12.8 (21.0) | ∞ |
| DCAC | $10^{-4}$ | 0 (0) | 9.4 (11.0) | 10.5 (14.8) | 12.0 (18.8) | ∞ |
| FPAC | $10^{-5}$ | 0 (0) | 10.7 (13.3) | 12.2 (19.0) | 14.3 (22.6) | ∞ |
| RPAC | $10^{-5}$ | 0 (0) | 10.7 (13.3) | 12.5 (19.3) | 15.2 (24.7) | ∞ |
| DCAC | $10^{-5}$ | 0 (0) | 10.7 (13.3) | 12.0 (18.7) | 14.0 (22.4) | ∞ |

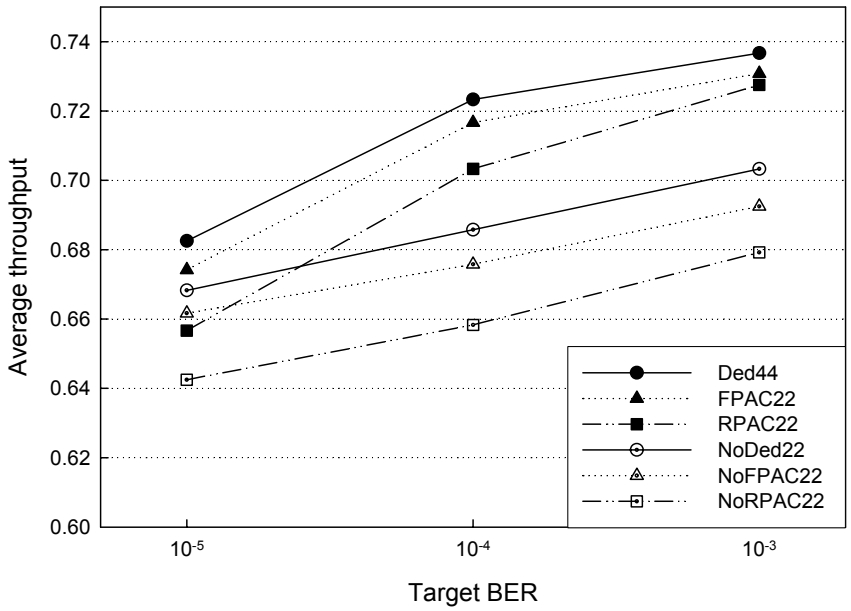


**Figure 22. Throughput performance of adaptive LDPC coded 2x2 ZF V-BLAST systems with(without) optimal ordering.**

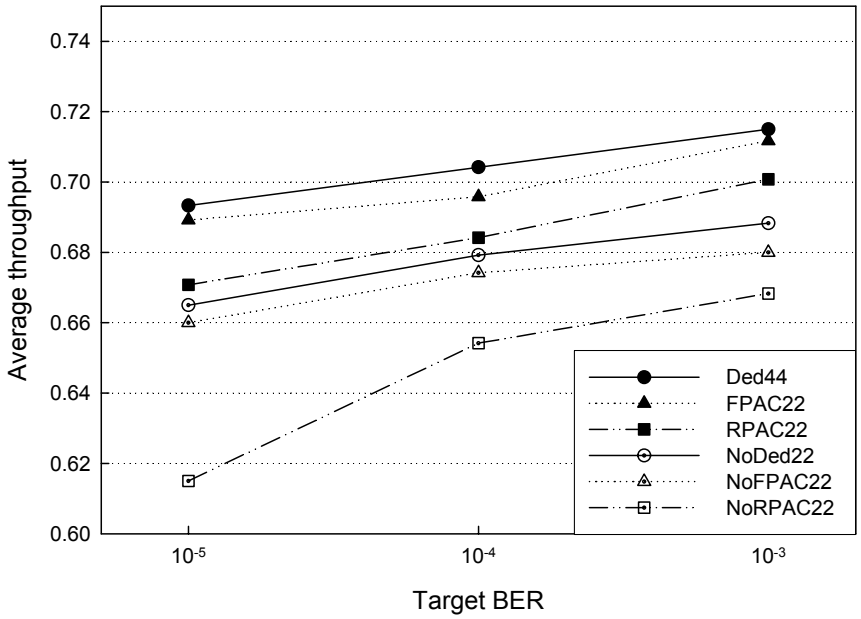


**Figure 23. Throughput performance of adaptive LDPC coded 4x4 ZF V-BLAST systems with(without) optimal ordering.**

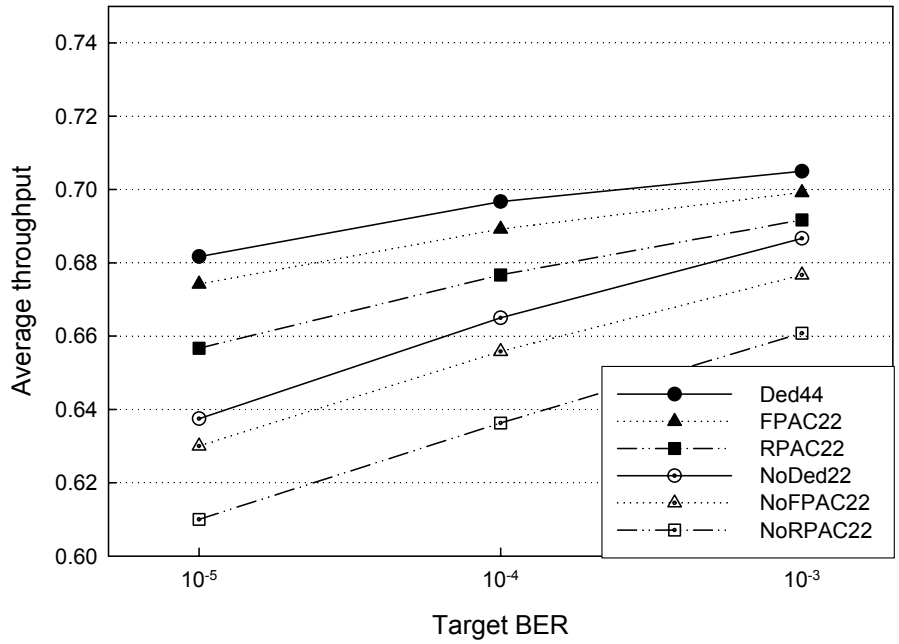


**Figure 24. Throughput performance of adaptive LDPC coded 2x2 MMSE V-BLAST systems with(without) optimal ordering.**

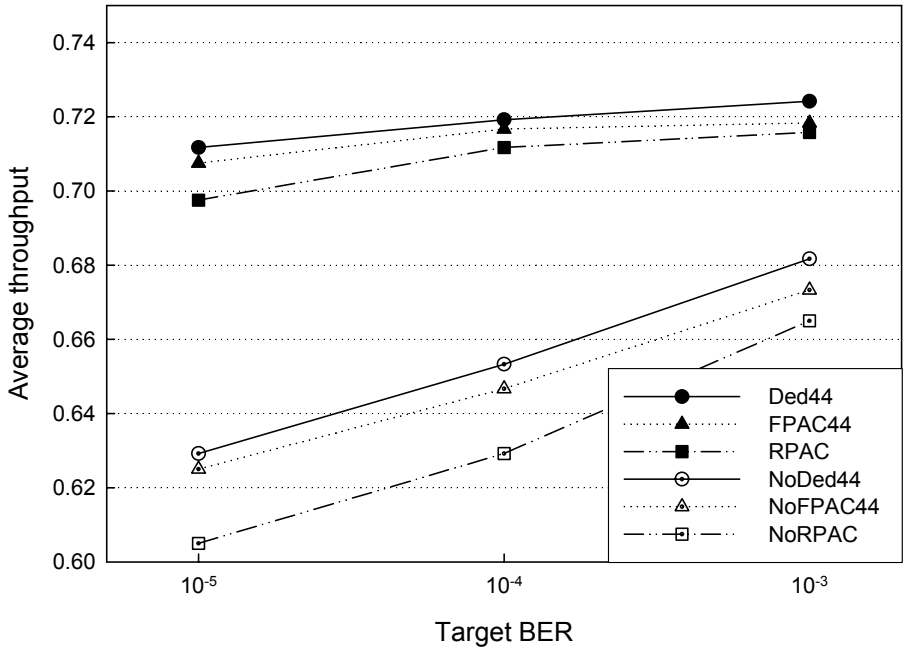


**Figure 25. Throughput performance of adaptive LDPC coded 2x2 MMSE V-BLAST systems with(without) optimal ordering.**

## 3.5 Conclusion

In this chapter, we present an adaptive LDPC coded V-BLAST system using finite-length punctured LDPC codes in a rate-compatible fashion, which we referred to as the FPAC V-BLAST system. The performance of our FPAC V-BLAST system is compared with the conventional RPAC system and the capacity-approaching DCAC system. From this simulation, our proposed FPAC V-BLAST system with low-complexity has comparable BER performance than the DCAC V-BLAST system with higher complexity that has near Shannon limit performance. Also, our FPAC system has better BER performance than the conventional RPAC system. From throughput simulations, we conclude that our FPAC V-BLAST system has similar performance like the capacity approaching DCAC V-BLAST system within 1% of the performance of average transmission rate. Also, our FPAC V-BLAST system improves average transmission rates of conventional RPAC system by 2% more at every target BER.

# CHAPTER 4

# INCREMENTAL REDUNDANCY LOW-DENSITY PARITY-CHECK CODES FOR HYBRID FEC/ARQ SCHEMES

## 4.1 Introduction

Wireless broadband communication for high data rate Internet services such as Wi-Max requires flexible and adaptive transmission techniques for confronting time-varying channels and enhancing spectral efficiency. For these systems, a careful design of the FEC codes can improve data throughput by incrementally transmitting a small fraction (so-called incremental redundancy) of the parity bits adaptively over time-varying channels [1].

Previous work in incremental redundancy hybrid ARQ systems [64] includes where the design of an ensemble [24][25] of FEC codes is considered. IR-HybridARQ systems require good frame error rate (FER) performance and should be adaptable to the time-varying nature of the channel. In this chapter we consider rate-compatible LDPC codes [65][66] for this purpose in V-BLAST architecture [9]. The conventional layered V-BLAST system uses a single code at each layer. We modify this system to use a fraction of this single code in all of the vertical antennas. For preparing an ensemble [67], we consider irregular LDPC codes together with an intentional puncturing algorithm [54], of which the maximum coding rate is increased here to support higher rates in IR-HybridARQ systems. We also exploit the IR-HybridARQ scheme [68] with an adaptive code selection algorithm to reduce the number of unnecessary traffic channels in IR-HybridARQ schemes at low operating SNR ranges. Note that excessive NACK signaling

traffics require the bigger queue size at transmitter and receiver end, and are the overhead of these systems.

This chapter is organized as follows. In section 4.2 and 4.3, we discuss design methods of the LDPC code ensembles for IR-HybridARQ schemes and explain the operation of IR-HybridARQ schemes over adaptive LDPC coded V-BLAST systems [69] model. In section 4.4, we present our V-BLAST MIMO system model, and provide simulation parameters and results. In section 4.5, we conclude with a brief summary about how our adaptive coded V-BLAST system is well behaved over time-varying MIMO channels.

## 4.2 Design of Incremental Redundancy LDPC Codes

The throughput performance of IR-HybridARQ schemes strongly depends on the design of the IR-LDPC codes, which is used as error correction codes. For this work, a careful design of the IR-LDPC codes is required for improving the throughput performance of IR-HybridARQ schemes. In this section, the way to extend the operating code range of IR-LDPC codes is presented for IR-HybridARQ schemes.

To design ensembles of IR-LDPC codes for IR-HybridARQ schemes, we consider a finite-length puncturing method that is suitable for punctured LDPC codes at short block lengths. However, previous attempts in this algorithm [54] have a maximum puncturing rate of about 0.8 for the mother code rate 0.5 because a parity-check matrix of LDPC codes has a finite number of $N$-step recoverable nodes in a given typical recovery tree. This algorithm in [54] is used and improved here to increase the maximum achievable coding rate for IR-HybridARQ schemes. The fundamental algorithm and basic terms used in this method are introduced in the previous section 3.2.

The proposed extended finite-length puncturing algorithm considers finding good puncturing locations in a given parity-check matrix with constraints on the group size, as shown in Figure 26.

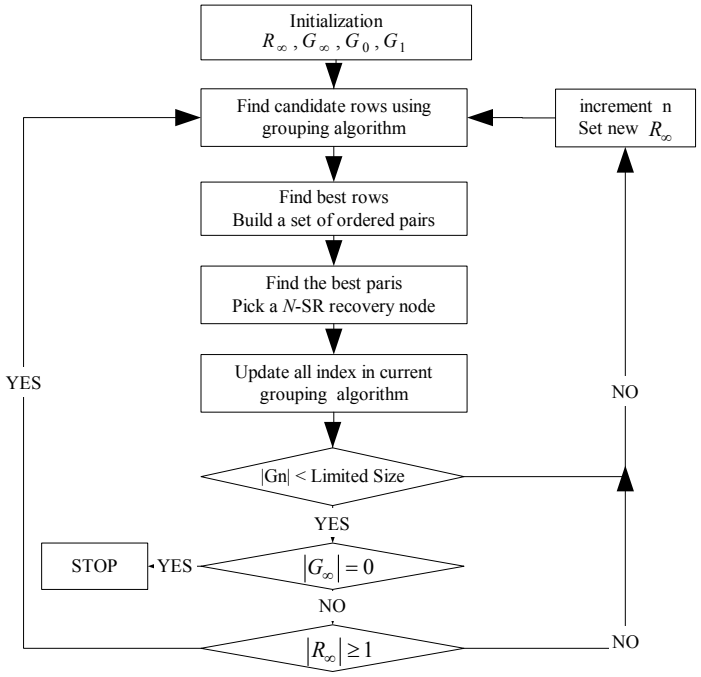


**Figure 26. Extended finite-length puncturing algorithm.**

A limited grouping step is applied to increase the maximum code rate whenever *N*-SR nodes are selected for each group. All of the variable nodes are separated into different groups that have a specific group size and the same recovery-error probabilities. Initially, empty sets $R_0$ and $R_1$, undetermined candidate row set $R_\infty$, and undetermined column set $G_\infty$ are defined. Next, the best column candidates in a given parity-check matrix are searched while finding the candidate rows and choosing the best survived check rows. Note that the number of column candidates for the next group is increased if the size of the previous group is limited in the finite-length puncturing method. If the best column and row pair is found, this column is set as a good puncturing location. This

algorithm is iterated until there exist no more undetermined columns, which equal $/G_\infty/ = 0$. From this method, the number of punctured locations in the given parity-check matrix can be increased while minimizing performance loss resulting from the puncturing.

### 4.3 Adaptive Incremental Redundancy Hybrid FEC/ARQ Schemes

The principle of IR-HybridARQ schemes is to avoid retransmission of all information and parity bits when the previous transmission fails. If decoding the previous frame fails, only additional fractional parts of parity bits are transmitted. In this IR-HybridARQ scheme, the adaptive code selection algorithm in the previous section is also used to enhance the throughput performance at low operating SNR ranges. The code combination procedures of this IR-HybridARQ scheme follow Chase's rule [70]. The procedure of our IR-HybridARQ scheme is described in the following steps.

Step 1. [Encoding] Encode information messages with LDPC forward error correction codes.

Step 2. [Grouping] Group all parity bits using the puncturing methods above.

Step 3. [Adaptive code selection] Select the code rate and the parity group for the next frame transmission using the adaptive code selection algorithm.

Step 4. [Sending] Transmit the best parity group.

Step 5. [Combining] Receive the parity group of current frame and combine it with the previous message and parity bits for constructing a frame at the receiver end.

Step 6. [Decision] Check the error in the frame. If there are some errors in the frame, send a NAK signal to the transmitter. Otherwise, send an ACK signal to the transmitter. After the transmitter receives an ACK signal, it stops sending the current frame and prepares the frame for the next transmission.

For an adaptive operation of IR-HybridARQ schemes, the adaptation threshold parameters need to be determined. The detailed algorithm for adaptive code selections is discussed in the previous section 3.3. The transmitter uses these threshold parameters for the code rate selection in the next transmission. The predicted channel states are partitioned into eight segments according to the adaptive code selection algorithm. The code rates from $R_0$ to $R_8$ are selected within the specified SNR range. In addition, the average number of retransmissions can be used as the criterion for adaptive transmission because the average number of retransmissions reflects partial information about the next channel state. To determine the code rate for the next frame, the transmitter selects the higher code rate between the values from adaptation threshold parameters and the code rate determined by subtracting one from the average retransmission number.

An important performance measure of IR-HybridARQ systems is the throughput, which is defined as the ratio of the number of information bits $k$ to the total number of bits, which the transmitter sends to the receiver until getting an ACK signal. In this IR-HybridARQ scheme, the system throughput $\eta$ is given by

$$\eta = \frac{k}{k(1-FER(1)) + \sum_{i=2}^{\infty} \left\{ \left( k + \sum_{j=1}^{i-1} r_j \right) \cdot (1-FER(i)) \prod_{j=1}^{i-1} FER(j) \right\}}, \tag{48}$$

where *FER(i)* is a probability of a frame error at the $i_{\text{th}}$ transmission after the $(i\text{-}1)_{\text{th}}$ unsuccessful transmission, and $r_j$ is the length of parity frame at the $j_{\text{th}}$ retransmission.

### 4.4 Performance Results

As a system model, an IR-HybridARQ scheme over an adaptive LDPC coded MIMO system is considered that employs an ensemble of IR-LDPC codes. The prepared

mother code is a half-rate irregular LDPC code with a length of 4096, which has degree distribution pairs in equations (33) and (34). The other code rates are prepared by puncturing this mother code with the proposed design methods and a random puncturing method.

### 4.4.1 Ensemble Designs of IR-HybridARQ Schemes

There are two design methods introduced in the previous section 4.2. Design method I is to design the ensemble of IR-LDPC codes with the finite-length puncturing algorithm. The ensemble of LDPC codes using design method I is shown in Table 5. The objective of method I is to maximize the number of *lower*-step recovery nodes, which reduces the total number of iterations of iterative decoding.

**Table 5. Ensemble of LDPC codes using design method I.**

| | $G_0$ | $G_1$ | $G_2$ | $G_3$ | $G_4$ | $G_5$ | $G_6$ | $G_7$ | $G_8$ |
|---|---|---|---|---|---|---|---|---|---|
| Size | 2560 | 1311 | 206 | 19 | 0 | 0 | 0 | 0 | 0 |

In this method, the grouping algorithm is first used for finding *N*-step recovery nodes from the given parity-check matrix of the mother code, which has a block length of 4096 and a half-code rate. The *n*-step recovery nodes of 1536 can be found exhaustively from the total parity bits of 2048. The number of total groups is minimized to three, as shown in Table 5. However, the maximal code rate is limited to 0.8 because there are no more *N*-step recovery nodes to support the code rates over 0.8 in this method. To prepare an ensemble supporting the code rates over 0.8 for IR-HybridARQ schemes, we randomly choose additional punctured bit positions of 256. Before this selection, the message nodes are assigned to the variable nodes with the highest degree from the remaining parity bits, which consist of the variable nodes of 512. After completing the

construction of the ensemble sets, we divide all punctured bits into eight groups for supporting the incremental redundancy transmission of IR-HybridARQ schemes.

A limitation of design method I is that the performance for higher puncturing (code rate above 0.8 for a rate 0.5 mother code) is not good enough to support the code rate over 0.8. Therefore, the other design method for designing an ensemble with subset codes needs to be considered, which has good frame error rate performance at higher rate above 0.8. This method is called a design method II. By applying the extended finite-length puncturing algorithm to finding the puncturing positions, additional *N*-step recovery nodes can be found in the given parity-check matrix of the mother code. Each group size is limited to 256. In Table 6, the eight groups from $G_0$ to $G_8$ and the *N*-step recovery nodes of 1792 are defined from the given typical recovery tree. This can support the higher data rate over 0.8 while increasing the dynamic operation of IR-Hybrid ARQ schemes.

**Table 6. Ensemble of LDPC codes using design method II.**

| | $G_0$ | $G_1$ | $G_2$ | $G_3$ | $G_4$ | $G_5$ | $G_6$ | $G_7$ | $G_8$ |
|---|---|---|---|---|---|---|---|---|---|
| Size | 2048 | 256 | 256 | 256 | 256 | 256 | 256 | 256 | 256 |
| | $R_0$ | $R_1$ | $R_2$ | $R_3$ | $R_4$ | $R_5$ | $R_6$ | $R_7$ | $R_8$ |
| Rate | 0.5 | 0.53 | 0.57 | 0.61 | 0.67 | 0.73 | 0.80 | 0.89 | 1 |

### 4.4.2 Frame Error Rate Performance of IR-HybridARQ Schemes

Two ensemble designs is introduced in the section 4.4.1. These two methods are compared to the conventional random punctured method to verify the error rate performance of each proposed ensemble of IR-LDPC codes. The incremental amount of IR-HybridARQ schemes in each transmission is set to 256. The code rates for the

ensemble of IR-LDPC codes are defined as shown in Table 6 according to the number of increased redundancy parity bits in each subset code.

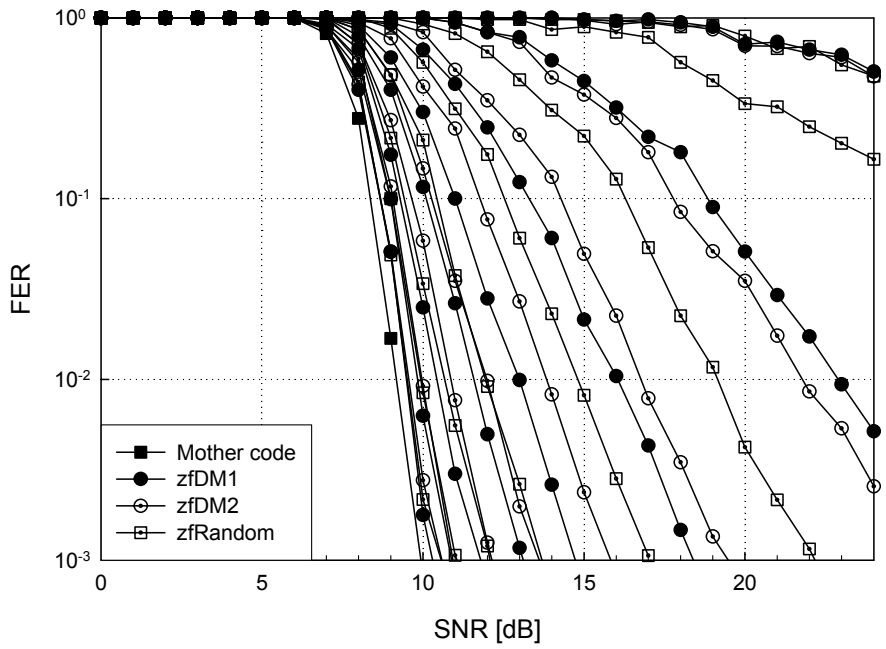


**Figure 27. Frame error rate performance of LDPC code ensembles in IR-HybridARQ ZF V-BLAST systems.**

The FER performance comparison of three different LDPC coded ZF V-BLAST systems with two transmit and receive antennas is shown in Figure 27. It is assumed that the channel state information is perfectly known to the transmitter and the receiver. The subset codes of each system have rates of 0.5, 0.53, 0.57, 0.61, 0.67, 0.73, 0.80, and 0.89 from the left to the right. The ensemble from design method I has better FER performance than design method II at lower rates under 0.8. Design method I maximizes the number of the lower-step recoverable nodes. It reduces the total number of iterations of iterative decoding and results in good FER performance. However, at a code rate over 0.8, the ensemble from design method I shows poor FER performance over the ensemble from design method II. The ensemble from design method II has more *N*-step recoverable

nodes, which can support code rates over 0.8. This fact guarantees that the ensemble of design method II has better FER performance than the ensemble of design method I at higher rates. Note that the ensemble of the conventional random puncturing method has inferior performance at higher rates over 0.73 compared to the ensembles of methods I and II. Especially, at a high rate 0.89, the ensembles of design method I and II outperform the random punctured ensemble.

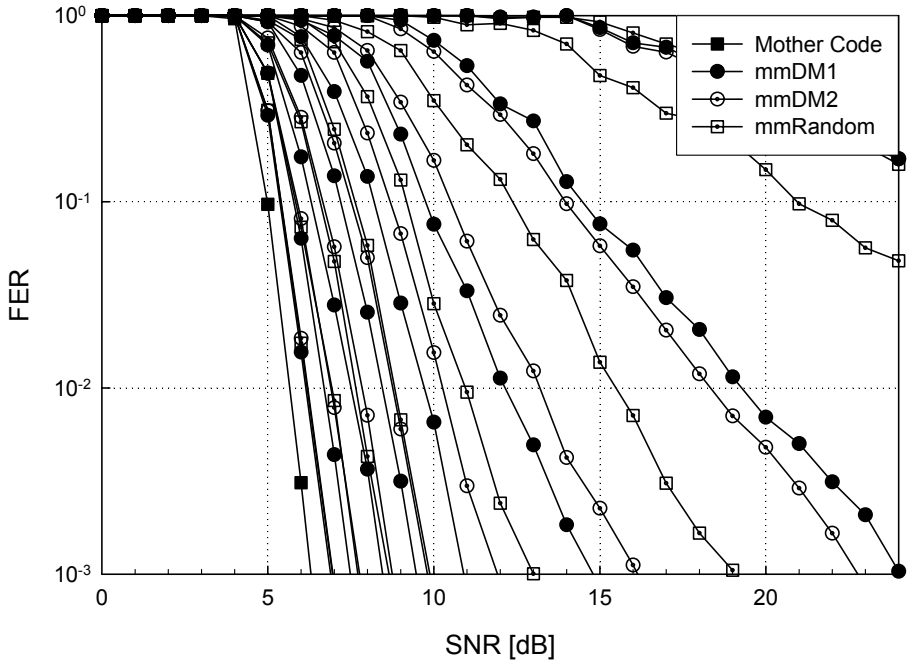


**Figure 28. Frame error rate performance of LDPC code ensembles in IR-HybridARQ MMSE V-BLAST systems.**

In Figure 28, the FER performances of LDPC coded MMSE V-BLAST systems with two transmit and receive antennas systems are compared. The overall FER performance of the three methods in MMSE V-BLAST systems shows about 3~4 dB $E_b/N_o$ improvement at each rate compared to the ZF V-BLAST systems as shown in

Figure 27. This performance improvement is resulting from the interference suppression, which is explained by equation (46).

### 4.4.3 Throughput Performance of LDPC Coded IR-HybridARQ Schemes

In this section, the throughput performance of non-adaptive and adaptive LDPC coded systems is compared. This throughput [71] is measured in two practical points. One is an average transmission code rate, which is defined as the system throughput $\eta$ in equation (48). This is measured as the ratio of the number of information bits to the total number of transmitted bits until the transmitter receives an ACK signal from the receiver. The other is an average number of NAK signals. The smaller number of NAK signals decreases the size of the required buffer at the transmitter and the receiver.

In Figure 29 and Figure 30, the throughput performance of non-adaptive IR-HybridARQ systems is shown. The performance of IR-HybridARQ schemes using the ensemble of design methods I and II, and the random punctured method is compared. The ensembles from design methods I and II have better throughput than the random punctured ensemble at a higher throughput region. In particular, for a throughput of 0.8, the ensembles of design method I and II have about a 3 dB $E_b/N_o$ improvement over the random punctured ensemble. Compared to the ensemble of design method I, the ensemble of design method II shows better throughput performance at higher throughput regions over 0.8. The throughput performance of these two systems has the performance limitation at higher throughput region 0.94, which is considered as the maximum throughput.

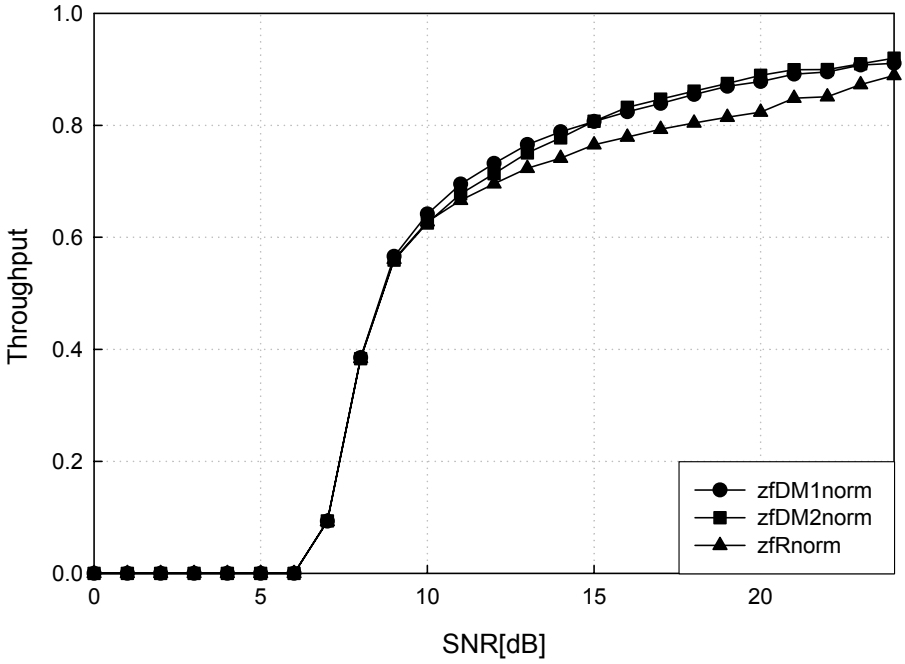


(a)

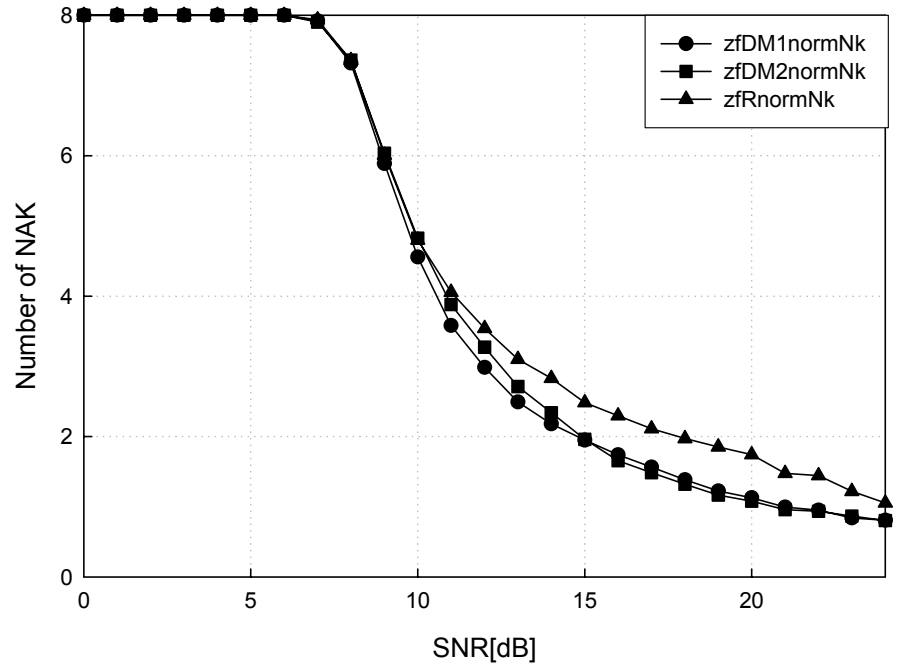


(b)

**Figure 29. Performance of non-adaptive IR-HybridARQ ZF-VBLAST systems: (a) throughput performance and (b) average number of NAK signals.**

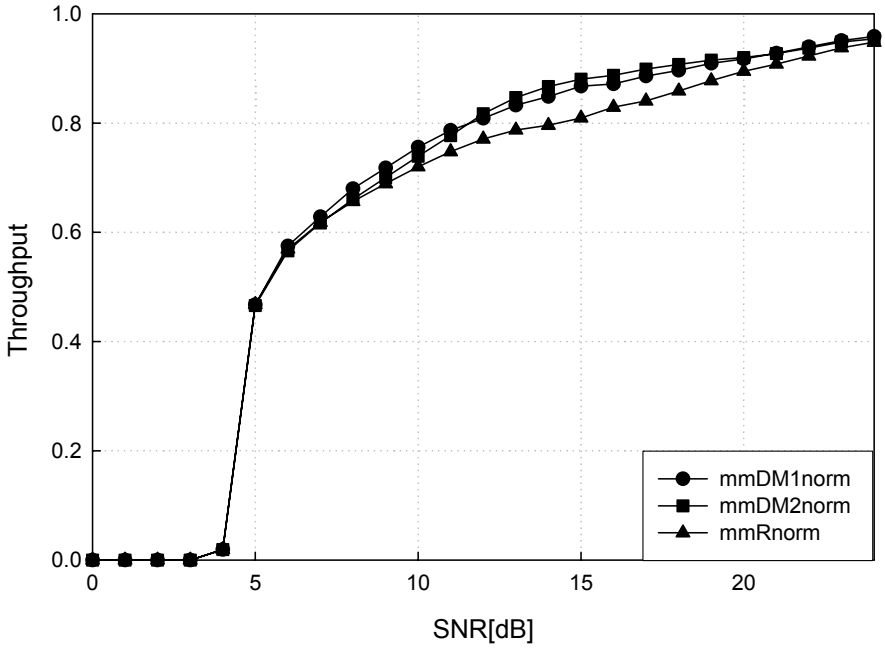


(a)

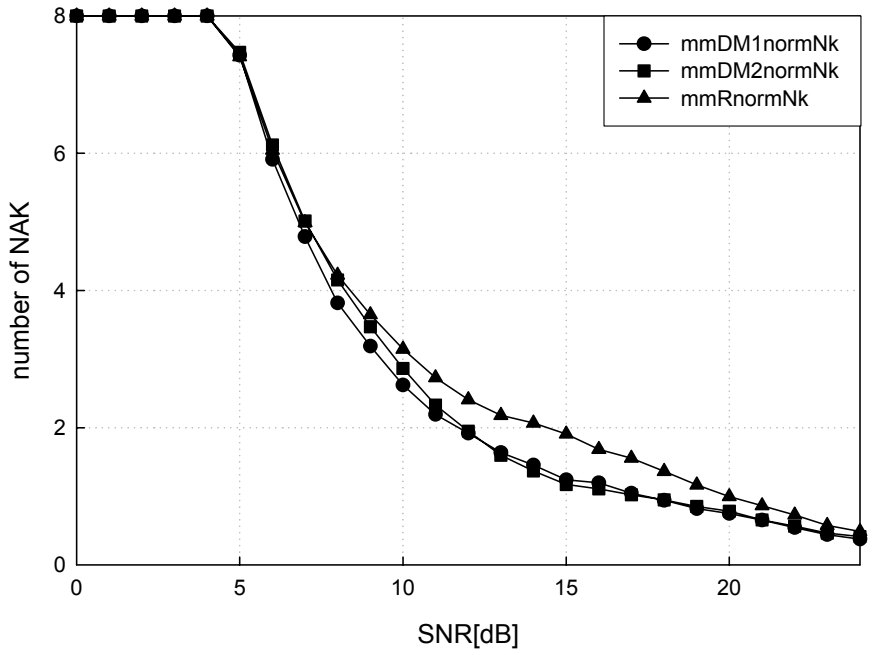


(b)

**Figure 30. Performance of non-adaptive IR-HybridARQ MMSE V-BLAST systems: (a) throughput performance and (b) average number of NAK signals.**

In Figure 31, Figure 32, and Figure 33, the throughput performance of LDPC coded V-BLAST systems are shown in different fading channels. We need to observe that the throughput performance of ensembles from design method I and II are about 3 dB better at high throughput regions than that of the random punctured system, where the coding rate is over 0.8 at all of different fading environments.

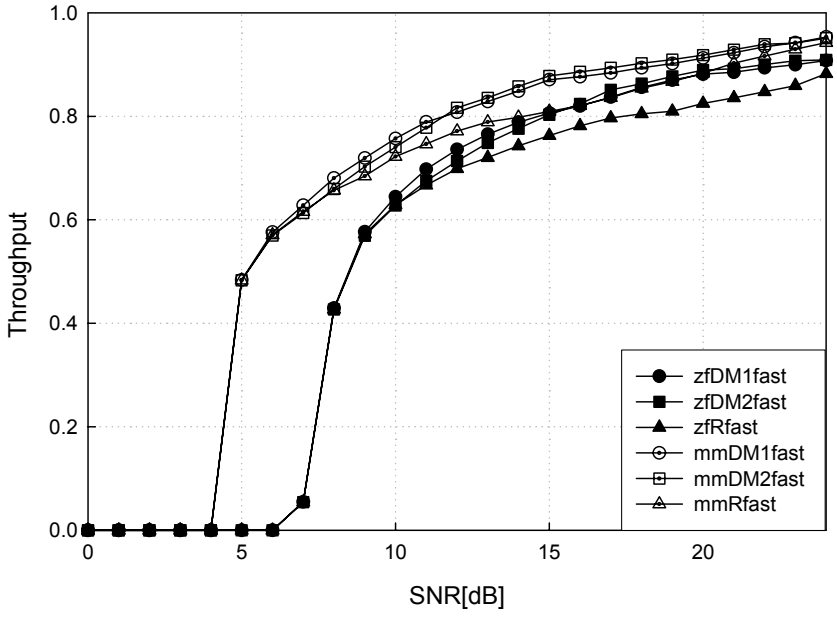


**Figure 31. Performance of non-adaptive LDPC coded V-BLAST systems in a fast fading channel. $f_D T_S = 0.02$.**

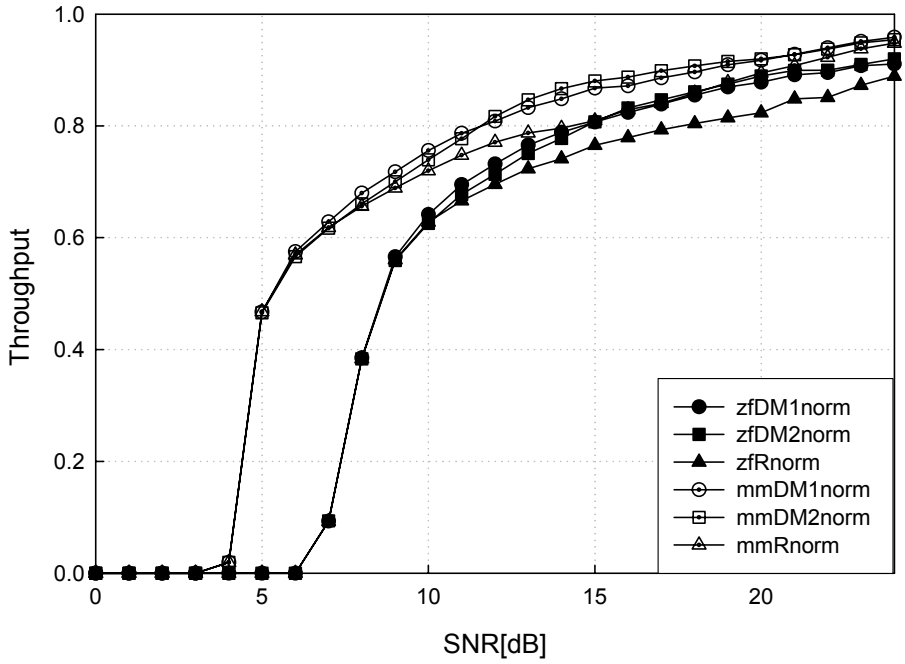


**Figure 32. Performance of non-adaptive LDPC coded V-BLAST systems in a fast fading channel. $f_D T_S = 0.01$.**

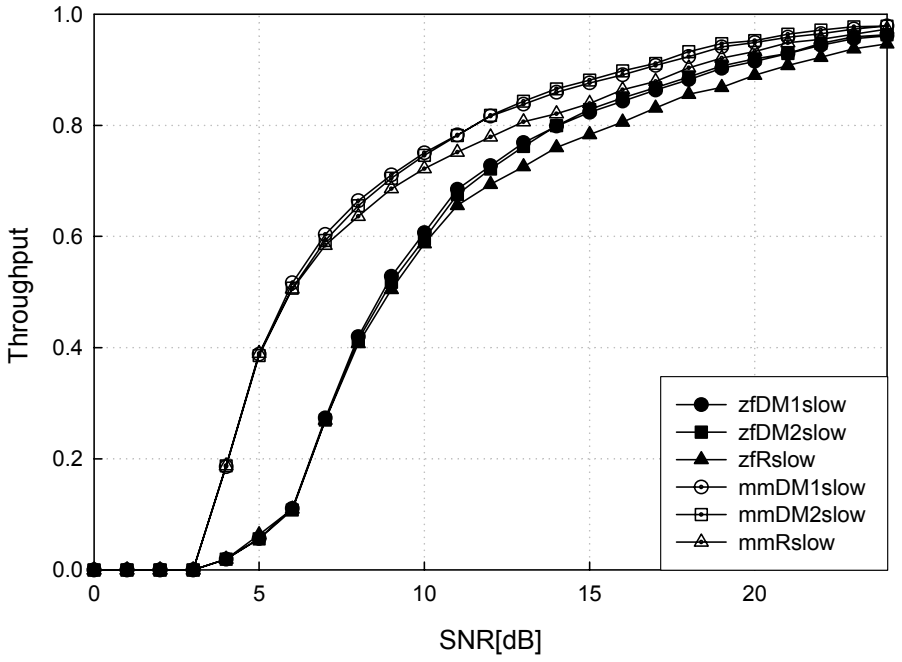


**Figure 33. Performance of non-adaptive LDPC coded V-BLAST systems in a fast fading channel. $f_D T_S = 0.001$.**

The throughput performance of adaptive IR-HybridARQ systems [72] is shown in Figure 34 and Figure 35. For fair comparison between the non-adaptive system and the adaptive system, all three IR-HybridARQ systems are compared. In these adaptive IR-HybridARQ systems, the transmitter selects the code rate for the next transmission with the threshold parameters in Table 7. These parameters are set by the adaptive code selection algorithm in the previous section 3.2. Comparing this result to the performance of non-adaptive IR-HybridARQ systems shown in Figure 30 and Figure 31, each IR-HybridARQ system shows comparable average transmission code rate performance while lowering the number of feedback traffic channels for NAK signals. In particular, the number of the NAK signals for retransmission is greatly reduced at lower operating SNR ranges, which reduces the required number of queue sizes at transmitter and receiver end in each IR-HybridARQ scheme.

**Table 7. Adaptation threshold parameters of IR-HybridARQ ZF and MMSE V-BLAST systems.**

| | [a]FP-MM I | [b]FP-ZF I | [c]FP-MM II | [d]FP-ZF II | [e]RP-MM | [f]RP-ZF |
|---|---|---|---|---|---|---|
| $TH_0$ | 0 | 0 | 0 | 0 | 0 | 0 |
| $TH_1$ | 6.3 | 10.0 | 6.3 | 10.0 | 6.3 | 10.0 |
| $TH_2$ | 6.9 | 10.3 | 6.9 | 10.6 | 6.9 | 10.6 |
| $TH_3$ | 7.5 | 10.9 | 7.8 | 11.2 | 7.7 | 11.1 |
| $TH_4$ | 8.4 | 11.8 | 8.7 | 12.5 | 8.6 | 12.4 |
| $TH_5$ | 9.5 | 13.1 | 9.8 | 13.7 | 9.9 | 13.8 |
| $TH_6$ | 10.9 | 14.7 | 12.0 | 15.8 | 13.0 | 17.0 |
| $TH_7$ | 14.8 | 18.4 | 16.1 | 19.4 | 19.0 | 22.2 |
| $TH_8$ | 24.0 | 29.0 | 22.7 | 25.8 | ∞ | ∞ |
| $TH_9$ | ∞ | ∞ | ∞ | ∞ | ∞ | ∞ |

[a, c]FP-MM I (II) :ensemble of design method I (II) in IR-HybridARQ MMSE V-BLAST system.

[e]RP-MM : random punctured ensemble in IR-HybridARQ MMSE V-BLAST system.

[b, d]FP-ZF I (II) :ensemble of design method I (II) in IR-HybridARQ ZF V-BLAST system.

[f]RP-ZF : random punctured ensemble in IR-HybridARQ ZF V-BLAST system.

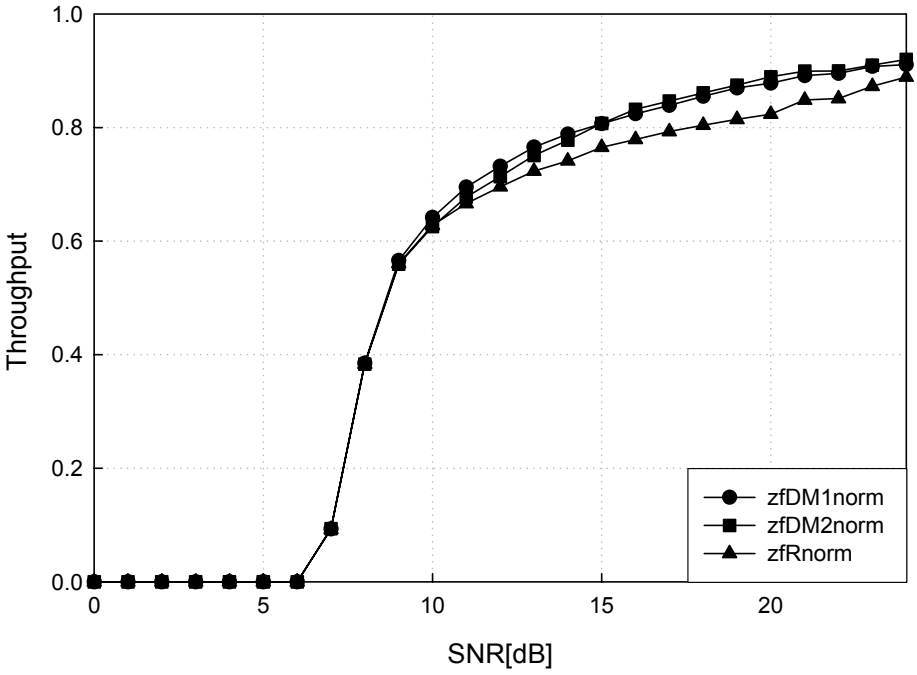


(a)

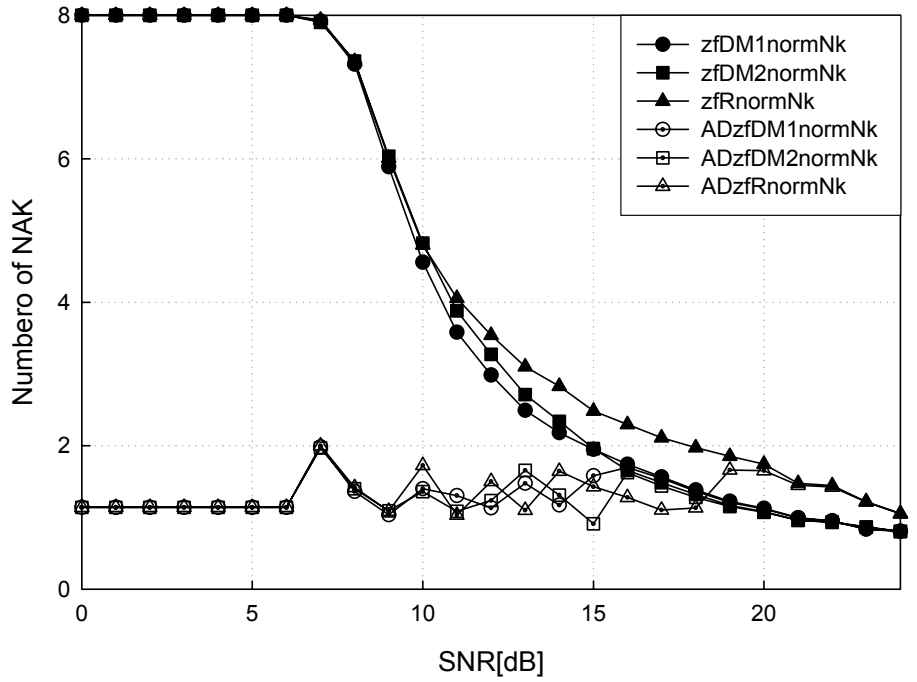


(b)

**Figure 34. Performance of adaptive IR-HybridARQ ZF V-BLAST systems: (a) throughput performance and (b) average number of NAK signals.**

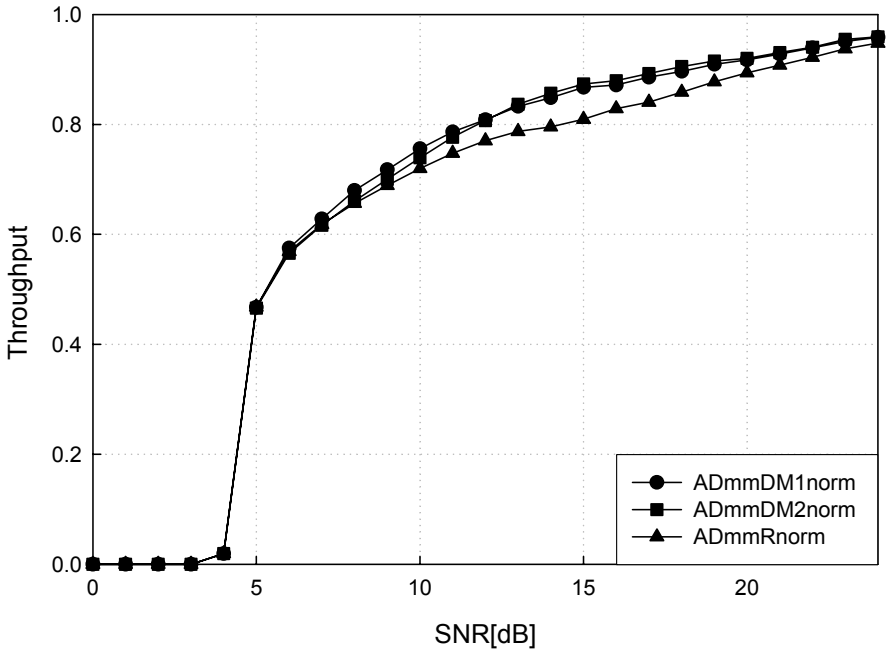


(a)

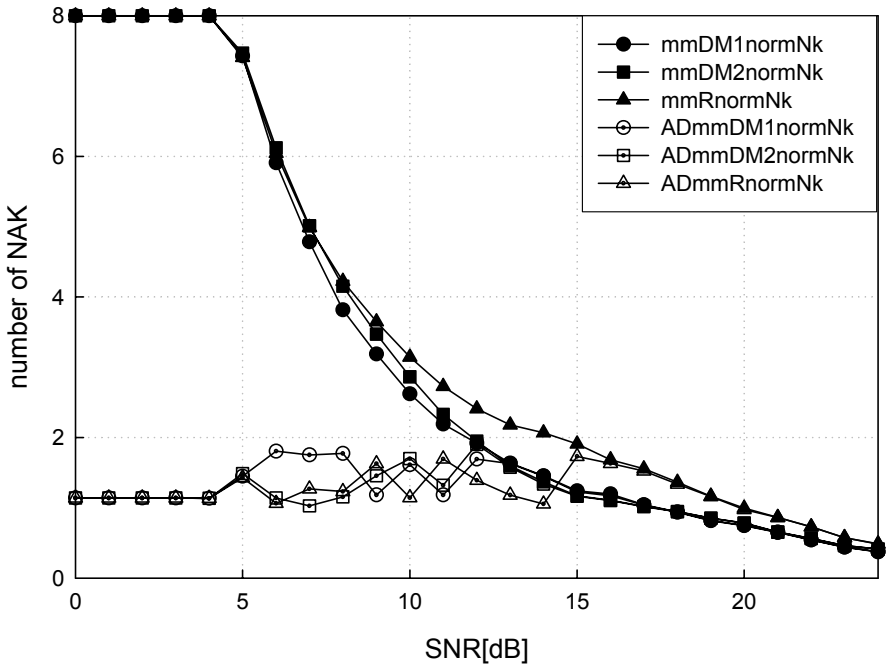


(b)

**Figure 35. Performance of adaptive IR-HybridARQ MMSE V-BLAST systems: (a) throughput performance and (b) average number of NAK signals.**

## 4.5 Conclusion

The throughput performance of IR-HybridARQ schemes strongly depends on the FER performance of the subset codes of an ensemble. In this chapter, we present two LDPC code ensembles for an IR-HybridARQ scheme by using a modified FP procedure. Simulation results show that LDPC coded ZF and MMSE V-BLAST systems using these ensembles yield a 3 dB improvement at high throughput regions over a conventional random punctured system in time-varying MIMO channels. In addition, we present an adaptive IR-HybridARQ scheme with an adaptive code selection algorithm. The unnecessary traffic of feedback channels requires bigger queue size at transmitter and receiver end. Simulation results show that the number of NAK signaling traffic can be significantly reduced in our adaptive LDPC coded systems without any significant throughput loss. In this chapter, our IR-HybridARQ scheme over an adaptive LDPC coded V-BLAST system using two ensembles is shown to be good candidate for the high-throughput wireless broadband communications in multiple antenna environments.

# CHAPTER 5

# INCREMENTAL REDUNDANCY IRREGULAR REPEAT ACCUMULATE CODES FOR HYBRID FEC/ARQ SCHEMES

## 5.1 Introduction

In next broadband wireless communication systems, the demand for efficient and reliable communications is tremendously increased. Also, powerful and flexible error control schemes are required for high-speed data service. For satisfying this demand, FEC coding and ARQ scheme must be combined for controlling transmission errors in broadband wireless systems. Among various combinations of FEC and ARQ schemes, this chapter is focused on an incremental redundancy Hybrid FEC/ARQ scheme [73]. This scheme can use punctured FEC codes [66] to adapt the system to the time-varying channels and utilize the incremental redundancy transmission for the transmitter to send the fractional parts of the parity bits to the receiver. In this scheme, we can maximize the throughput performance by sending only required parity bits to the receiver according to the channel state information.

This chapter presents incremental redundancy IRA codes for throughput improvement of HybridARQ systems. IRA codes can be good FEC codes for IR-HybridARQ scheme with the aid of their simple structure and low-complexities with good error rate performance. The IRA codes for IR-HybridARQ scheme should have following requirements. It can support the variable code rates in the system, and can be implemented in a rate-compatible fashion [54] for a low-complexity design. Also, it should have minimum performance loss at higher code rates, and have good error rate

performance over wide operating code ranges. Using the IRA codes in IR-HybridARQ schemes can also make the system simpler because it has simple generator matrix. These IRA codes are also examined as FEC codes in many wireless standards for high throughput and low-complexity applications [74][75][76]. However, the structure of these codes, which have many degree 2 nodes in parity part, leads to high error rate performance in burst error channels. Then, we need to propose adaptive rate-compatible puncturing patterns for these IRA codes [77][78] to maximize the throughput performance of IR-HybridARQ schemes. For the MIMO system for high-data-rate transmissions, we consider QR decomposition based V-BLAST systems because ZF/MMSE based V-BLAST systems require prohibitive computational complexities. This IR-HybridARQ scheme using a QR decomposition based detector and IRA codes can be one of the good candidate MIMO systems for low-complexity and high throughput performance. Through the simulation, we verify that IR-HybridARQ schemes using adaptive puncturing patterns of IRA codes have good throughput performance in all of SNR regions since their performance is adaptive to the time-varying channels.

This chapter is organized as follows. In section 5.2, we discuss the construction of IRA codes for IR-HybridARQ scheme and propose an adaptive transmission method using adaptive punctured patterns of given IRA codes. In section 5.3, we explain the system model using a QR decomposition based detector for a low-complexity design and introduce adaptive HybridARQ transmission for maintaining the high-throughput performance. In section 5.4, we present the system parameter and results of the error rate and throughput performance of IRA codes in HybridARQ schemes. In final section 5.5, we conclude with a brief summary about how our proposed IR-HybridARQ scheme using

IRA codes and their adaptive punctured patterns is well behaved with a low-complexity and moderate performance loss over time-varying MIMO channels.

## 5.2 Code Construction of Incremental Redundancy Irregular Repeat Accumulate Codes for Hybrid FEC/ARQ Scheme

In this section, we consider a punctured scheme for higher code rate from the mother code. For the punctured scheme using one of the adaptive puncturing patterns from eIRA structure in Figure 38, we prepare the code rates 0.5 to 0.94. The prepared eIRA codes have a rate-compatible structure, and show good FER performance at all coding rate, which inherit a single mother code's characteristics.

### 5.2.1 Irregular Repeat Accumulate Codes

We consider the IRA codes as FEC codes for IR-HybridARQ scheme. The basic structure of IRA codes is illustrated in Figure 36. The IRA codes are attractive choice for constructing a low-complexity system because the encoder structure is very simple while their performance is quite competitive with other LDPC codes. The IRA codes are first introduced in [29]. In an IRA code, a block of information bits is encoded by an irregular repetition outer code. Each information bit is repeated with its different number of repetition. Then, the block of repeated bits is interleaved and encoded by an inner accumulator. Those resulting bits are randomly permuted. Obviously, this encoding method has linear complexity as the length of the codes increases.

In an IRA code, the random code ensemble can be represented by parameters ($\{ \lambda_i \}$, $a$), which is called as degree profile. Here, $\lambda_i$ is referred to as the degree distribution of the ensemble with degree $i$, for $i = 2, \ldots, d$, such that $\sum_{i=2}^{d} \lambda_i = 1$. Also, $a$

is referred to as the grouping factor before the accumulator, which outputs one bit for the group of input symbols with the size $a$. The rate of the codes can be expressed by

$$R = \frac{a \sum_{i=2}^{d} \lambda_i / i}{1 + a \sum_{i=2}^{d} \lambda_i / i} = \frac{a}{a + \bar{d}}, \tag{49}$$

where the average degree is given by $\bar{d} \square 1/(\sum_{i=2}^{d} \lambda_i / i)$. These IRA codes can be considered as a special class of LDPC codes of which parity nodes can be constructed with only degree-2 variable nodes.

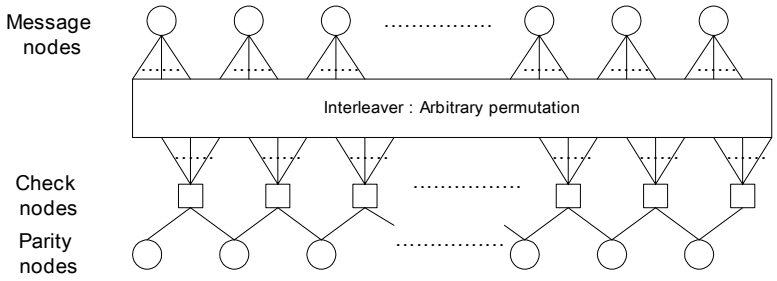


**Figure 36. Tanner graph representation for irregular repeat accumulate codes.**

### 5.2.2 Proposed Adaptive Transmission Method using Puncturing Patterns of eIRA Codes

We consider a finite-length puncturing algorithm [54] for searching the punctured bits location to support the variable code rates. On a typical recovery tree [54] in a finite-length punctured algorithm, we can represent the IRA codes as following representation in Figure 37. If we select the parity group for each higher punctured code rate as shown in Figure 37, we can increase the number of possible punctured nodes in a recovery tree to certain maximum number. For example, if we increase the number of lower step nodes in a recovery tree by maximizing the number of lower step recovery nodes using a finite-length puncturing algorithm, we can obtain the maximum punctured code rate, 0.67. Over

the code rate 0.67, the punctured code performance is degraded due to the lack of more available punctured nodes in the finite-length puncturing algorithm. To increase the punctured code rate of eIRA codes [78], we can apply the limited grouping algorithm in the previous chapter to get the good error rate performance in higher code rates. However, we cannot get the good throughput performance in all of SNR ranges with that algorithm, because the maximum code rate approach shows some performance limitation in the middle area of dynamic operating code ranges.

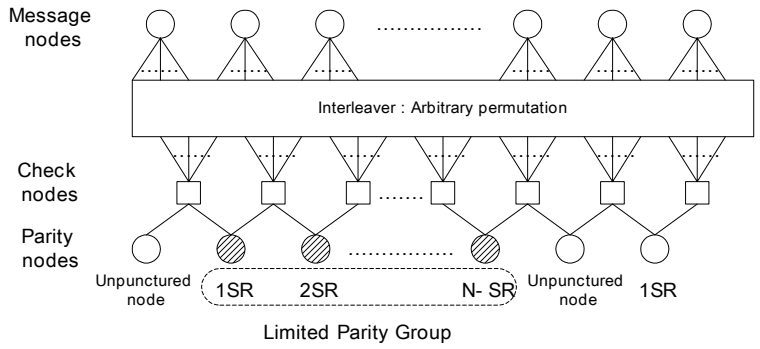


**Figure 37. Tanner graph representation for an example of a group of the punctured nodes in a recovery tree.**

In this chapter, an adaptive transmission method using adaptive puncturing patterns from the eIRA structure is presented to support the good throughput performance in all of SNR ranges. In eIRA codes, we can consider the several puncturing pattern based on the finite-length puncturing algorithm. However, for the best performance of given code rates, we need to select carefully some of special patterns for good error rate performance among them.

In Figure 38, possible adaptive puncturing patterns are shown on the basis of eIRA structures. The $L_{th}$ circled node means the $L_{th}$ step recovery node in a recovery tree of the finite-length punctured algorithm. Suppose given e-IRA codes have $K$ parity bits.

The largest step of given e-IRA codes in the group of punctured bits is $L$, which is the same as the number of puncturing pattern modes.

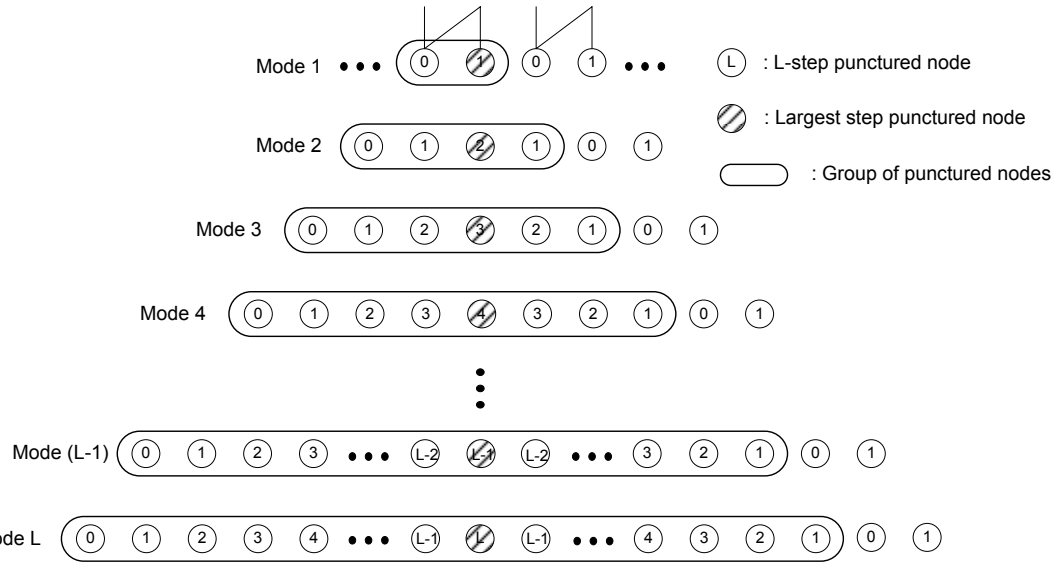


**Figure 38. Adaptive puncturing pattern in eIRA codes.**

If the size of group of the punctured nodes is $P$, $P$ can be calculated with following relationship with $L$.

$$P = 2 \cdot L \,. \tag{50}$$

In the mode 1, the number of the first step recovery node is half number of the total parity bits in given eIRA codes. In the other mode, the number of the $L$-step recovery node is expressed by

$$S_m = \left\lfloor \frac{K}{P} \cdot 2 \right\rfloor = \left\lfloor \frac{K}{2 \cdot L} \cdot 2 \right\rfloor = \left\lfloor \frac{K}{L} \right\rfloor \qquad , L > 1 \,. \tag{51}$$

Also, the number of largest step of the given e-RIA codes is given by

$$S_L = \left\lfloor \frac{K}{P} \right\rfloor = \left\lfloor \frac{K}{2 \cdot L} \right\rfloor \quad , L > 1 \,. \tag{52}$$

The number of unpunctured nodes is calculated by

$$S_U = \left\lfloor \frac{K}{P} \right\rfloor = \left\lfloor \frac{K}{2 \cdot L} \right\rfloor \quad , L > 1 . \tag{53}$$

So, the total number of parity bits in given eIRA codes becomes

$$K = \sum_{m=1}^{m=L-1} S_m + S_L + S_U . \tag{54}$$

If we use eIRA codes in IR-HybridARQ schemes, we can send optimized punctured bits for a specific mode to adapt the throughput performance of IR-HybridARQ schemes to the time-varying channels. Using these adaptive puncturing patterns, we can maximize the throughput performance in all of SNR ranges by using the proper punctured bits, which is selected for good error rate performance at a given code rate.

## 5.3 System Model

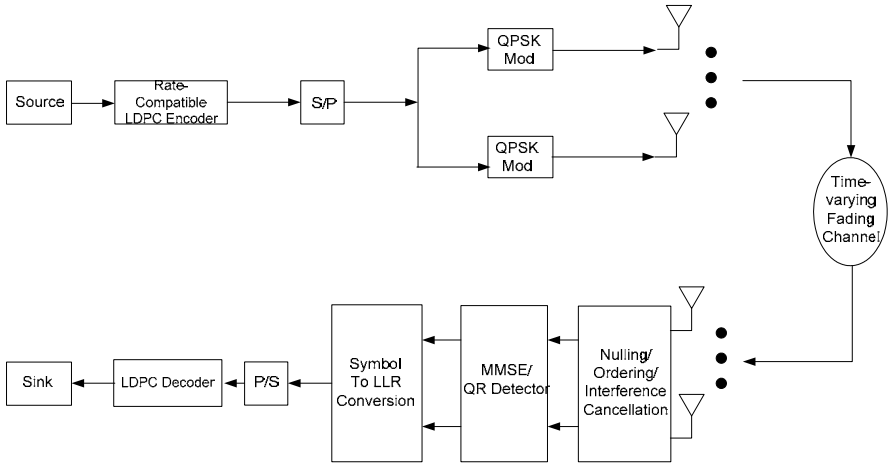


**Figure 39. MMSE/QR based V-BLAST MIMO Systems.**

The V-BLAST MIMO system model with a single LDPC code is shown in Figure 39. The detection of this V-BLAST system consists of nulling signal and cancelling interference while estimating the information symbol **x** given **y** and ***H*** in

$$\mathbf{y} = \boldsymbol{H}\ \mathbf{x}\ + \mathbf{n} , \tag{55}$$

where **n** is an AWGN noise vector. In this equation, the channel matrix ***H*** is assumed as full rank matrix, and each channel is uncorrelated. This detection algorithm involves following three steps.

Step 1. Ordering : Determine the optimal detection order to minimize error propagation in detection process.

Step 2. Nulling and slicing: Use the nulling vector to null out all the other symbols except the strongest symbol. Then, slice obtained symbol to the nearest value in the signal constellation.

Step 3. Cancelling: Cancel the effect of new decoded symbol from the remaining transmitted symbols.

### 5.3.1 QR Decomposition Based Detection

The V-BLAST decoding algorithm with MMSE detection has prohibitive computational complexity because it requires pseudoinverse calculations for matrix inversion. In this chapter, we now consider V-BLAST detection based on QR decomposition, which are less complex to solve a system of linear equations.

In our system, we consider the number of transmit antennas *m* and the number of receive antennas *n*. The channel matrix ***H*** in equation (55) can be factorized as

$$\mathbf{y} = \boldsymbol{H}\ \mathbf{x}\ + \mathbf{n} = \boldsymbol{QR}\ \mathbf{x} + \mathbf{n} \tag{56}$$

where the matrix ***Q*** has orthogonal columns with unit norm, and the matrix ***R*** is an upper triangular matrix. Multiplying hermitian matrix of ***Q*** in (56), the detected signal ***y*** can be represented as

$$\begin{aligned}\tilde{\mathbf{y}} = \boldsymbol{Q}^{H}\mathbf{y} \;\; &= \boldsymbol{Q}^{H}\boldsymbol{H}\mathbf{x} + \boldsymbol{Q}^{H}\mathbf{n} \\ &= \boldsymbol{Q}^{H}(\boldsymbol{Q}R)\mathbf{x} + \boldsymbol{Q}^{H}\mathbf{n} = (\boldsymbol{Q}^{H}\boldsymbol{Q})\,R\mathbf{x} + \boldsymbol{Q}^{H}\mathbf{n} \\ &= \boldsymbol{R}\mathbf{x} + \tilde{\mathbf{n}}\,.\end{aligned} \tag{57}$$

In this equation, the statistical properties of the noise term are unchanged because $\boldsymbol{Q}$ is a unitary matrix. Then, the upper triangular matrix $\boldsymbol{R}$ can be expressed by

$$\begin{pmatrix} r_{11} & r_{12} & \cdots & r_{1m} \\ 0 & r_{22} & \cdots & r_{2m} \\ 0 & 0 & \cdots & r_{3m} \\ \vdots & \vdots & \vdots & \vdots \\ 0 & 0 & \cdots & r_{nm} \end{pmatrix}. \tag{58}$$

If we consider the number of each transmit and receive antenna $m = n$ in this equation, the $n_{\text{th}}$ received symbol of $\boldsymbol{y}$

$$\tilde{y}_n = r_{nn}x_n + \tilde{n}_n\,. \tag{59}$$

Then the $n_{\text{th}}$ decision statistic $d_{\text{n}}$ is

$$d_n = \frac{1}{r_{nn}}\tilde{y}_n = x_n + \frac{1}{r_{nn}}\tilde{n}_n\,. \tag{60}$$

Once a decision is made on $d_{\text{n}}$, its effect can be subtracted from the remaining symbols. In general the $k_{\text{th}}$ received symbol and the $k_{\text{th}}$ decision statistic $d_{\text{k}}$ are given by

$$\tilde{y}_k = r_{kk}x_k + \tilde{n}_k + \sum_{i=k+1}^{m} r_{ki}x_i\,. \tag{61}$$

$$d_k = \frac{1}{r_{kk}}\left(\tilde{y}_k - \tilde{n}_k - \sum_{i=k+1}^{k} r_{ki}\hat{x}_i\right). \tag{62}$$

### 5.3.2 Structure of an eIRA Mother Code

In this chapter, we consider eIRA codes as FEC codes in IR-HybridARQ scheme. The eIRA codes form the parity bit in the bi-diagonal structure which satisfies the

following design rules. The rules are (i) assigning degree-2 nodes to nonsystematic bits, (ii) ensuring that the degree-2 nodes do not form a cycle amongst themselves and (iii) avoiding cycles of length-4 in the Tanner graph of the code.

The eIRA codes have the simple parity-check matrix $\boldsymbol{H}$, which consists of a $(n-k)\times k$ sparse matrix $\boldsymbol{H}_1$ without degree-2 nodes and a $m\times m$ matrix $\boldsymbol{H_2}$ with degree-2 nodes in equation (63). The $\boldsymbol{H}_2$ matrix has a bi-diagonal structure with degree-2 nodes, as illustrated in Figure 40. In this structure, the generator matrix $\boldsymbol{G}$ [78] for the parity-check matrix $\boldsymbol{H}$ in equation (63) can be expressed by equation (64).

$$H_2 = \begin{bmatrix} 1 & & & & & & & \\ 1 & 1 & & & & & & \\ & 1 & 1 & & & & & \\ & & 1 & & & & & \\ & & & \cdots\cdots & & & & \\ & & & & 1 & 1 & & \\ & & & & & 1 & 1 & \\ & & & & & & 1 & 1 \end{bmatrix}$$

**Figure 40. $\boldsymbol{H}_2$ matrix of parity check matrix of eIRA codes.**

$$H = [H_1 \; H_2] \tag{63}$$

$$G = [I \; P] = [I \;\; H_1^T H_2^{-T}] \tag{64}$$

From these equations, we can encode eIRA codes easily by performing the parity-check equations recursively. The simple structure of efficient encoders [78] for the eIRA codes are as illustrated in Figure 41. This class of LDPC codes has the advantage of a low-complexity encoder if the multiplication with $H_2^{-T}$ in equation (64) can be implemented efficiently. These codes have the systematic form of IRA codes with the matrix $\boldsymbol{H}_1^{\mathrm{T}}$ which has dimension $k\times n$ in Figure 41. For this reason, these codes are called extended IRA codes.

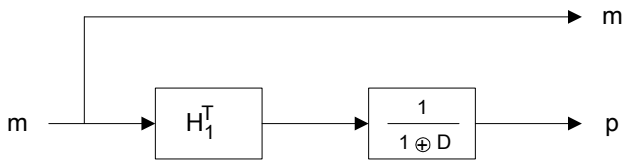


**Figure 41. Encoder structure of eIRA codes.**

### 5.3.3 Adaptive Hybrid FEC/ARQ Schemes for High-Throughput Transmission

The objective of IR-HybridARQ scheme is to improve the throughput by retransmitting the required fractional part of parity bits rather than the whole information and parity bits when the previous transmission fails. The code combining process of this IR-HybridARQ scheme follows the Chase's rule [70]. For the HybridARQ scheme using eIRA codes with adaptive puncturing patterns in this chapter, we need to modify the HybridARQ protocol. The steps of our modified IR-HybridARQ scheme are shown in Figure 42.

First, a frame for transmission is encoded by LDPC codes for an error correction. This encoded message is grouped by puncturing patterns in previous section. In this IR-HybridARQ scheme, we use the adaptive puncturing patterns for confronting time-varying channels. The transmitter selects the puncturing pattern from mode 1 to mode L according to the channel state information in a previous frame. It is assumed that the receiver knows the exact channel state information and sends it the transmitter without delay. Therefore, the transmitter sends the chosen parity group for specific puncturing pattern. At the receiver side, the transmitted frame is combined with the previous message and parity bits for completing the whole frame. The receiver checks the error in the frame. If there are some errors in the frame, it sends a NAK signal to the transmitter. Otherwise, it sends an acknowledgement (ACK) signal to the transmitter. After

transmitter receives the ACK signal, it discontinues transmitting the remaining parts of the current frame, and prepares a frame for the next transmission.

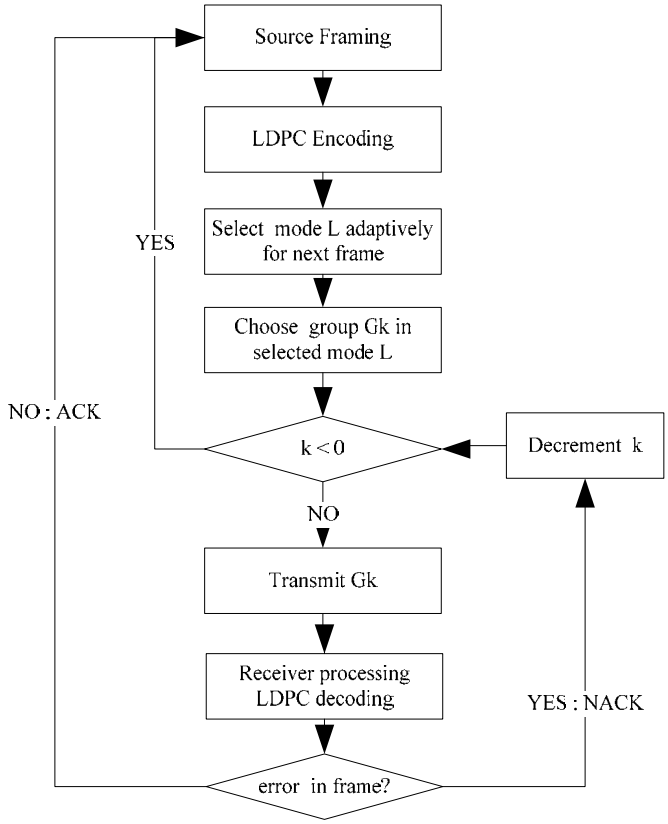


**Figure 42. Operation of an IR-HybridARQ scheme using adaptive puncturing patterns from e-IRA codes.**

### 5.4 Performance Results

The performance of our system model is simulated at 2x2 and 4x4 MIMO system with MMSE and QR methods with optimal ordering detection. Also, we pay more attention to the QR based MIMO system with e-IRA codes because this system has low-complexity and high-throughput performance than MMSE V-BLAST MIMO system. Our code ensembles for IR-HybridARQ have 128 bits at each step of the transmission in IR-HybridARQ scheme. The mother code of eIRA codes has a code rate, 0.5. In this

simulation, we prepare two mother codes, which are optimized in AWGN channel independently.

The first mother code of eIRA codes have following degree distributions. We try to keep the same degree distributions as those in [78] for a rate-1/2 code, which are optimized in AWGN channel maintaining eIRA structure. This code is called as eIRA1 in this section.

$$\lambda(x) = 0.00015 + 0.30235x + 0.27132x^2 + 0.42618x^6 \tag{65}$$

$$\rho(x) = 0.35555x^5 + 0.64445x^6 \tag{66}$$

The second mother code of eIRA codes, which is called as eIRA2, is designed with the degree distributions from LDPC codes, which have performance gap from the Shannon limit, about 0.442 dB. The degree distributions of this mother codes are as shown in equations (67) and (68). We apply the progressive edge growth algorithm [61] to $\boldsymbol{H}_1$ design of both eIRA codes for having the better girth characteristics.

$$\lambda(x) = 0.00014 + 0.28547x + 0.21432x^2 + 0.5007x^6 \tag{67}$$

$$\rho(x) = 0.000837 + 0.9991634x^6 \tag{68}$$

The ensemble code rates for punctured scheme are 0.5, 0.53, 0.57, 0.62, 0.67, 0.73, 0.80, and 0.89. This simulation is done using Monte Carlo methods over frequency-flat fading channels generated by a modified Jake's fading model. The normalized Doppler spread is $fdTs = 0.01$.

### 5.4.1 FER Performance of eIRA Codes in Different Puncturing Modes

The throughput performance of IR-HybridARQ schemes depends on the frame error rate performance of an ensemble of a given FEC codes. For an adaptive transmission with variable puncturing patterns according to the channel state information,

we need to verify the error rate performance of each puncturing pattern. Here, we measure the error rate performance of the prepared two mother codes, eIRA1 and eIRA2 in puncturing mode 1, mode 2, and mode 4. The mode 1 is prepared for supporting the code rates from 0.5 to 0.67, and the mode 2 is prepared for supporting the code rates from 0.67 to 0.80. The mode 4 is prepared for code rates over 0.8.

In Figure 43, Figure 44, and Figure 45, performance of an eIRA1 code in each mode is presented. The supported code rates of the ensemble of the eIRA1 code are from 0.5 to 0.94, as shown in Table 8. Each mode has different puncturing locations in all of groups, which can support good error rate performance at target code rates.

**Table 8. Ensemble of eIRA codes**

| | $G_0$ | $G_1$ | $G_2$ | $G_3$ | $G_4$ | $G_5$ | $G_6$ | $G_7$ | $G_8$ |
|---|---|---|---|---|---|---|---|---|---|
| Size | 1024 | 128 | 128 | 128 | 128 | 128 | 128 | 128 | 64 |
| | $R_0$ | $R_1$ | $R_2$ | $R_3$ | $R_4$ | $R_5$ | $R_6$ | $R_7$ | $R_8$ |
| Rate | 0.5 | 0.53 | 0.57 | 0.61 | 0.67 | 0.73 | 0.80 | 0.89 | 0.94 |

In Figure 43, the performance of eIRA1 codes in mode 1 shows good error rate performance in code rate 0.53, 0.57, 0.62, and 0.67. However, FER performance of the ensemble over code rate 0.67 has poor error rate performance. This is because the number of possible punctured locations is limited to 512 among 1024 parity bits in mode 1. In Figure 44, eIRA1 codes in mode 2 shows good error rate performance at code rates 0.73 and 0.80 over the eIRA1 codes in mode 1. The puncturing pattern in mode 2 has 773 punctured locations in all of groups, while the mode 1 supports only 512 bits. So, eIRA1 codes in mode 2 have better error rate performance in code rates 0.73 and 0.80 than the eIRA1 codes in mode 1.

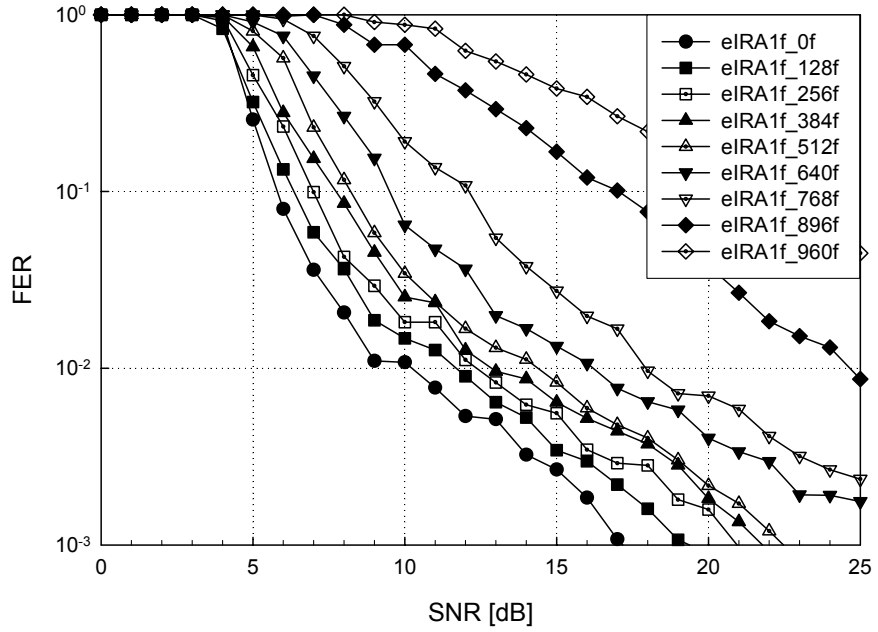


**Figure 43. Frame error rate performance of eIRA1 codes in mode 1 in 2x2 MMSE V-BLAST systems.**

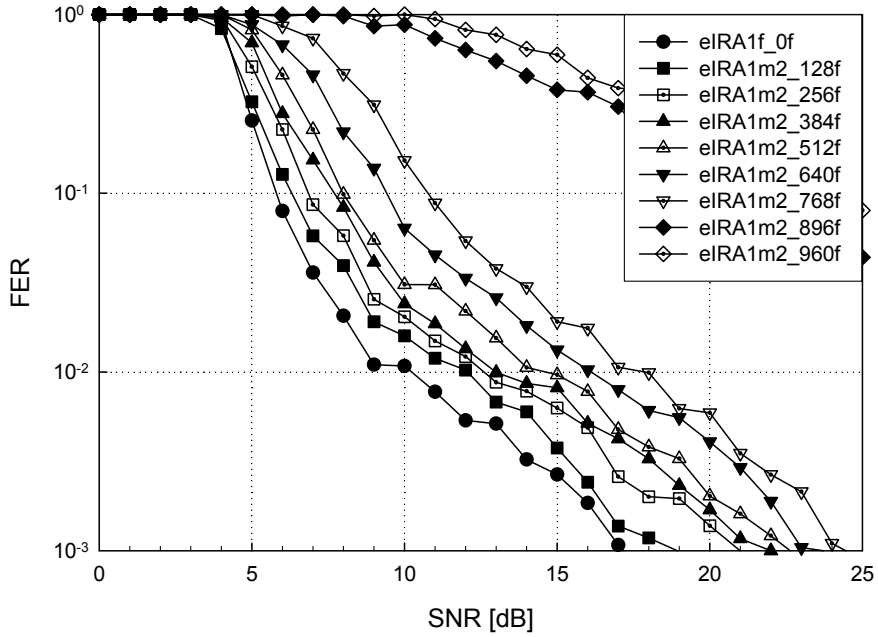


**Figure 44. Frame error rate performance of eIRA1 codes in mode 2 in 2x2 MMSE V-BLAST systems.**

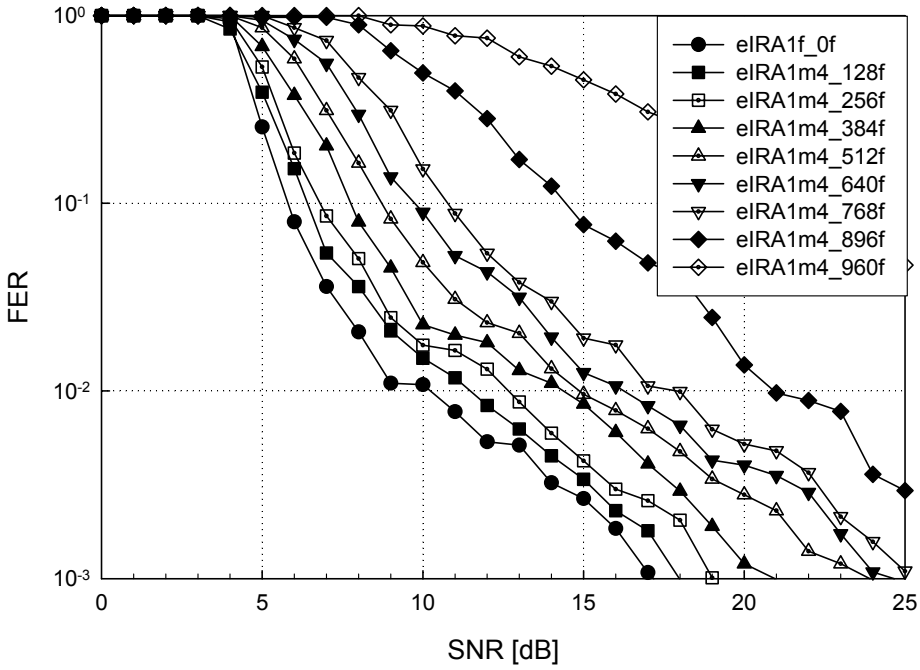


**Figure 45. Frame error rate performance of eIRA1 codes in mode 4 in 2x2 MMSE V-BLAST systems.**

In Figure 45, frame error rate performance of eIRA1 codes in mode 4 is presented. The puncturing pattern in mode 4 has 902 punctured bit locations, which can support code rate up to 0.9. A higher code rate 0.89 in mode 4 has better error rate performance than the ensemble in mode 1 and mode 2. This is because the mode 1 and mode 2 have limited number of the punctured locations, while the mode 4 can have enough punctured locations to support the higher code rates. However, the ensemble of lower code rates in mode 1 and mode 2 has better error rate performance than the one in the mode 4. Then, if we can maximize the throughput performance of IR-HybridARQ schemes with eIRA codes, we need to consider the adaptive puncturing pattern according to the target code rates.

In next figures, frame error rate performance of the second eIRA codes is also presented for verifying the performance difference according to the puncturing mode of eIRA codes. Here, we also present the QR based V-BLAST system for low-complexity approach. The two systems of MMSE and QR based V-BLAST system with an eIRA2 code is also compared, as shown in Figure 46, Figure 47, and Figure 48 in MMSE V-BLAST systems, and Figure 49, Figure 50, and Figure 51 in QR-based V-BLAST systems.

In Figure 46 and Figure 49, error rate performance of the ensemble of an eIRA2 code in mode 1 is shown. The ensemble in a QR V-BLAST scheme shows about 2 dB worse error rate performances than the one in MMSE based V-BLAST scheme. However, QR based scheme don't need to use pseudoinverse or inverse calculation in detection process, so it has less complexity and moderate error rate performance.

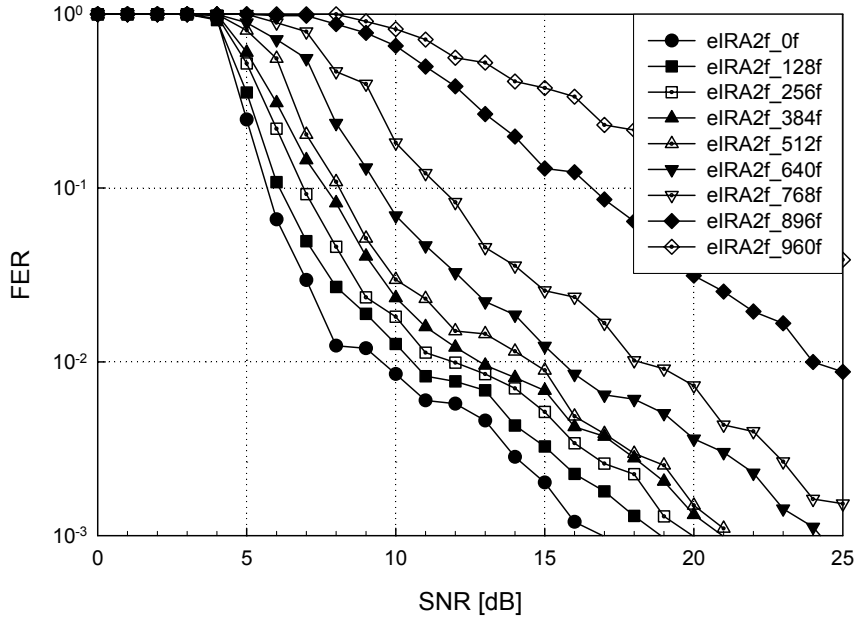


**Figure 46. Frame error rate performance of eIRA2 codes in mode 1 in 2x2 MMSE V-BLAST systems.**

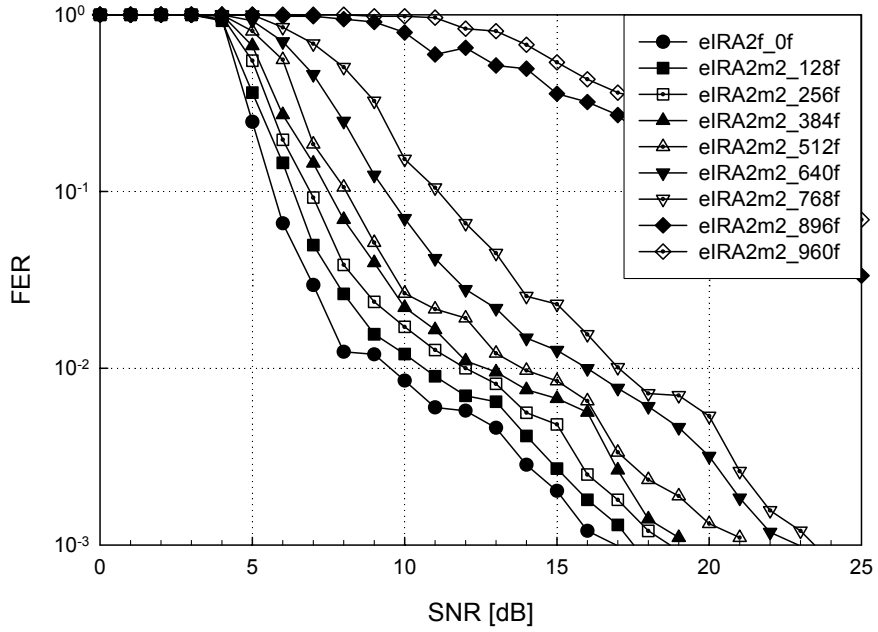


**Figure 47. Frame error rate performance of eIRA2 codes in mode 2 in 2x2 MMSE V-BLAST systems.**

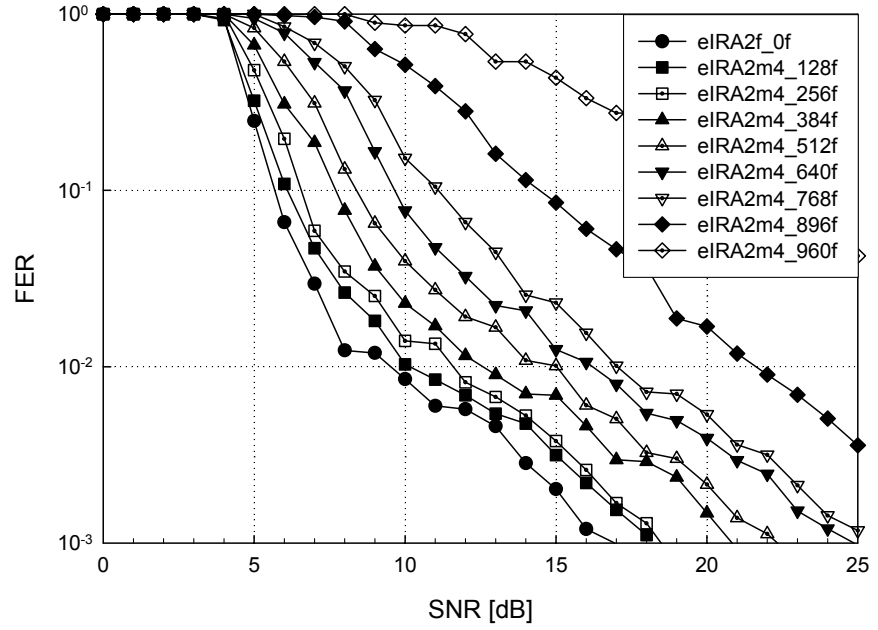


**Figure 48. Frame error rate performance of eIRA2 codes in mode 4 in 2x2 MMSE V-BLAST systems.**

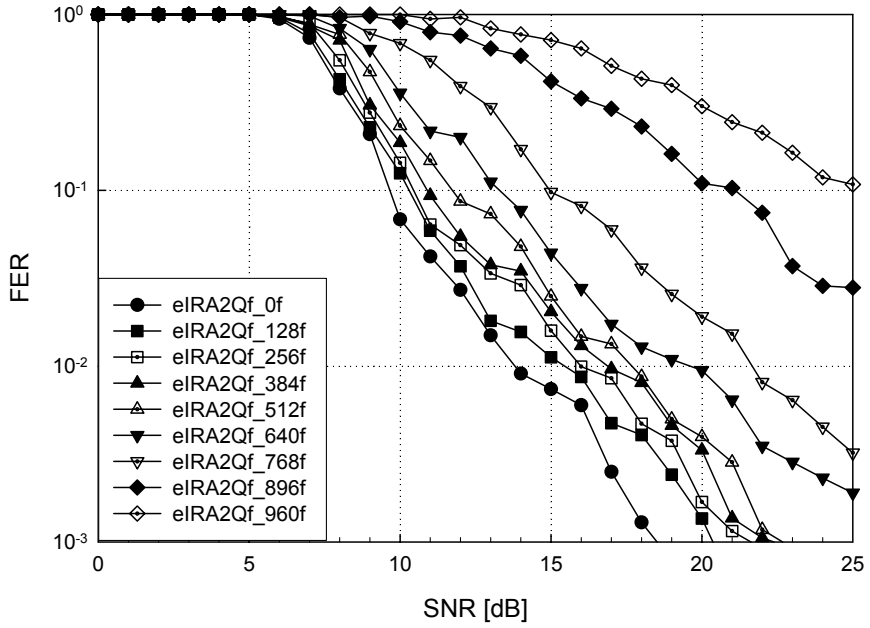


**Figure 49. Frame error rate performance of eIRA2 codes in mode 1 in 2x2 QR V-BLAST systems.**

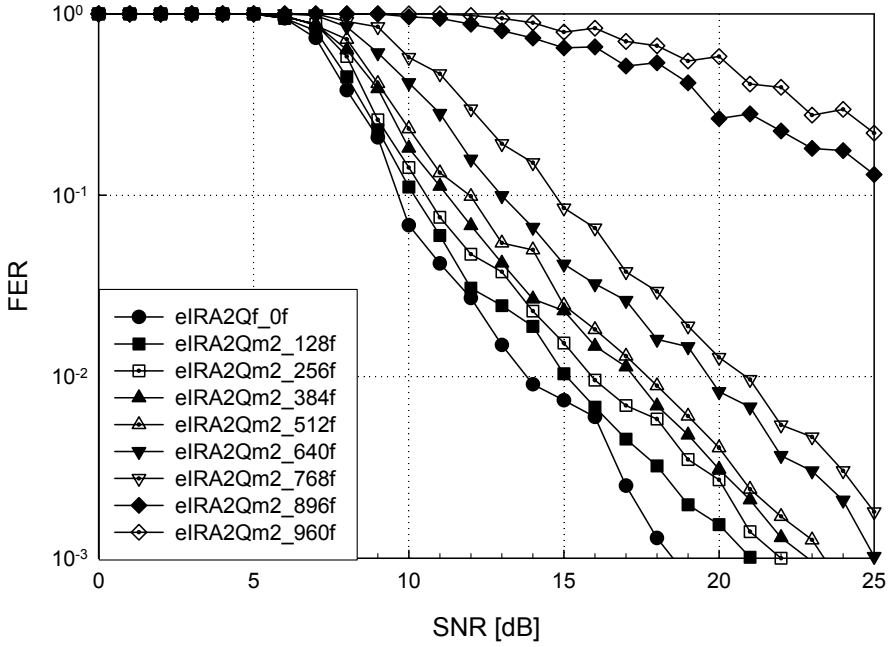


**Figure 50. Frame error rate performance of eIRA2 codes in mode 2 in 2x2 QR V-BLAST systems.**

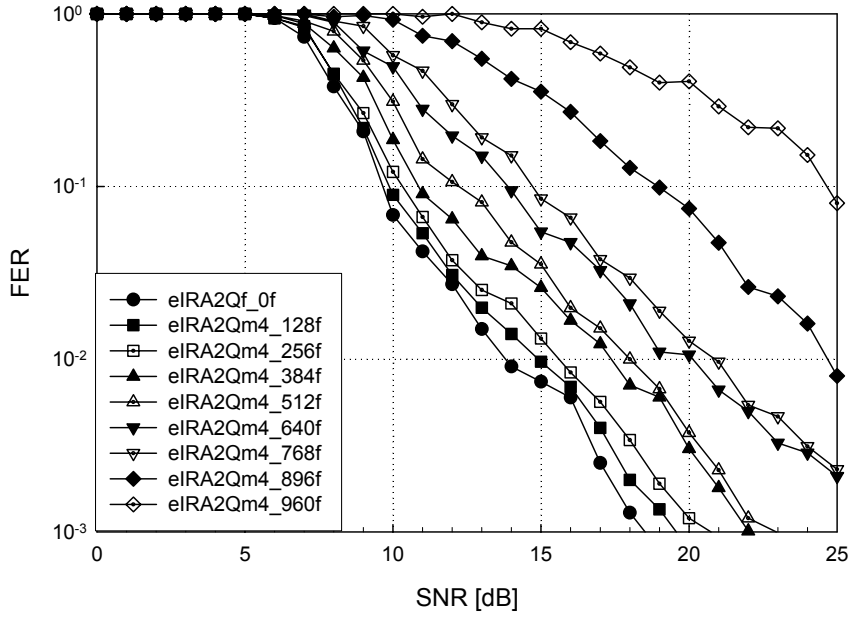


**Figure 51. Frame error rate performance of eIRA2 codes in mode 4 in 2x2 QR V-BLAST systems.**

In Figure 47 and Figure 50, error rate performance of the ensemble of eIRA2 codes in mode 2 is presented. In this mode, the ensemble with code rates 0.73 and 0.80 has better error rate performance than the one in mode 1. This is because the ensemble in the mode 2 has more available punctured locations than the one in mode 1 from its grouping structure. Then, the ensemble in mode 2 can support the code rate over 0.67 with higher performance. However, this mode cannot support the code rates over 0.80 because there are no more available punctured locations in its structure. In Figure 48 and Figure 51, the performance of eIRA2 codes in mode 4 is shown. This mode can have enough punctured locations to support the code rates over 0.8, so the ensemble in this mode have better error rate performance than the one in mode 1 and mode 2 in higher code rate over 0.8.

In Figure 52, Figure 53, and Figure 54, this QR based V-BLAST scheme with an eIRA2 code are presented in 4x4 multiple antennas. All of the characteristics of an eIRA2 code in 4x4 QR V-BLAST schemes have same trends as the ones of an eIRA2 code in 2x2 antenna scheme. The ensemble in mode 1 has good error rate performance in code rates 0.53, 0.57, 0.62, and 0.67, while the ensemble in mode 2 has good error rate performance in code rates 0.73 and 0.80. Also, the ensemble in mode 4 has better error rate performance over code rates 0.8 than the one in mode 1 and mode 2.

Compared these performance to previous results of the ensemble in 2x2 scheme, the ensemble of this scheme has about 2 dB performance degradation over 2x2 multiple antennas scheme. However, in terms of throughput performance, this scheme has twice throughput improvement than the 2x2 antenna schemes. In next section, the throughput performance of these ensembles is compared in IR-HybridARQ schemes.

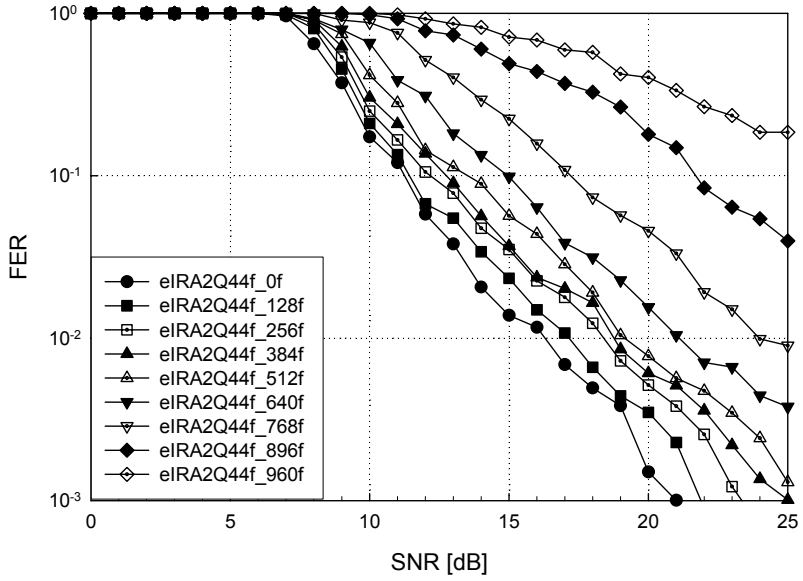


**Figure 52. Frame error rate performance of eIRA2 codes in mode 1 in 4x4 QR V-BLAST systems.**

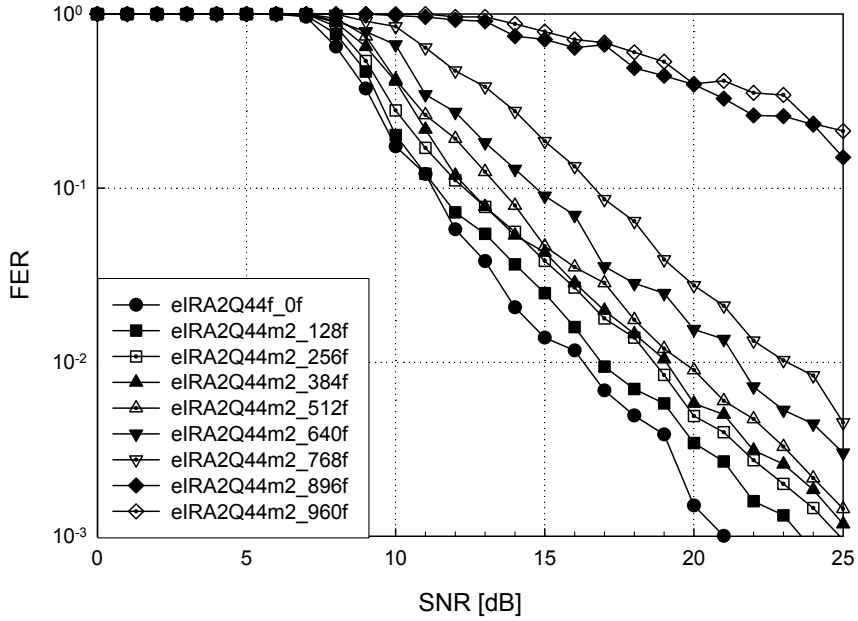


**Figure 53. Frame error rate performance of eIRA2 codes in mode 2 in 4x4 QR V-BLAST systems.**

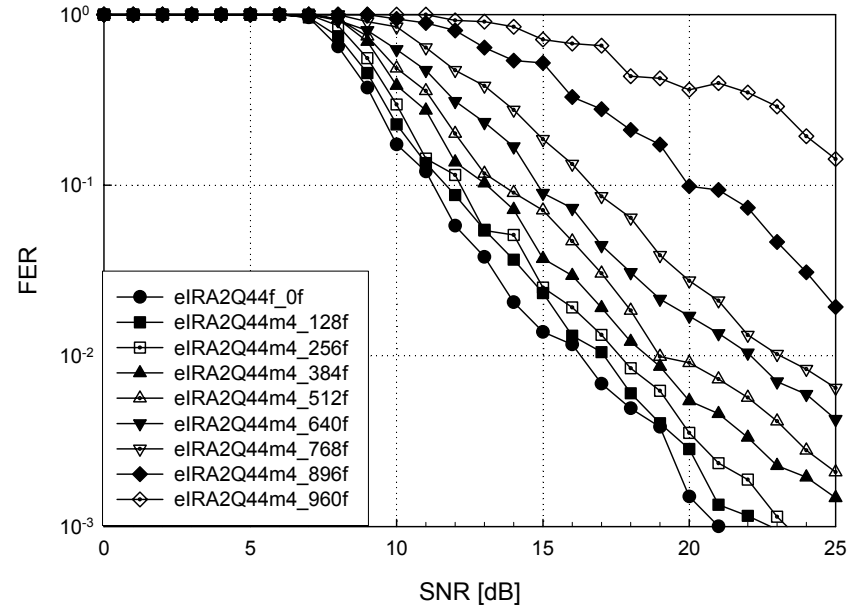


**Figure 54. Frame error rate performance of eIRA2 codes in mode 4 in 4x4 QR V-BLAST systems.**

### 5.4.2 Throughput Performance

In Figure 55, Figure 56, Figure 57, and Figure 58, the throughput performance of eIRA codes in MMSE and QR V-BLAST schemes are shown. In each scheme, the IR-HybridARQ scheme using adaptive puncturing scheme is compared to the other single mode schemes. We need to observe that the IR-HybridARQ scheme using adaptive puncturing pattern have higher throughput performance in all of SNR operating ranges in all of different systems. Especially, this scheme have comparable throughput performance to mode 1 in lower code rates under 0.67, and mid-range code rates between 0.67 and 0.80 to mode 2, and higher code rates over 0.8 to mode 4. In a single mode operation, the ensemble in mode 1 and mode 4 has good error rate performance, while the one in mode 2 have poor throughput performance over code rate 0.8.

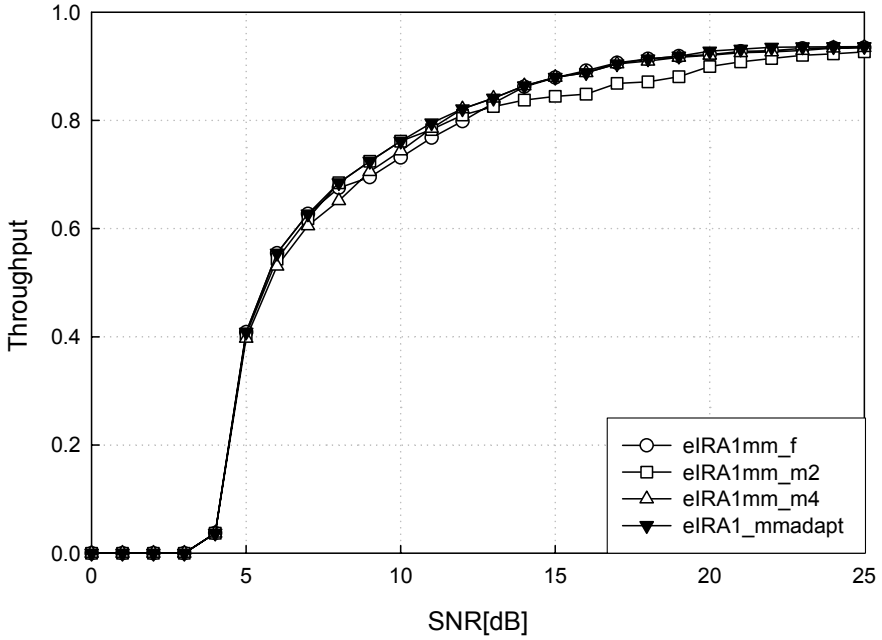


**Figure 55. Throughput performance of eIRA1 codes in 2x2 MMSE V-BLAST systems.**

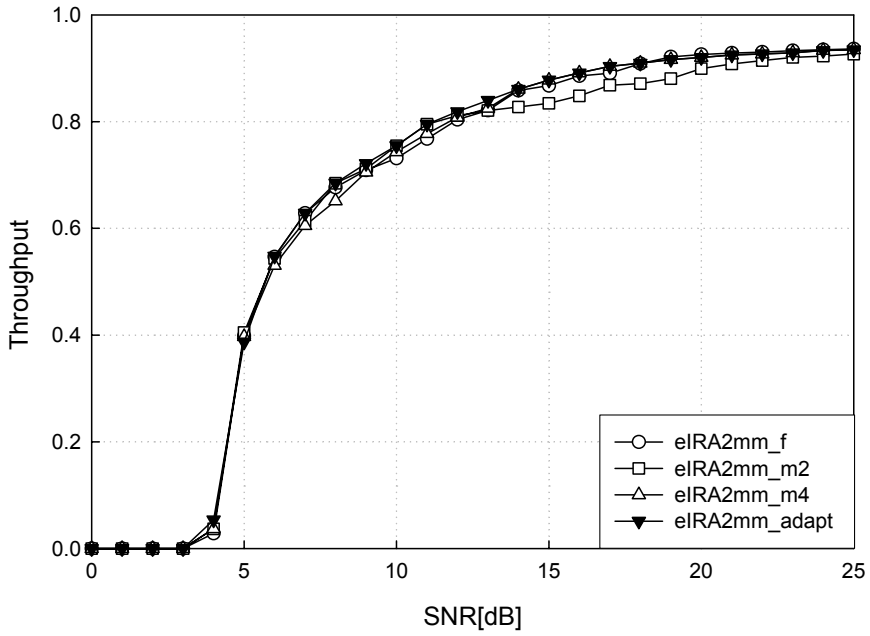


**Figure 56. Throughput performance of eIRA2 codes in 2x2 MMSE V-BLAST systems.**

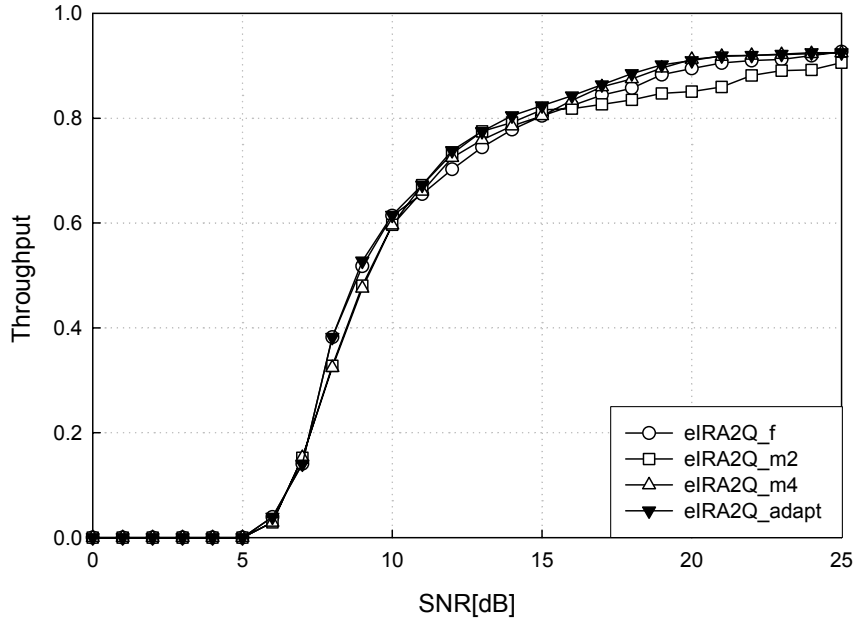


**Figure 57. Throughput performance of eIRA2 codes in 2x2 QR V-BLAST systems.**

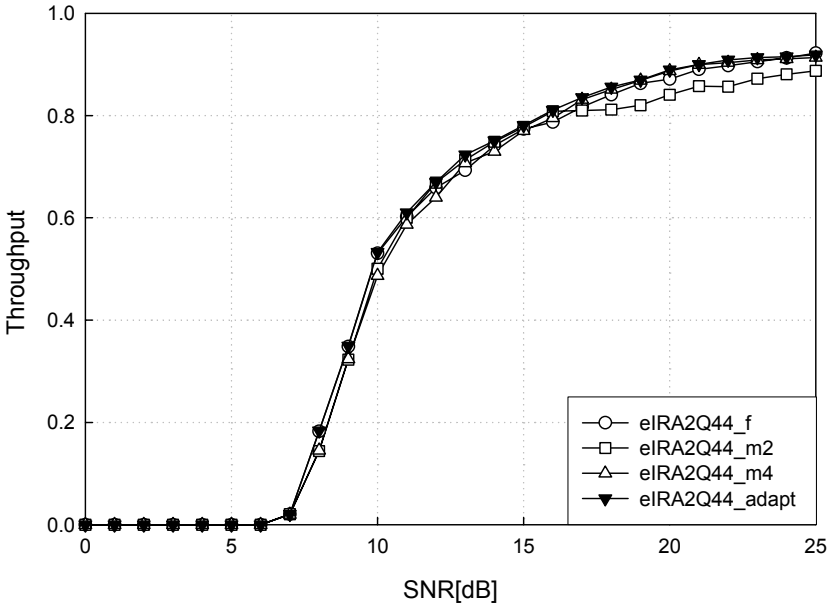


**Figure 58. Throughput performance of eIRA2 codes in 4x4 QR V-BLAST systems.**

## 5.5 Conclusion

This chapter presents the IR-HybridARQ scheme in QR V-BLAST system with eIRA codes for low-complexity and higher throughput performance. IRA codes can be good FEC codes for HybridARQ scheme with the aid of their simple structure and low-complexities with good error rate performance. However, the structure of these codes, which have many degree 2 nodes in parity part, leads to high error rate performance in burst channels. Then we propose an adaptive rate-compatible puncturing pattern for these IRA codes to maximize the throughput performance.

Through the simulation, we verify that the IR-HybridARQ scheme using adaptive puncturing pattern of IRA codes have higher throughput performance in all of SNR regions than the schemes with any other single mode, since its puncturing pattern is carefully adaptive to the time-varying channels. For the MIMO system for high-data-rate

transmission, we consider QR decomposition based V-BLAST system because MMSE based V-BLAST systems require prohibitive computational complexities at pseudoinverse calculation. Our proposed IR-HybridARQ scheme using a QR decomposition based detector and IRA codes shows higher throughput performance with moderate performance loss and low-complexity over a MMSE V-BLAST scheme.

# CHAPTER 6

# SUMMARY AND FUTURE WORK

This dissertation researches incremental redundancy LDPC codes for hybrid FEC/ARQ schemes to meet different code rates and quality of service requirements over time-varying channels.

To approach this work, we study the design and performance evaluation of IR-LDPC codes, which are optimized at short block lengths. In chapter 3, each performance of the IR-LDPC subset codes is compared to the performance of LDPC codes prepared by conventional random puncturing and dedicated multiple coded methods. This is a necessary step for designing the IR-LDPC codes because the throughput performance of IR-HybridARQ schemes strongly depends on the error rate performance of a family of the IR-LDPC codes. As a system model for this work, we present a new adaptive coded system with the proposed IR-LDPC codes. This adaptive coded system can confront the nature of time-varying channels. It can also reduce the complexity of a receiver by using only one channel code to support variable data rates. In addition, it shows performance comparable to multiple dedicated coded systems. The performance of the dedicated LDPC coded systems is considered to have upper-limit performance with high-complexity capacity-approaching schemes. As shown in the results, our adaptive LDPC coded system with the proposed IR-LDPC codes shows at least a 2% higher average transmission rate improvement than a conventional random punctured system. Its throughput performance also comes within 1% of a system that uses multiple dedicated codes at every target error rate in time-varying channels.

The previous IR-LDPC codes [28] have some of the limitations of a maximum achievable code rate. In chapter 4, a careful design of IR-LDPC codes is considered to increase the operating code range of IR-HybridARQ schemes. To address this issue, we propose a design of IR-LDPC codes using the extended finite-length puncturing algorithm [69]. Throughput results show that, compared to a conventional random punctured system in time-varying MIMO channels, LDPC coded V-BLAST systems using this approach yield a 3 dB improvement at high throughput regions. This IR-HybridARQ scheme is also operated with an adaptive code selection algorithm. In IR-HybridARQ schemes, unnecessary traffic channels for a negative acknowledgement signal require larger queue size at both transmitter and receiver ends. Simulation results show that the amount of NAK signaling traffic can be significantly reduced in our adaptive LDPC coded systems without any significant throughput loss.

For low-complexity and high-throughput IR-HybridARQ schemes, in chapter 5, we consider eIRA codes as FEC codes. The eIRA codes can be good FEC codes for the HybridARQ scheme with low-complexities and good error rate performance. However, the structure of these codes leads to high error rate performance in burst channels. To compensate for this problem, we propose an adaptive rate-compatible puncturing pattern for these eIRA codes to maximize the throughput performance of IR-HybirdARQ scheme. Through simulation results, we verify that the IR-HybridARQ scheme using adaptive puncturing patterns of eIRA codes has higher throughput performance in all of SNR regions than does any other single mode scheme. For the MIMO system for high-data-rate transmission with low-complexity, we consider QR decomposition based V-BLAST systems because MMSE based V-BLAST systems require prohibitive computational

complexities. This IR-HybridARQ scheme using a QR decomposition based detector and eIRA codes shows moderate performance loss and low-complexity compared to MMSE V-BLAST schemes.

## 6.1 Future Research Directions

The research presented in this dissertation focuses on designing and evaluating IR-LDPC codes and effective IR-HybridARQ scheme with high-throughput performance and low-complexity in time-varying channels. In this section, a number of future research directions are outlined.

**Extending Method for Increasing Dynamic Operating Code Range of IR-HybridARQ Scheme**

In this dissertation, IR-HybridARQ schemes using the proposed IR-LDPC codes have the operating code range from 0.5 to 0.9. For dynamic IR-HybridARQ schemes having a wider code range, IR-LDPC codes need to be designed to support lower code rates under a code rate, 0.5 [28]. We will continue our work on the design and performance evaluation of IR-LDPC codes in IR-HybridARQ schemes with wider operating code ranges by studying effective structures for lower code rates.

**Adaptive Coding and Modulation for Maximizing Throughput Performance of IR-HybridARQ Scheme**

In this research, we consider only an adaptive coded system in IR-HybridARQ schemes using capacity-approaching LDPC codes. In order to get the capacity of a given channel, it is necessary to study the combining of coding and modulation with optimal power and rate allocations [79][80]. Also, for bandwidth efficient modulation, we need to

consider higher order signal constellations such as 16 quadrature amplitude modulation (QAM) and 64 QAM. Then, we will study proper combination of LDPC codes and modulation to maximize the performance of IR-HybridARQ schemes.

**Iterative Receiver Design in IR-HybridARQ Scheme**

For many communication systems joint decoding and interference cancellation is required for optimum performance. Iterative algorithms for joint channel coding and interference cancellation have been studied in [81][82]. In this scheme, output of the soft decision decoder is used again to estimate the interference. This soft output is encoded and mapped again for input to the soft interference cancellation. Through these steps, the residual interference in previous iterations can be corrected. We need to achieve throughput improvement of IR-HybridARQ schemes with the least iteration between the interference cancellation and the iterative decoder.

# REFERENCES


[1] Rober H. Deng and Hong Zhou, "An adaptive coding scheme with code combining for mobile radio systems," *IEEE Transactions on Vehicular Technology*, vol. 42, no. 4, pp. 469-476, November 1993.

[2] M. S. Alouini, X. Tang, and A. Goldsmith, "An adaptive modulation scheme for simultaneous voice and data transmission over fading channels," *IEEE Transactions on Communications*, pp. 837-850, May 1999.

[3] "The 3rd generation partnership project (3GPP)," http://www.3gpp.org., Mar 2002.

[4] V. Tarokh, A. Naguib, N. Seshadri, and A. R. Claderbank, "Combined array processing and space-time coding," *IEEE Transactions on Information Theory*, vol. 45, no. 4, pp. 1121-1128, May 1999.

[5] V. Tarokh, H. Jafarkhani, A. R. Claderbank, "Space-time block coding for wireless communications: performance results," *IEEE Journal on Selected Areas in Communications*, vol. 17, pp. 451-460, March 1999.

[6] S. M. Alamouti, "A simple transmit diversity technique for wireless communications," *IEEE Journal on Selected Areas in Communications*, vol. 16, pp. 1451-1458, 1998.

[7] T. L. Marzetta and B. Hochwald, "Capacity of a mobile multiple-antenna communication link in Rayleigh flat fading," *IEEE Transactions on Information Theory*, vol. 45, pp. 139-157, January 1999.

[8] SoonYoung Yoon, "Introduction to WIBRO technology," *ITU-D IMT2000 Documents*, 2004.

[9] G .J. Foschini, "Layered space-time architecture for wireless communication in a fading environment when using multiple antennas," *Bell Lab. Tech. Journ.*, vol. 1, pp. 41-59, 1996.

[10] G. J. Foschini, G. D. Golden, A. Valenzela, and P. W. Wolniansky, "Simplified processing for high spectral efficiency wireless communications employing multi-element arrays," *IEEE Journal on Selected Areas in Communications*, vol. 17, no. 11, pp. 1841-1852, November 1999.

[11] G. J. Foschini and M. J. Gans, "On limits of wireless communications in a fading environment when using multiple antennas," *Wireless Personal Communications*, pp. 311-335, vol. 6, no. 3, March 1998.

[12] S. Lin and D. J. Costello, Jr., *Error Control Coding: Fundamentals and Applications*, Englewood Cliffs, NJ: Prentice Hall, 1983.

[13] S. Lin, D. J. Costello Jr., and M. J. Miller, "Automatic repeat request error control schemes," *IEEE Communication on Magazine,* vol. 22, no. 12, pp. 5-17, December 1984.

[14] J. Hagenaure and E. Lutz, "Forward error correction coding for fading compensation in mobile satellite channels," *IEEE Journal on Selected Areas on Communications*, vol. 5, pp. 215-225, February 1987.

[15] Siemens, "ARQ error control techniques," *3GPP, TSGR2n2, 085/99*, 1999.

[16] T. C. Ancheta, "Convolutional parity check automatic repeat request," *IEEE Int. Symp. Inform. Theory*, 1979.

[17] R. Mantha and F. R. Kschischang, "A capacity approaching hybrid ARQ scheme using Turbo codes," *IEEE Globecom.*, pp. 2341-2345, 1999.

[18] D. N. Rowitch and L. B. Milstein, "On the performance of hybrid FEC/ARQ systems using Turbo codes," *IEEE Transactions on Communications*, vol. 48, no. 6, pp. 948-959, June 2000.

[19] Y. M. Wang and S. Lin, "A modified selective-repeat type II hybrid ARQ system and its performance analysis," *IEEE Transactions on Communications*, vol. 31, pp. 593-608, May 1983.

[20] D. M. Mandelbaum, "An adaptive feedback coding scheme using incremental redundancy," *IEEE Transactions on Information Theory*, vol. 20, pp.388-389, 1974.

[21] N. Rowitch and L. B. Milstein, "Rate compatible punctured Turbo codes in a hybrid FEC/ARQ system," *IEEE Globecom.*, vol. 4, pp. 55-59, 1997.

[22] Q. Zhang and S. A. Kassam, "Hybrid ARQ with selective combining for fading channels," *IEEE Journal of Selected Areas on Communication*, vol. 17, no. 5. pp. 867-879, May 1999.

[23] S. Lin and P. S. Yu, "A hybrid ARQ scheme with parity retransmission for error control of satellite channels," *IEEE Transactions on Communications*, vol. 30, pp. 1701-1719, 1982.

[24] Stefania Sesia, Giusepp Caire, and Guillaume Vivier, "Incremental redundancy hybrid ARQ schemes based on low-density parity check codes," *IEEE Transactions on Communications*, vol. 52, no. 8, pp. 1311-1321, 2004.

[25] Nedeljko Varnica, Emina Soljanin, and Philp Whiting, "LDPC code ensembles for incremental redundancy hybrid ARQ," *ISIT*, pp. 995-999, 2005.

[26] M. R. Yazdani and A. H. Banihashemi, "On construction of rate-compatible low-density parity check codes," *IEEE Communications Letters*, vol. 8, no. 3, pp. 159-161, 2004.

[27] Emina Soljanin, Ruoheng Liu, and Predrag Spasojevic, "Hybrid ARQ with random transmission assignments," *Advances in Networking Information Theory*, vol. 66, pp. 321-334, 2004.

[28] J. Li and K. Narayanan, "Rate-compatible low-density parity-check codes for capacity-approaching ARQ scheme in packet data communications," *CIIT*, 2002.

[29] H. Jin, A. Khandekar, and R. McEliece, "Irregular repeat-accumulate codes," *Proc. 2nd Int. Symp. Turbo Codes and Related Topics*, pp. 1-8, September 2000.

[30] R. G. Gallager, "Low density parity check codes," *IRE Transactions on Information Theory*, IT-8, pp. 21-28, January 1962.

[31] C. Berrou, A. Glavieus, P. Thitmajshima, "Near Shannon limits error-correcting coding and decoding: Turbo-codes," *Proc. IEEE Int. Conference on Communications*, Geneva, pp. 1064-1070, 1993.

[32] D. J. C. MacKay, "Good error-correcting codes based on very sparse matrices," *IEEE Transactions on Information Theory*, vol. 45, no. 2, pp. 399-431, 1999.

[33] J. Pearl, "Probabilities reasoning in intelligent systems: networks of plausible inference," *Morgan Kaufman Publishers*, 1988.

[34] D. J. C. MacKay, R. M. Neal, "Near Shannon limit performance of low-density parity-check codes," *IEEE Electronics Letters*, vol. 32, no. 18, pp. 1645-1646, 2001.

[35] T. J. Richardson, A. Shokrollahi, R. Urbanke, "Design of capacity-approaching low-density parity-check codes," *IEEE Transactions on Information Theory*, vol. 47, 2001, pp. 617-637, 2001.

[36] T. J. Richardson and R. Urbanke, "The capacity of low-density parity-check codes under message-passing decoding," *IEEE Transactions on Information Theory*, vol. 47, no. 2, pp. 599-618, 2001.

[37] S. Y. Chung, G. D. Forney, T. J. Richardson, and R. L. Urbanke, "On the design of low-density parity-check codes within 0.0045 dB of the Shannon limit," *IEEE Electronics Letter*, vol. 5, no. 2, pp. 58-60, 2001.

[38] R. Tanner, "A recursive approach to low complexity codes," *IEEE Transactions on Information Theory*, vol. 27, pp. 533-547, 1981.

[39] T. Tian, C. Jones, J. D. Villasenor, and R. D. Wesel, "Selective avoidance of cycles in irregular LDPC code construction," *IEEE Transactions on Communications*, vol. 52, no. 8, pp. 1242-1247, 2004.

[40] T. J. Richardson and R. Urbanke, "Efficient encoding of low-density parity-check codes," *IEEE Transactions on Information Theory*, vol. 47, no. 2, pp. 638-656, 2001.

[41] F. R. Kschischang, B. J. Frey, and H. A. Loeliger, "Factor graphs and the sum-product algorithm," *IEEE Transactions on Information Theory*, vol. 47, pp. 498-519, February 2001.

[42] William E. Ryan, "An introduction to low-density parity-check codes," University of Arizona, April 2001.

[43] E. Telatar, "Capacity of multi-antenna Gaussian channels," *European Transactions on Telecommunications*, vol. 10, no. 6, pp. 585-595, November 2000.

[44] B. Hochwald, S. ten Brink, "Achieving near-capacity on a multiple antenna channel," *IEEE Transactions on Communications*, vol. 51, no. 3, March 2003.

[45] E. Biglieri, J. Proakis, and S. Shamai, "Fading channels: Information-theoretic and communications aspects," *IEEE Transactions on Information Theory*, vol. 44, pp. 2619-2692, October 2001.

[46] Stephan Baro, Gerhard Bauch, Aneta Pavlic, and Andreas Semmler, "Improving BLAST performance using space-time block codes and turbo decoding," *IEEE Globecom.*, vol. 2, pp. 1067-1071, 2000.

[47] K. L. Lo, Z. Chen, P. Alexaner, and B. Vucetic, "Layered space-time coding with joint iterative detection, channel estimation and decoding," *IEEE Int. Symp. on Spread-spectrum Tech. & Appl.*, pp. 308-312, 2002.

[48] E. Biglieri, G. Taricco, and A. Tulino, "Decoding space-time codes with BLAST architecture," *IEEE Transactions on Signal Processing*, vol. 50, no. 10, pp. 2541-2551, October 2002.

[49] E. Armanious, D.D. Flaconer, and H. Yanikomoeroglu, "Adaptive Modulation, Adaptive Coding, and Power Control for Fixed Cellular Broadband Wireless Systems: Some New Insights," *WCNC*, vol. 4, pp.238-242, Mar 2003.

[50] M. A. Kousa and M. Rahman, "An adaptive error control system using hybrid ARQ schemes", *IEEE Transactions on Communications*, vol. 39, no. 7, pp. 1049-1057, July 1991.

[51] T. Keller and L. Hanzo, "Adaptive multicarrier modulation: a convenient framework for time-frequency processing in wireless communications," *Proceedings of the IEEE*, vol. 88, no. 5, pp. 611-640, May 2000.

[52] J. Hou, P. H. Siegel, and L. B. Milstein, "Performance analysis and code optimization of low-density parity-check codes on Rayleigh fading channels," *IEEE Journal on selected Areas on Communications*, vol. 19, pp. 924-934, May 2001.

[53] B. Lu, B. X. Wang, and K. R. Narayanan, "LDPC based space-time coded OFDM systems over correlated fading channels: performance analysis and receiver

design," *IEEE Transactions on Communications,* vol. 50, no. 1, pp. 74-88, January 2000.

[54] J. Ha, J. Kim, D. Klinc, and Steven W. McLaughlin, "Rate-compatible punctured low-density parity-check codes with short block lengths," *IEEE Transactions on Information Theory*, vol. 52, no. 2, pp. 728-738, February 2006

[55] King F. Lee and Douglas B. Williams, "A mulitrate pilot-symbol assisted channel estimator for OFDM transmitter diversity systems," *ICASSP*, vol. 4, pp. 2409-2412, 2001.

[56] W. Hur and S. W. McLaughlin, "Throughput improvements of incremental redundancy LDPC Coded MIMO V-BLAST system," *International Wireless Communication and Mobile Computing Conference*, July 2006.

[57] K. Rice and R. Storn, "Differential evolution- A simple and efficient heuristic for global optimization over continous spaces," *J. Global Optimization,* vol. 11, pp. 341-359, September 1997.

[58] C. Di, D. Proietti, I. E. Telatar, T. J. Richardson, and R. L. Urbanke, "Finite-length analysis of low-density parity-check codes on the binary erasure channel," *IEEE Transactions on Information Theory*, vol. 47, pp. 657-670, February 2001.

[59] Klinc. D, Jeongseok Ha, Jaehong Kim, and Steven W. McLaughlin, "Rate-compatible punctured low-density parity-check codes for ultra wide band systems," *IEEE GlobeCom*, vol. 6, pp. 3856-3860, November 2005.

[60] J. Ha and Steven W. McLaughlin, "Low-density parity check codes over Gaussian channels with erasures," *IEEE Transactions on Information Theory*, vol. 49, no. 7, pp. 1801-1809, July 2003.

[61] X. Hu, E. Eleftheriou, and D.M. Arnold, "Progressive edge-growth tanner graphs," *IEEE Globecom.*, pp. 995-1001, November 2001.

[62] Y. Kou, S. Lin, and M. P. C. Fossorier, "Low-density parity-check codes based on finite geometries: a rediscovery and new results," *IEEE Transactions on Information Theory*, vol. 47, pp. 2711-2736, November 2001.

[63] S. Verdu, *Multiuser detection*, 2nd edition Cambridge, U.K.: Cambridge university press, 1998.

[64] Jun Wu, et al. "The incremental redundancy H-ARQ for convolutional coding," *IEEE 802.16 Broadband Wireless Access Working Group*, Document Number IEEE C802.16e-04/246r3, 2004.

[65] P. Jung, J. Plechinger, M. Doetsch, and F. M. Berens, "A pragmatic approach to rate compatible punctured turbo-codes for mobile radio applications," *Proc. 6th Int. Conf. on Advances in Commun. And Control,* June 1997.

[66] J. Hagenauer, "Rate-compatible punctured convolutional codes and their applications," *IEEE Transactions on Communications*, vol. 36, no. 4, pp. 389-400, 1988.

[67] S. Litsyn and V. Shevelev, "On ensembles of low-density parity-check codes," *IEEE Transactions on Information Theory*, vol. 48, pp. 1451-1461, June 2002.

[68] J. Metzner, D. Chang, "Efficient selective repeat ARQ Strategies for very noisy and fluctuating channels, " *IEEE Transactions on Communications*, vol. 33, no. 5, pp. 409-416, 1985.

[69] W. Hur and S. W. McLaughlin, "Incremental redundancy LDPC codes for MIMO V-BLAST system," *Conference on Information Science and System*, March 2006.

[70] David Chase, "Code Combining – A maximum-likelihood decoding approach for combining an arbitrary number of noisy packets," *IEEE Transactions on Communications.*, vol. 1, no. 5, pp. 385-393, 1985.

[71] S. Keallel, R. Link, and S. Bakthiyari, "Throughput performance of memory ARQ schemes," *IEEE Transactions on Vehicular Technology,* vol. 48, no. 3, pp. 891-899, May 1999.

[72] S. Kallel, S. Bakhtiyari, and R. Link, "An adaptive hybrid ARQ scheme," *Wireless Personal Communications*, vol. 12, no. 3, pp.297-311, Mar 2000.

[73] J. Kim, W. Hur, A. Ramamoorthy, and S. W. McLaughlin, "Design of rate-compatible irregular LDPC codes for incremental redundancy hybrid ARQ systems," *Proc. Int. Symp. Inform. Theory*, July 2006.

[74] ETSI ETS 300 744, "Digital video broadcasting: frame structure, channel coding and modulation for digital terrestrial television (DVB-T)," ETSI, Tech. Rep., March 1997.

[75] R. Nee, G. Awater, M. Morikura, H. Takanashi, M. Webster, and K. W. Halford, "New high-rate wireless LAN standards," *IEEE Communications on Magazine*, pp. 82-88, December 1999.

[76] B. Bangerter, E. Jacobsen, M. Ho, A. Stephens, A. Maltsev, A. Rubtsov, and A. Sadri, "High-throughput wireless lan air interface," *Intel Technology Journal,* vol. 7, no. 7, pp. 47-57, August 2003.

[77] J. Sun and O. Y. Takeshita, "Interleavers for turbo codes using permutation polynomials over integer rings," *IEEE Transactions on Information Theory*, vol. 51, no. 1, pp. 101-119, January 2005.

[78] M. Yang, W. E. Ryan, and Y. Li, "Design of efficiently encodable moderate-length high-rate irregular LDPC codes," *IEEE Transactions on Communications*, vol. 52, no. 4, pp. 564-571, April 2004.

[79] S. T. Chung, A. Lozano, and H.C. Huang, "Approaching eigenmode BLAST channel capacity using V-BLAST with rate and power feedback," *IEEE VTC Fall*, vol. 2, pp. 915-919, October 2001.

[80] S. T. Chung, A. Lozano, H. C. Huang, A. Sutivong, and J. M. Cioffi, "Approaching the MIMO capacity with a low-rate feedback channel in V-BLAST," *EURASIP J. APPL. Signal Processing*, pp. 761-771, May 2004.

[81] Yang Hu, Changchuan Yin, and Guanxin Yue, "Turbo receiver with hybrid interference cancellation for coded V-BLAST system," *Int. Conf. Mobile Technology, Applications and Systems*, November 2005.

[82] Wu Yan and Sumei Sun, "Iterative interference cancellation and decoding for convolutional coded VBLAST systems," *4th Int. Conf. Information, Communication and Signal Processing*, vol. 3, pp. 1511-1515, December 2003.